Megawatt Charging for Medium- and Heavy-Duty Electric Vehicles:

Battery Thermal Management System Design

Jeffry Dijkhuis

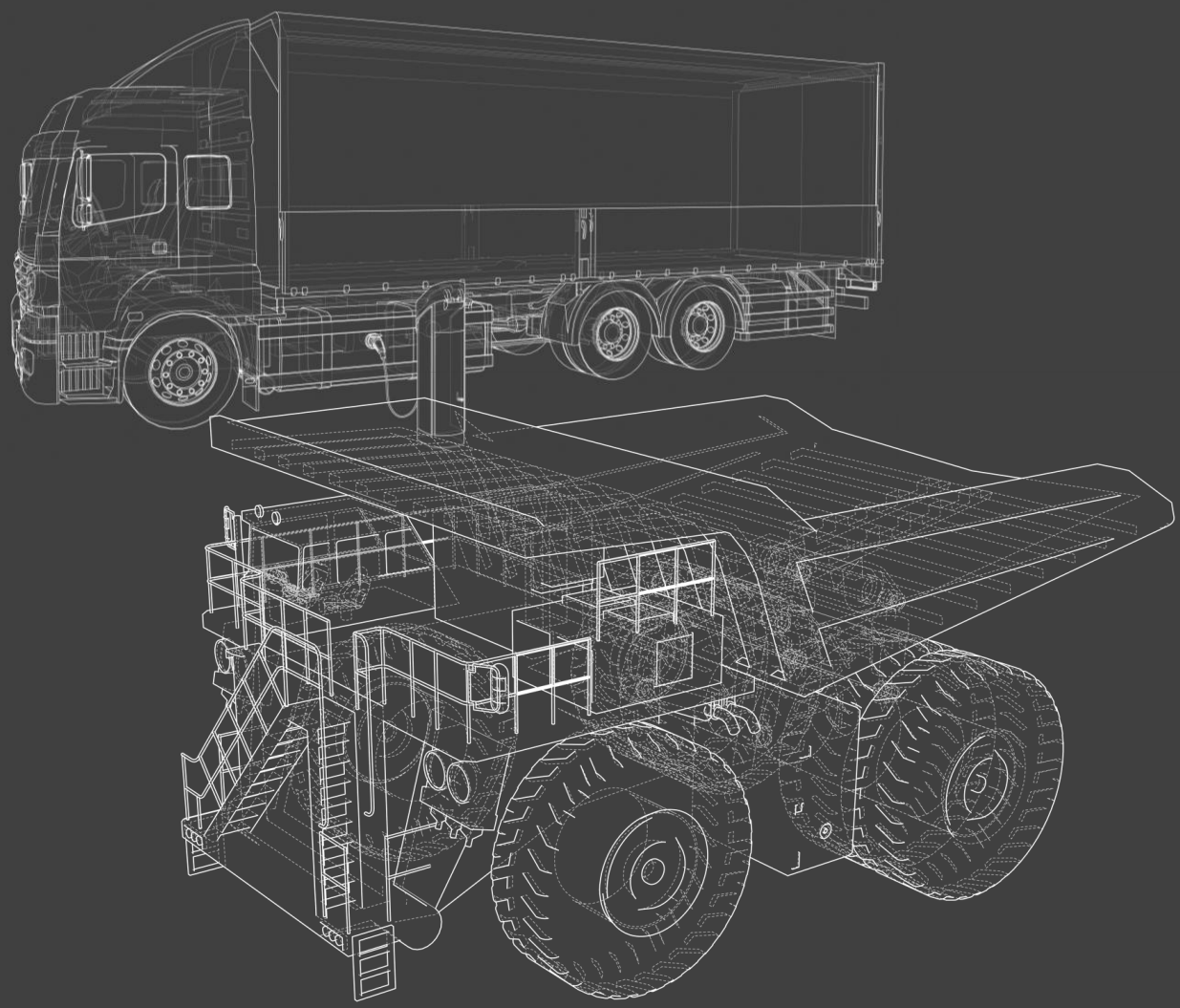

TU Delft Delft University of Technology

This page is intentionally left blank

Megawatt Charging for Medium- and Heavy-Duty Electric Vehicles: Battery Thermal Management System Design

Master thesis submitted to Delft University of Technology

in partial fulfilment of the requirements for the degree of

MASTER OF SCIENCE

in **Mechanical Engineering**

Faculty of Mechanical, Maritime and Materials Engineering

by

Jeffry Dijkhuis

Student number: 4605438

To be defended in public on November 24th, 2023

Thesis committee:	Prof.dr. K. Hooman,	TU Delft, Chair
	Dr. A.M.J. Felden,	TU Delft, Graduation Committee
	Dr. E. Zanetti,	TU Delft, Graduation Committee
	Ir. J. Hermans,	Shell, Supervisor
	Dr. ir. D. Palanisamy,	Shell, Supervisor
	Ir. R. Shah,	Shell, Supervisor

TU Delft Delft University of Technology

This page is intentionally left blank

Preface

This document represents my thesis as part of the study MSc Mechanical Engineering – Energy, Flow, and Process Technology at the Delft University of Technology. The title of the thesis is: “Megawatt Charging for Medium- and Heavy-Duty Electric Vehicles: Battery Thermal Management System Design”.
With the successful completion of this thesis, I proudly mark the conclusion of my academic journey at the Delft University of Technology, where I pursued a Master of Science in Mechanical Engineering and a Master of Science in Management of Technology.

I would like to express my gratitude to prof. dr. K. Hooman from the TU Delft as well as the Shell eMobility organization for the opportunity to conduct this research. Furthermore, I would like to thank my Shell colleagues, D. Palanisamy, R. Shah, J. Hermans, A. Ramaswamy, and R. R. Vegesna, who supported me regularly during my research and shared their expertise. I deeply appreciate their contributions and the enriching experiences we shared together. Moreover, I am thankful to the TU Delft for providing me with a nurturing academic environment and access to world-class resources during my studies. Lastly, I extend my appreciation to my friends and family, whose unwavering support and encouragement have fueled my determination to complete this work.

Jeffry Dijkhuis
November, 2023

This page is intentionally left blank

Abstract

This report presents a comprehensive study aimed at addressing the design of battery thermal management systems (BTMS) for medium- and heavy-duty electric vehicles (MHDEVs) utilizing Megawatt Charging Systems (MCS). With the increasing adoption of electric vehicles in the transportation industry, the development of an efficient and effective BTMS is of paramount importance. This study strives to shed light on the design requirements and best practices for MHDEV BTMS', providing valuable insights into the BTMS requirements, battery heat generation during Megawatt charging, and BTMS dimensioning and development.

The primary research question guiding this study is: "*How should the battery thermal management system be designed for medium- and heavy-duty electric vehicles utilizing Megawatt Charging Systems (MCS)?*"

The research process adheres to a system engineering approach, in which research is conducted on the various methodological steps of BTMS design.
First, the requirements for BTMS' being used in MHDEV's for MCS up to 4.5MW have been identified. Furthermore, the heat generation of the battery pack has been quantified for MCS charging which guides the required duty of the BTMS.
Moreover, temperature uniformity of the battery cells has been assessed through the Biot number for lumped capacitance models and it has been found that temperature gradients occur in the battery cells.
Two assessment steps have been proposed to assess BTMS strategies. These BTMS strategies include forced air BTMS, immersion cooling BTMS, cooling plates with coolant BTMS, and cooling plates with refrigerant BTMS. This resulted in design requirements for heat transfer areas and mass flow rates for being able to maintain the battery cells below 35 ℃.
Furthermore, the concepts of an active BTMS with refrigerant as well as passive storage of heat generated during charging with a thermal energy storage (TES) system have been developed and investigated. This included the dimensioning of a condenser and compressor for the vapor-compression refrigeration cycle and included the dimensioning of the required mass and volume of TES medium. The TES media assessed are immersion coolant, paraffin PCM, and hydrated salt PCM.
Implementing a PCM material as heat storage during the charging session appeared to be the most optimal BTMS strategy and utilizing a hydrated salt PCM is the most advantageous for this. When requiring one BTMS for both driving as well as Megawatt charging, a vapor-compression refrigeration system is found to be more beneficial, as it can operate continuously compared to the discontinuous PCM thermal storage.

Recommendations for future research are given related to the need for increased fidelity of heat generation prediction and BTMS models. Furthermore, research should be conducted on how to best combine the BTMS for MCS with the MHDEV HVAC and vehicle power electronics thermal management.

This page is intentionally left blank

Table of Contents

List of Figures

List of Tables

Nomenclature

Acronyms

AC	Alternating Current
BTMS	Battery Thermal Management System
COP	Coefficient of performance
C-rate	Charge/Discharge rate
DC	Direct Current
DOD	Depth of Discharge
ECM	Equivalent Circuit Model
EV	Electric Vehicle
GHG	Global Greenhouse Gas
HVAC	Heating, Ventilation, and Air Conditioning
LFP	Lithium Iron Phosphate
LIB	Lithium-ion battery
Li-ion	Lithium-ion
LMO	Lithium-ion Manganese Oxide
LTO	Lithium Titanium Oxide
MCS	Megawatt Charging System
MHDEV	Medium- and Heavy-Duty Electric Vehicle
MHT	Mining Haul Truck
NCA	Nickel Cobalt Aluminum Oxide
Ni-MH	Nickel-Metal Hydride
NMC	Nickel Manganese Cobalt Oxide
OEM	Original Equipment Manufacturer
PCM	Phase Change Material
PTC	Positive Temperature Coefficient
SEI	Solid Electrolyte Interface
SOC	State of Charge
SOH	State of Health
TMS	Thermal Management System

Latin symbols

A	Surface area	m^2
c_p	Specific heat capacity	$J/kg \cdot K$
h_c	Heat transfer coefficient for convection	$W/m^2 \cdot K$
I	Electric current	A
$\dot{m}$	Mass flow rate	kg/s
m	Mass	kg
Q	Heat	J
$\dot{Q}$	Heat transfer rate	W
$\dot{Q}_{gen}$	Heat generation rate	W
$\dot{Q}_v$	Volumetric internal heat generation rate	W/m^3
R	Battery internal resistance	Ω
T	Temperature	$°C$
ΔT	Temperature difference	$°C$
U	Overall heat transfer coefficient	W/K
V	Voltage	V

Greek symbols

λ	Thermal conductivity	$W/m \cdot K$
ρ	Density	kg/m^3

Subscripts

abs	Absorbed
amb	Ambient
bat	Battery
cell	Battery cell
gen	Generated
in	Inlet
irrev	Irreversible
lm	Logarithmic mean
max	Maximum
out	Outlet
pack	Battery pack
rej	Rejected
rev	Reversible
TES	Thermal Energy Storage
vap	Vaporization

1

Introduction

This chapter highlights the imperative for implementing a robust thermal management system in fleets of medium- and heavy-duty electric vehicles. Section 1.1 provides an overview of the background and motivation for this study, emphasizing the ongoing transition towards medium- and heavy-duty electric vehicles and underscoring the crucial role of thermal management systems in ensuring optimal battery performance.
Section 1.2 elucidates the specific research objective of this study, outlining the primary focus and purpose. It aims to investigate and propose an efficient thermal management system tailored to the unique requirements of medium- and heavy-duty electric vehicles, particularly concerning battery temperature regulation. Lastly, Section 1.3 offers an outline of the report, providing readers with a clear roadmap of the subsequent chapters and sections.

1.1 Background and motivation

The transportation sector is a major contributor to global greenhouse gas (GHG) emissions, accounting for 25% of global total emissions, with road vehicles alone responsible for 75% of that share (Al-Hanahi, et al., 2021). Of these road vehicles, less than 8% are trucks and buses, however, they are contributing to more than 35% of the road vehicle emissions (IEA, 2023). To address this challenge, European bus and truck manufacturers have committed to achieving net-zero emissions in vehicle operations by 2050, despite the current reliance on fossil fuels, which power 97.8% of trucks and 94.5% of buses in Europe (ACEA, 2021) (Al-Saadi, et al., 2022).
To accelerate the transition towards net-zero emissions, 27 countries signed a global Memorandum of Understanding (MoU) to increase the share of medium- and heavy-duty electric vehicles up to a 100% share by 2040 (Drive to Zero, 2022). In Europe, the number of medium- and heavy-duty electric vehicles in operation is projected to reach 40,000 by 2025 and 270,000 by 2030 (ACEA, 2021).

However, the shift towards electrification in the transportation sector, particularly for medium- and heavy-duty vehicles, significantly increases the demand for mined minerals, including cobalt, nickel, lithium, manganese, graphite, copper, and silver. This transition is projected to be much more mineral-intensive than previous energy transitions (Heredia, et al., 2022) (Marín & Goya, 2021) (Watari, et al., 2019) (Carballo & Sahla, 2022). The minerals find application in various areas, such as electric vehicle batteries, solar panel production, magnets for wind turbines and EV motors, and electricity networks (International Energy Agency, 2022) (Muralidharan, et al., 2019). Consequently, the mining industry plays a crucial role in

facilitating this energy transition (Heredia, et al., 2022). Notably, the International Energy Agency has determined that the production of an electric car requires six times the amount of minerals compared to a conventional car (Carballo & Sahla, 2022) (International Energy Agency, 2022). As a consequence, lithium demand is growing more than 40 times in demand in 2040 compared to 2020, and demand for other minerals is growing significantly as well (International Energy Agency, 2022). Clean energy technologies, in particular, are becoming the fastest-growing demand segment for rare earth materials and the total global mineral demand is anticipated to be up to six times higher in 2040 compared to 2020, depending on the extend of efforts to achieve the climate goals outlined in the Paris Agreement (International Energy Agency, 2022).

In addition to the commitments in the on-road medium- and heavy-duty vehicles sector, the mining industry has set objectives to achieve net-zero scope 1 and 2 greenhouse gas emissions by 2050 as outlined by the International Council on Mining and Metals (ICMM), representing 28 mining companies and several commodity associations (McKinsey, 2021) (KPMG, 2021) (O'Brien, 2020) (Leonida, 2022) (Feng, et al., 2022) (ChargeOn, 2023). This ambitious goal is being pursued through the adoption of clean powertrain solutions for mining fleets, including the use of fully battery-electric mining haul trucks (Schmidt, et al., 2021) (Barkh, et al., 2022). Mining haul trucks are a type of heavy-duty vehicle and play a crucial role in transporting ore and overburden (waste material above exploited area) in open-pit mines. The electrification of fleets can in the long term also enable fleet owners to participate in the energy market by providing ancillary services, and reduce grid congestion (Al-Saadi, et al., 2022).

To operate these medium- and heavy-duty electric vehicle fleets effectively without disrupting their operations, high charge rates are required to be able to fully charge the vehicle in a short time.

When considering long-haul trucks, the U.S. mandates a 30-minute break after 8 hours of driving and the European Union a 45-minute break after 4.5 hours of driving. To be able to fully recharge the vehicle in 30-45 minutes, high charging speeds such as Megawatt charging are required (IEA, 2023).

When considering mining haul trucks, the current diesel-powered mining haul trucks can typically operate for approximately 24 hours before requiring refueling, which can be done in about 10 – 20 minutes, whereas electric mining haul trucks are expected to have a maximum operating time of 1-3 hours, depending on the battery technology employed (Leonida, 2022). This implies that fully electric mining haul trucks need to be recharged very frequently during operation. Consequently, achieving a high charging speed is essential for electric mining haul trucks to effectively compete with their diesel-powered counterparts.

While the fast-charging technology to meet these demands is in an early stage and general electric vehicle technology in the medium- and heavy-duty vehicle segment has been classified as Technology Readiness Level 5, several collaborations have been set up to develop Megawatt Charging Systems (MCS) (Muralidharan, et al., 2019).

In China, the China Electricity Council and CHAdeMO's "ultra ChaoJi" are jointly developing a heavy-duty electric vehicle charging standard for charging up to several megawatts (IEA, 2023). Furthermore, institutions including the National Renewable Energy Lab (NREL), Argonne National Laboratory (ANL) and the Oak Ridge National Laboratory (ORNL) have been developing new levels of Megawatt Charging Systems which are currently being facilitated by MCS taskforce initiated by CharIN (CharIN, 2023). The charging standards

include an SAE J3271 and ISO 5474-3 charging standard up to 4.5 MW aimed for medium- and heavy-duty electric vehicles and are set to be published between 2024 and 2025 (Meintz, et al., 2021) (Bohn, 2020) (SAE, 2021) (CharIN, 2022).
For heavy-duty electric vehicles in the mining sector, the demand for MCS' has been indicated by the ChargeOn innovation challenge, which had the objective to find effective solutions for charging large electric mining haul trucks by collaborating with technology companies (ChargeOn, 2023).

The process of charging medium- and heavy-duty electric vehicle batteries in a short duration requires a significant amount of electrical power, leading to substantial heat generation in the battery pack. This heat generation is a result of the batteries' internal resistance and electrochemical processes (Liang, et al., 2021) (Al-Zareer, et al., 2018) (Akinlabi & Solyali, 2020).
During the operation of the vehicles, the system is subjected to not only heat generation during charging and discharging but can also face extreme ambient temperatures, particularly for mining haul trucks, which can range from -40 ˚C to 50 ˚C (Koellner, et al., 2004). If the heat in the battery pack is not removed quick enough, the temperature of the battery will rise. Lithium-ion batteries' lifetime and performance, as well as their safety, are very sensitive to temperature and therefore it is important to maintain the battery temperature in its optimal temperature range and reduce temperature differences between individual battery cells (Kim, et al., 2019) (Lin, et al., 2021) If the battery temperature becomes too high, a fire or explosion can occur (Liang, et al., 2021).
Consequently, a well-designed thermal management system is essential for the battery system of medium- and heavy-duty electric vehicles. This system ensures the safe operation of the trucks throughout their lifetime (Jilte, et al., 2021) and is essential for operation in all climates (Pesaran, 2001).
The primary purpose of the thermal management system is to regulate and maintain the temperature of the battery within the optimal temperature range, optimizing its performance and lifespan (Al-Zareer, et al., 2018) (Buidin & Mariasiu, 2021) and is arguably the most vital component of any electric vehicle (Akinlabi & Solyali, 2020) (Buidin & Mariasiu, 2021).

1.2 Research objective

The primary objective of the study is to explore the optimal design of a thermal management system for medium- and heavy-duty electric vehicles that can accommodate extremely high charging speeds categorized as Megawatt Charging Systems (MCS). The investigation will focus on various aspects, including comprehending the heat generation within the vehicle's battery pack, exploring different thermal management strategies, and selecting suitable heat transfer fluids. The development of an efficient thermal management system is vital to maintain the battery's temperature within the optimal range, ensuring safe and reliable operation of the vehicle. This aspect holds significant importance for the widespread commercial use of medium- and heavy-duty electric vehicle fleets.

1.3 Research outline

This study comprises several chapters that contribute to a comprehensive exploration of the research topic. Chapter 2 presents the literature review that has been done for heat generation in Li-ion batteries, Thermal Management Systems, and thermal modelling efforts. The literature review chapter delves into the existing body of knowledge, examining relevant studies, theories, and advancements in these areas. Chapter 3 highlights the research question that guides the study and describes the methodology used. Chapter 4 presents the results of the study. Chapter 5 is dedicated to the Discussion, where the analysis and interpretation of results are discussed. Chapter 6 concludes the study and summarizes its key findings. Lastly, Chapter 7 delves into the Recommendations of the study.

2

Literature Review

This chapter provides a comprehensive literature review, delving into various aspects relevant to the study. It commences by examining the operating conditions specific to medium- and heavy-duty electric vehicles, providing crucial insights into their operational requirements. Additionally, the review investigates heat generation phenomena in electric vehicle batteries, analyzing the factors that contribute to high battery temperatures and the associated risks. It also explores existing thermal management systems implemented in electric vehicles, outlining their objectives and design guidelines.

Moreover, the literature review evaluates various thermal management strategies, thoroughly assessing their respective advantages and disadvantages. It also delves into the significance of heat transfer fluids in battery thermal management, discussing their role in optimizing performance.

Finally, modeling efforts in battery thermal management are examined, highlighting the research and development in this area.

The literature review aims to provide a comprehensive overview of the current state of knowledge and advancements in the field.

2.1 Fleet Electrification and Charging Demands

Fleets of trucks, buses, and mining vehicles currently mainly rely on diesel fuels as their primary source of power (ACEA, 2021) (Al-Saadi, et al., 2022). However, as part of the fleet electrification efforts, an increasing number of medium- and heavy-duty electric vehicles is being developed and introduced to the market (CALSTART, 2023).

While electric trucks and buses have already established a presence in the market, the adoption of electric mining haul trucks is still in its early stages. As of 2023, there are approximately 54,000 large mining trucks with a payload of 90 metric tonnes and higher (The Parker Bay Company, 2023). Most of these trucks operate as diesel-electric, meaning they do not have an external power source or onboard traction battery (Lindgren, et al., 2022). A few cases exist where overhead trolley lines supply power to the diesel-electric trucks, similar to electric trains. However, commercially available fully electric mine hauling trucks specifically designed for open-pit mines are not yet available (Muralidharan, et al., 2019). Nonetheless, a pilot project conducted in Switzerland in 2018 retrofitted a diesel-powered Komatsu haul truck with a battery pack and electric motor, converting it into a relatively small fully electric haul truck with a capacity of 123 tonnes when fully loaded (Rizzo, et al., 2018) (Muralidharan, et al., 2019).

For any electric medium- and heavy-duty vehicle to become a viable alternative to its diesel-powered counterpart, it is crucial that the electric vehicle maximizes its operational time each day, minimizing the time spent on charging or battery swapping, as this is lost time to transport materials or passengers. Considering mining haul trucks as an example, their primary objective is to achieve the lowest possible cost per ton of hauled material, typically achieved through larger truck sizes and improved system efficiency (Mazumdar, 2013) (Koellner, et al., 2004)
Extended periods of charging for medium- and heavy-duty electric vehicles would elevate the total cost of ownership (TCO) of the fleet, thereby diminishing the appeal of the electric vehicles compared to their conventional diesel-powered counterparts for fleet owners.

Medium- and heavy-duty electric vehicles operate for approximately 18 hours per day on average, significantly more than light-duty electric vehicles (Al-Saadi, et al., 2022).
While diesel-powered mining haul trucks can operate for around 24 hours before refueling, electric mining haul trucks are projected to run for a maximum of 1-3 hours, depending on the battery technology employed (Koellner, et al., 2004) (Leonida, 2022). Consequently, electric mining trucks require frequent recharging during operation. Furthermore, (Leonida, 2022) explains that diesel-powered MHTs can refuel in just 10-20 minutes, highlighting the high demand for fast charging speeds in electric MHTs to compete effectively with their diesel counterparts.
Charging systems that facilitate the charging speeds demanded from medium- and heavy-duty electric vehicles are referred to as Megawatt Charging Systems (MCS) and supply up to 4.5 MW of power (CharIN, 2023) (CharIN, 2022) (SAE, 2021). These Megawatt Charging Systems should not be mistaken for Extra-Fast Charging (XFC) systems designed for normal passenger EVs, which typically operate at power levels of approximately 350 kW (Suarez & Martinez, 2019). Al-Saadi, et al. (2022) indicated that by 2030, a number of 30,000 chargers of over 500kW are needed in Europe alone to enable operations of the expected size of medium- and heavy-duty vehicle fleet. Pilot projects for Megawatt Charging Systems (MCS) are taking place in 2023 and commercialization is planned for 2024 (Bernard, et al., 2022).
An alternative to Megawatt charging is battery swapping, during which a drained vehicle battery is replaced by a fully charged battery at a swapping station. Benefits include reduced upfront investment costs and recharging times of as little as 3-5 minutes. However, disadvantages involve the need for battery- and vehicle standardization, requiring more than one battery per vehicle, and associated material demand and costs (IEA, 2023). Therefore, the choice between Megawatt charging and battery swapping depends on factors including the requirements of a specific fleet, regional conditions, and future developments.
Research conducted by Rafi, et al. (2020) on mining haul truck operations demonstrates that while battery swapping yields similar productivity to charging, it incurs significantly higher costs over a five-year period. Consequently, charging MHTs and aiming to reduce charging durations emerges as a more attractive option.

Notably, the majority of medium- and heavy-duty truck and bus purchases are through leasing or acquired through a loan, as price is a concern for buyers (IEA, 2023). Furthermore, fleet owners demand a high lifetime milage of the vehicles. Consequently, LFP cathode battery chemistries are the preferred choice for fleet owners. In China, over 95% of heavy-duty trucks produced were equipped with these LFP batteries in 2021 (IEA, 2023).

Furthermore, fleet electrification offers an opportunity to integrate Internet of Things (IoT) technologies, such as autonomous vehicles and data analysis, to enhance safety, efficiency, and reduce operational costs (Ertugrul, et al., 2020). Additionally, the connection of these vehicles to smart grids enables their utilization as distributed energy storage systems, contributing to the balancing of electricity grids.
Moreover, electric vehicles, including medium- and heavy-duty ones, have to comply with the ECE R100 regulatory framework. This is a regulation developed by the United Nations Economic Commission for Europe (UNECE) that sets technical specifications and procedures for evaluation of electric and hybrid electric vehicles and their components.
Testing requirements include assessing the performance, durability, and safety of the battery system, which includes the thermal management. Furthermore, it includes an assessment of the energy efficiency, which also involves the thermal management system. This underscores the importance of these factors for the design of a thermal management system for medium- and heavy-duty electric vehicles.

2.2 Heat Generation in Electric Vehicle Batteries

2.2.1 Li-ion batteries and optimal temperature range

Nowadays, lithium-ion (referred to as Li-ion) batteries are widely utilized as energy storage devices in electric vehicles (EVs) (Lai, et al., 2022) (Chu, et al., 2016) (Lu, et al., 2013) (Wu, et al., 2019). These batteries consist of a positive electrode, a negative electrode, an electrolyte, a membrane that allows only lithium-ions to flow through, and a battery shell (Zhang, et al., 2022). Li-ion batteries are well suited for electric vehicles due to a long cycle life, a high specific energy (energy per unit mass), a high energy density (energy per unit volume), and low self-discharge, compared to other rechargeable cell chemistries such as Ni-MH and lead-acid batteries (Rao & Wang, 2011) (Bandhauer, et al., 2011) (Zhang, et al., 2022) (Lu, et al., 2013). However, the increased use of high-capacity Li-ion batteries in EVs has raised concerns regarding durability, safety, cost, and cold conditions performance, which hindered the commercial adoption of these batteries in EV's (Bandhauer, et al., 2011) (Lu, et al., 2013)).
Lithium-ion batteries used in automotive applications are classified into three types: battery cell, battery module, and battery pack. Multiple lithium ion cells are configured in parallel or series to constitute a module, with usually hundreds of battery cells in one battery pack (Kalaf, et al., 2021) (Wu, et al., 2019).

To ensure optimal performance and safety, it is important to consider a battery's operating temperature range. Pesaran (2001) stated that the desired operating temperature range for batteries in EV's depends on the battery type (due to the different electrochemistry's) and is typically narrower than the specified temperature operating range for the vehicle itself by the vehicle manufacturer (Pesaran, 2001). Studies have determined that the desired temperature range of lithium-ion batteries is 15-35 ˚C (Xia, et al., 2017) (Chen, et al., 2016) (Pesaran, et al., 2013) (De Vita, et al., 2017). While some scholars mention a slightly higher operating range of 25-40 ˚C, this range is not specific for Li-ion batteries but also includes Ni-MH and lead acid batteries (Pesaran, 2002) (Rao & Wang, 2011). An upper limit of 50 ˚C for battery's surface temperature has been adopted in literature (Rao, et al., 2013) (Bandhauer, et al., 2011) (Sato, 2001). Previous research aimed for a maximum cell temperature of 40 ˚C (Park & Jaura,

2003). A lower temperature limit described in literature is -10 ˚C, as this temperature corresponds with significant lithium plating and battery capacity reduction (Bandhauer, et al., 2011).

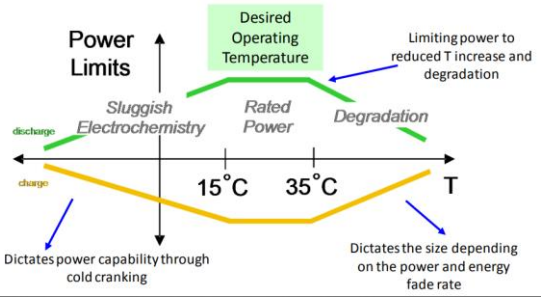

Figure 1: Battery optimal temperature range and power limits. Adapted from (Pesaran, et al., 2013)

In addition to maintaining a battery in its optimal temperature range, uneven temperature distribution in a battery pack should also be avoided. Temperature differences between individual battery cells can lead to different charge- and discharge behavior for each cell and could reduce battery pack performance (Poal, et al., 2021).

To ensure temperature uniformity in a battery pack comprising Li-ion battery cells and modules, the temperature distribution from battery module to module is desired to be less than 5 ˚C (Pesaran, 2002) (Rao & Wang, 2011) (Tete, et al., 2021). On a more detailed level, researchers such as (Mahamud & Park, 2011) (Park & Jaura, 2003) (Rao, et al., 2017) define this constraint as the maximum temperature gradient anywhere in the battery pack not exceeding 5 ˚C, implying that the temperature differences between cells should be less than 5 ˚C.

One measure defined in literature to assess temperature non-uniformity is cell maximum temperature difference (CMTD), which represents the largest temperature difference between any two points in the battery (Sabbah, et al., 2008).

2.2.2 Heat generation phenomena

To maintain lithium-ion batteries in the optimal temperature range, the implementation of an effective battery thermal management system (BTMS) that considers battery heat generation is essential (Liu, et al., 2021). Therefore, gaining a comprehensive understanding of heat generation in batteries is crucial for ensuring the performance and safety of lithium-ion batteries (Liu, et al., 2021).

Heat generated in batteries can be classified into reversible and irreversible components (Huang, et al., 2006) (Xia, et al., 2017). An overview of these classifications is shown in Figure 2. Reversible heat production arises from the entropy change associated with the reversible chemical reaction taking place in the battery's anodes and cathodes (Liu, et al., 2021). Specifically, during the charge- and discharge processes, lithium ions insertion and extraction occurs between cathode and anode and cause this change in entropy. Irreversible heat production encompasses polarization heat and Joule/ohmic heat, primarily caused by internal resistance of a battery, with ohmic resistance being the major contributor to irreversible heat generation (Liu, et al., 2021) (Bai, et al., 2019) (Huang, et al., 2006).

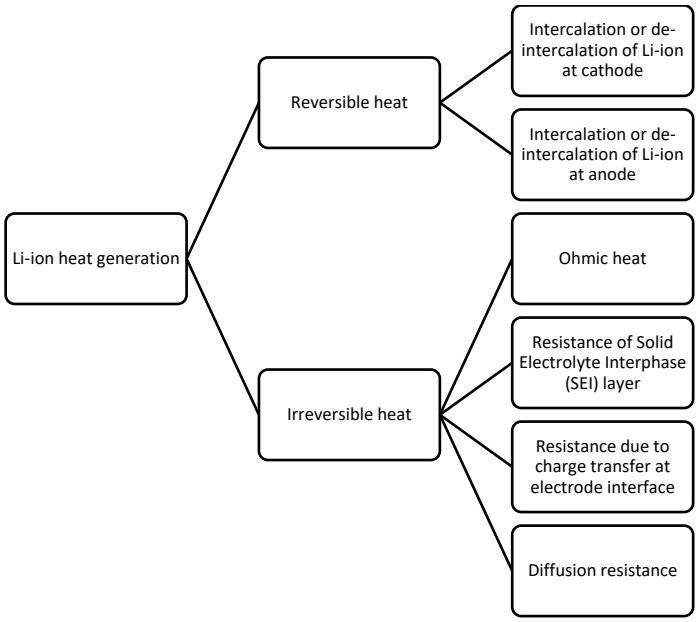

Figure 2: Heat generation classifications in Li-ion batteries. Adapted from (Choudhari, et al., 2020)

Extensive research has been done in evaluating quantities of irreversible heat generation versus reversible heat generation. Huang et al. (2006) stated that in general, the irreversible heat production is much larger than the reversible heat production. Thermal behavior analyses conducted by Bai et al. (2019) on NCA (nickel-cobalt-aluminum) li-ion pouch cell batteries revealed that irreversible heat production accounted for over 90% of the total heat generation at various charge/discharge rates, whereas reversible heat production contributed less than 10%.

To further specify these differences between irreversible and reversible heat generation, research revealed that whether either irreversible or reversible heat generation will be the largest contributor to total heat generation will depend on the charging or discharging rate, also known as the C-rate. It was found that the irreversible heat generation is typically dominant at high C-rates (1 C and larger) and the reversible heat generation is dominant at low C-rates (Nazari & Farhad, 2017). These findings are aligned with the findings of the studies from both Jeon & Baek (2011) and Ye et al. (2012) who found that for low discharge rates (less than 1C) reversible heat is dominant in heat generation. Furthermore, during higher rates of discharge, reversible heat was found to be negligible, and the contribution of Ohmic heat is then significant. The study from Liu et al. (2021) arrived at the same conclusion and stated that Joule heat (Ohmic heat) generated by lithium-ion batteries is much greater than the reversible heat production at high discharge rates, however, also found that the opposite is true at low discharge rates.

To quantify the amount of irreversible heat generation, Choudhari, et al. (2020) stated that the irreversible heat contributes to more than 70% of total heat generation. However, they did not further specify how the irreversible heat generation depends on battery type and (dis)charging rate.

Nazari & Farhad (2017) found that ignoring the reversible heat generation results in relatively small errors in total heat production, where the exact contribution of reversible heat generation appeared to depend on cathode and anode materials. For example, at C-rates higher than 2 and Li-ion nominal capacity higher than 18 A*h/m^2, ignoring the reversible heat generation results in an error of less than 1% for the prediction of total heat production of G/LMO Li-ion batteries.

However, for other cathode/anode materials the errors are found to be larger. It remains unclear whether the reversible heat generation factor decreases sufficiently to become negligible at larger than 5 C.

Ohmic heating that is part of the irreversible heat generation, also known as Joule heating, is defined as:

$$Q = I^2 * R \tag{2.1}$$

From equation 1, it can be seen that if the resistance and/or battery current increases, more irreversible heat is generated as also highlighted in the study of (Sabbah, et al., 2008). Ohmic heating is used in practice in heating devices such as electrical heaters and electrical stoves. The devices use a resistive element to generate heat. Generally in Li-ion batteries, the battery resistance increases with aging of the battery (cycling and calendar aging) and this results in more heat generation at later stages of the battery's lifetime (Raijmakers, et al., 2019) (Schmitt, et al., 2017).

Several effects in heat generation can be observed that should be considered. Firstly, it is found that heat generation in Li-ion batteries is affected by several parameters such as the depth of discharge (DOD), discharge rate (DR), and ambient temperature (Liu, et al., 2021).
Furthermore, Huang et al. (2006) found that for certain lithium-ion batteries, the heat produced at the positive electrode is about three times as much than that of the overall battery. The study suggests taking this in consideration when optimizing thermal management systems for rapid charging and discharging of Li-ion batteries.
Another effect that has to be taken into account is that heat generation differences between charging and discharging processes can be observed. Huang et al. (2006) state that at small currents, it could be assumed that the irreversible heat production during charging and discharging (ceteris paribus) is equal. However, it is questionable whether this is a valid assumption, as other research demonstrates that the internal resistance of batteries differs between charging and discharging, such as the study by Bai et al. (2019) which revealed more heat generation during discharge compared to charge processes. Choudhari et al. (2020) found the opposite effect and mentioned that the heat generation in Li-ion batteries is higher during charging than during discharging, as the internal battery resistance is claimed to be higher during charging.
It might be that the observation of the internal resistance differences between charging and discharging have not been taken into account in the research of Huang et al. (2006).
Furthermore, ambient temperature effects influence the heat generation. An example of this is the study of Smith & Wang (2006) who simulated a hybrid-electric vehicle (HEV) driving a US06 drive cycle at 25 ˚C. At this temperature it was found that the lithium-ion battery pack generated 320W of heat. However, at lower ambient temperatures the heat production was found to be higher. The cause of this may be the change of battery internal resistance as a result of temperature changes. Lastly, the study found that heat production in the battery was dominated by ohmic heating effects (Smith & Wang, 2006).

2.2.3 Risks of insufficient thermal management

A battery thermal management system plays a critical role in preventing excessive heat accumulation within the battery pack and mitigating the risk of thermal runaway (Zhao, et al.,

2021). Thermal runaway is a phenomenon that can occur in batteries, when an increase in temperature leads to a positive feedback loop leading to further increases in battery temperature. Studies conducted by Feng et al. (2015) have revealed that if thermal runaway occurs in a battery, less than 12% of its total heat released is already enough to trigger thermal runaway in adjacent battery cells, highlighting the significant risk involved. Thermal runaway is characterized by a substantial heat release, reaching magnitudes on the order of $10^7 \frac{W}{m^3}$ leading to rapid increases in battery and surrounding temperatures (Xu, et al., 2017). Such thermal runaway events can result in safety hazards like short circuits, combustion, and even explosions (Zhang, et al., 2022). Feng et al. (2018), Mali et al. (2021), and Wang et al. (2016) reported a significant number of Li-ion battery accidents that happened in EVs caused by thermal runaway, which led to the complete destruction of the vehicle.
At (extremely) low temperatures, lithium dendrites may appear in Li-ion batteries, causing short circuit, failure to start, and other operational faults (Zhang, et al., 2022). Additionally, low temperatures contribute to increased electrolyte viscosity, decreasing the diffusion rate of lithium-ions and significantly elevating the battery's internal resistance (Zhang, et al., 2022).

To address safety concerns, the ISO 6469-1:2019 international standard sets forth safety standards for electric vehicles, including battery safety (ISO, 2019) (Wang, et al., 2016). It is important to consider that the safety risks of lithium-ion batteries are directly related with the amount of energy contained within the battery cell and pack (Weinert, et al., 2007).
In an effort to enhance safety, new cathode materials have been introduced in the past, such as $LiFePO_4$ (LFP), which has demonstrated significant improvements in safety (Weinert, et al., 2007). An overview of cathode (positive electrode) materials used in Li-ion batteries is shown in studies by Liu et al. (2017) and (Choudhari, et al., 2020). While graphite-based carbon has been the most widely used material for the anode (negative electrode) in the last decade, alternative materials like lithium-titanate or lithium-titanium-oxide (LTO or $Li_4Ti_5O_{12}$) anodes have been developed to improve battery durability, enhance performance for fast charging, and has proved to be a promising anode material (Lu, et al., 2013) (Liu, et al., 2017) (Zhang, et al., 2018) (Liu, et al., 2014) (Feng, et al., 2018). However, these alternative materials are relatively more expensive and have a lower energy density compared to conventional LFP batteries (Wu, et al., 2012). Lithium-ion batteries utilizing LTO as anode material have demonstrated the ability to tolerate up to 10 C charging and discharging rate, possess a long cycle life exceeding 20,000 cycles, and have a working temperature range of -35 °C to 55 °C (Zhang, et al., 2018). Research from Belharouak et al. (2011) indicates that the total heat generated during the reaction of LTO with the electrolyte is much smaller than when using the conventional graphite as battery anode material. Additionally, LTO-based batteries exhibit minimal dendrite formation at high C-rates and/or at low temperatures as LTO has a high redox potential (Wu, et al., 2012).

Another consequence as a result of prolonged high battery temperatures is the increased speed of battery degradation. Yuksel et al. (2017) reviewed various studies on the degradation of Li-ion batteries, considering factors such as charge rates, temperatures, and depths-of-discharge. The review concluded that the primary degradation mechanism in LFP Li-ion batteries is lithium loss due to solid electrolyte interface (SEI) growth. Aging of Li-ion batteries, higher temperatures, and C-rates, contribute to SEI growth, although the magnitude of this effect varies among studies (Yuksel, et al., 2017) (Heiskanen, et al., 2019) (Wang, et al., 2011).

2.3 Thermal Management Systems in Electric Vehicles

In the field of heat transfer, three fundamental processes play a crucial role in establishing the temperature of an object or space: heat generation, heat transport, and heat dissipation (Xia, et al., 2017). The previous chapter has already provided a comprehensive overview of heat generation in batteries. Heat generation, heat transport, and heat dissipation can be effectively harnessed as strategic tools for heating or cooling objects or spaces. By leveraging these heat transfer phenomena, a thermal management system can effectively regulate and control the temperature of a system. The thermal management system is arguably the most vital component of an electric vehicle (Akinlabi & Solyali, 2020) (Buidin & Mariasiu, 2021). Furthermore, the integration of thermal management with battery energy storage is one of the most important technical issues to be addressed in in EV's according to (Zhao, et al., 2021).

Over the past two decades, the number of yearly publications on the topic of thermal management systems has increased significantly as shown in Figure 3. This trend signifies a growing interest in the study of thermal management systems (Zhang, et al., 2022). Similarly, (Tete, et al., 2021) observed a similar increase in the annual publications of review papers on thermal management systems.

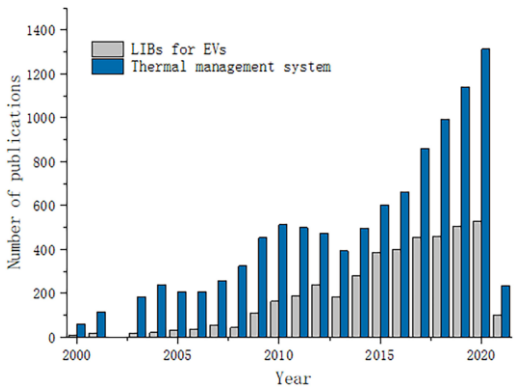

Figure 3: Number of publications on thermal management systems and EV Li-ion batteries (Zhang, et al., 2022)(source: Scopus, data from January 20, 2021)

2.3.1 TMS subsystems

Thermal management systems are employed to regulate the temperature of diverse components in electric vehicles. As a result, the overall thermal management of the vehicle can be divided into multiple subsystems. In the case of fully electric vehicles, the thermal management system can be categorized into two primary parts: battery thermal management and cabin thermal management (also known as the HVAC system) (Liang, et al., 2021).

Additionally, power electronics thermal management represents a third category of thermal management systems. In electric vehicle drivelines, the electric motor is integrated with the gearbox, inverters, and can even be integrated with the HVAC and battery cooling system (Wang, et al., 2022). Cooling these power electronics components typically involves the use of a water-ethylene glycol mixture (Moreno, et al., 2022). Furthermore, heat sinks to dissipate heat are often applied to inverters. However, optimizing the thermal management systems for power electronics is a complex task that requires consideration of various technical fields. Challenges arise when design choices that optimize thermal management may not be

compatible with mechanical and electromagnetic factors, leading to practical problems. Consequently, a comprehensive multi-physical analysis is necessary to evaluate the overall effectiveness of thermal management technologies in power electronics (Wang, et al., 2022).

This study places specific emphasis on battery thermal management. However, integration of this system with thermal management of HVAC and power electronics could optimize the overall effectiveness and efficiency. Therefore, it is important to clarify that the thermal management of power electronics and HVAC in the vehicle is not considered within the scope of this study.

2.3.2 BTMS objective

The objective of a battery thermal management system is to maintain a battery pack in its optimal temperature range while ensuring even temperature distribution within the battery pack (Pesaran, 2001) (Lyu, et al., 2019). This aligns with the broader objectives defined by Smith et al. (2018) which is increasing the Li-ion batteries' lifetime and overall battery system lifetime, as well as preventing thermal runaway from occurring to improve safety as indicated by Yang et al. (2019). In addition to maintaining the temperature of the battery within the optimal temperature range and increasing lifetime, another objective is to optimize its performance and lifetime (Al-Zareer, et al., 2018) (Buidin & Mariasiu, 2021) (Zhao, et al., 2021).
To achieve these objectives, a battery pack incorporates several temperature sensors that are connected to the thermal management system. The TMS utilizes this temperature data to determine the mass flow rate of the cooling medium, as explained by (De Vita, et al., 2017).

Thermal management systems must be designed for the battery to ensure safe usage of electric vehicles during its lifetime (Jilte, et al., 2021) and is essential for operation in all climates (Pesaran, 2001).
According to the study of Pesaran (2001), the battery thermal management system should have the following four essential functions: cooling to remove heat from the battery, heating to improve the battery temperature when the temperature is too low, insulation to prevent sudden temperature change of battery, and ventilation to exhaust the potentially hazardous gases from the battery (Pesaran, 2001). This study primarily focuses on the cooling and heating of the battery, however, does consider the ease of ventilation and insulation when evaluating cooling and heating strategies.

It is worth noting that implementing a thermal management system may have some disadvantages, such as increased system complexity, higher costs, reduced reliability, and additional energy consumption for operation, as pointed out by (Pesaran, et al., 2013). Therefore, these factors should be carefully considered when designing a thermal management system. As an example of commitment to overcoming the drawbacks typically associated with thermal management, electric vehicle OEM's strive to optimize power consumption to enhance the driving range of their vehicles (Poal, et al., 2021).
Ultimately, the benefits of the battery thermal management system in terms of extending battery life and enhancing performance outweigh the expenses and complexities associated with the additional components of the system (Pesaran, et al., 2013).

2.3.3 BTMS design guidelines

When designing a battery thermal management system (BTMS), it is crucial to follow an established approach or set of guidelines. One such systematic approach, proposed by Pesaran (2001) and Pesaran et al. (1999) consists of seven essential steps. The actual implementation of this approach depends on factors such as the desired level of sophistication, information availability, and project budget. The magnitude of heat generation of the battery and other heat generation sources dictate the size and design of the thermal management system (Pesaran, 2001). The following steps outline the process involved in designing and evaluating a battery thermal management system:

1. Define the BTMS objective and constraint
2. Obtain battery module heat generation and heat capacity
3. Perform a first-order BTMS evaluation
4. Predict the behavior of the battery module and pack
5. Design a preliminary BTMS
6. Build and test the BTMS
7. Optimize the BTMS

While it is ideal to follow all these steps for an optimized BTMS, executing some of the steps at a lower level of detail or skipping some of the steps may be necessary depending on project requirements, budget, and time (Pesaran, et al., 1999).

Literature by An et al. (2017) suggests that the selection of thermal management technology should also be based on the cooling demand and the specific application (Zhao, et al., 2021). Yang et al. (2019) have a similar view and highlight that the first required parameter to identify for thermal management system design is the quantity of heat that has to be removed.
Furthermore, it is important to evaluate the proposed BTMS configuration and its optimal performance before implementing it in practice, as different types of TMS have distinct characteristics, as mentioned by (Olabi, et al., 2022).

2.3.4 BTMS specifications and design requirements

While the guidelines discussed in previous section provide clarity in the steps to design a BTMS, it is important to determine the specific requirements involved. There are two sets of requirements to consider; information resources required for designing a BTMS and assessment requirements for evaluating the final product.

Regarding the information resources required in designing a BTMS for electric vehicles, Pesaran et al. (2013) have identified the following points:

- The acceptable temperature range for cell components at all times
- The acceptable temperature difference within cells and from cell to cell
- Maximum and minimum temperature limits for battery life specifications, performance ratings, and safety considerations
- Thermo-physical properties of cells or components
- Heat generation rate under average and aggressive drive profiles
- Heat rejection rate by thermal management system

- Configurations and dimensions of cells and proposed battery thermal management system
- The parasitic power needed to circulate fluids through battery thermal management system

Regarding assessment requirements, Rao & Wang (2011) have defined the following requirements for a thermal management system:

- Maintain optimum operating temperature range for every cell and all battery modules, rejecting heat in hot climates/adding heat in cold climates.
- Ensure small temperature variations within a cell and module.
- Ensure small temperature variations among various modules
- Compact and lightweight, reliable, low-cost, easily packaged, and easy maintenance
- A provision for ventilation if the battery generates potentially hazardous gases

Additional assessment requirements have been identified in literature. Pesaran (2001) outlined several essential assessment requirements for a battery thermal management system, including alignment with vehicle manufacturer specifications for the vehicle in which the BTMS is placed, lightweight and compact design, low cost, easily packaged, reliable, easy maintenance, using low parasitic power, facilitate battery operation across diverse climate conditions, provide ventilation in the presence of hazardous gases, and allow for seamless integration of the BTMS in the vehicle. Greco et al. (2015) also emphasize the importance of a lightweight, compact, reliable, and low-cost BTMS.
Sundin & Sponholtz (2020) mention two additional requirements for the thermal management system. Firstly, the heat removal capacity of the BTMS must exceed the heat generated by the battery, represented by the equation:

$$U > \frac{Q_{battery}}{T_{battery} - T_{ambient}} \tag{2.2}$$

Secondly, the mass of the heat transfer medium used must be sufficient to absorb all the heat generated by the battery.
By considering the requirements mentioned in this section, a comprehensive and effective battery thermal management system can be designed and evaluated.

2.3.5 BTMS classifications and evaluation

A battery thermal management system can be classified based on various factors such as its operating mode, heat transfer type, heat transfer medium, and method of application (Tete, et al., 2021). This section aims to explore each classification and provide a more detailed understanding of their respective characteristics.
Table 1 provides an overview of these classifications for easy reference.
Considering the extensive number of studies conducted on battery thermal management strategies employing different configurations and thermal media, it becomes impractical to review all the existing research, as noted by Liu et al. (2017). Therefore, this study aims to provide an overview of the key distinctions, advantages, and disadvantages, of the most widely utilized battery thermal management methods.

Mode
Heating
Cooling
Heating & Cooling
Power consumption
Active
Passive
Combination of active and passive
Heat transfer medium
Air
Liquid
PCM
Combination of media
Contact type
Direct
Indirect
System design
Coolant-based
Refrigerant-based

Table 1: Classification of thermal management systems

Various thermal management methods are currently applied in passenger electric vehicles available on the market. Table 2 provides an overview of different EV models along with their respective thermal management systems (Yuksel, et al., 2017) (Xia, et al., 2017).

Year	OEM	Product	Thermal Management Method
2019	Mercedes-Benz	EQR	Liquid cooling
2018	Volkswagen	IDR	Air cooling
2017	BMW	i8	Refrigerant-based cooling
2017	Toyota	Prius Prime	Air cooling
2016	GM	Chevrolet Bolt	Liquid cooling
2015	BMW	X5 PHEV	Refrigerant-based cooling
2014	Audi	A6 PHEV	Refrigerant-based cooling
2014	Tesla	Model 3	Liquid cooling
2013	Tesla	Model X	Liquid cooling
2012	Nissan	e-NV200	Air cooling
2011	Toyota	iQ	Liquid cooling
2010	Mercedes-Benz	S400 Blue	Refrigerant-based cooling
2009	BMW	i3	Refrigerant-based cooling

Table 2: Overview of battery thermal management methods for EVs (Shen & Gao, 2020)

While a multitude of techniques and heat transfer media exist for thermal management purposes, electric vehicles have so far only adopted air- and indirect liquid-based cooling methods (including the use of refrigerants) (Tete, et al., 2021).

This chapter evaluates each type of thermal management system and highlights the key differences and characteristics. The thermal management types selected for evaluation in this study are the ones that are most commonly used in EVs. Novel thermal management types or strategies that are significantly immature and only experienced limited testing in lab

environments have been left out of the scope, as their effectiveness in practice is not proven sufficiently.

Active and passive cooling

Heat transfer can be either passive or active (Kalaf, et al., 2021) (Keklikcioglu, et al., 2018). In passive heat transfer, thermal performance is improved without the need for additional energy input, relying solely on ambient conditions and geometric surface modifications within flow channels. Examples of passive heat transfer techniques include nozzle turbulators, heat sinks, coiled or tangled wires, and twisted tapes (Keklikcioglu, et al., 2018). On the other hand, active cooling involves the use of specialized heat transfer equipment that requires external power to enhance the heat transfer rate.

In some cases, a combination of active and passive cooling methods can be employed to cool or heat a battery. For instance, active cooling may be implemented on the inside of a battery pack, while passive heat transfer from ambient conditions can be utilized on the outside of the pack. This hybrid approach maximizes the efficiency of the thermal management system by leveraging the advantages of both active and passive cooling techniques.

Heat transfer medium

Thermal management systems for batteries can be categorized into different cooling methods based on the heat transfer medium used. According to Rao & Wang (2011), there are four main categories:

- Air for heating/cooling/ventilation
- Liquid for heating/cooling
- Phase change materials (PCMs)
- A combination of the options above

Other scholars such as Abdelkareem et al. (2022) provided a similar overview of thermal management types based on thermal medium, including indirect liquid cooling, direct liquid cooling, forced air cooling, and phase change materials. Each of these cooling options possesses its own set of advantages and disadvantages.

Air cooling

Zhao et al. (2021) indicated that air-cooled battery thermal management systems have been widely used in EV's due to a demand for cost-reduction. Furthermore, its advantages are its simplicity and generally lighter weight (Liu, et al., 2017). The method of air cooling also has been studied intensively (Liu, et al., 2017).

Air cooling can be utilized through natural convection (passively) and through forced convection (actively). However, the heat transfer coefficient for convection by air is generally lower in natural convection than in forced convection. Liu et al. (2017) state that therefore, cooling by natural convection is only effective when used with low energy density batteries. Furthermore, the study found that air cooling is improper for applications in abuse conditions such as high ambient temperatures and/or at high charge- and discharge rates, due to the low thermal conductivity of air. For these applications, cooling strategies such as liquid cooling are advised. The findings of Choudhari, et al. (2020) align with this observation, emphasizing the inadequacy of air cooling at high charge- and discharge rates.

Sabbah et al. (2008) also studied the effectiveness of air-cooling under high discharge rates and high operating and ambient temperatures, and concluded that the performance of air-cooled

thermal management systems is not sufficient to keep the cell temperatures within the desirable operating range without significant fan power.
Sundin & Sponholtz (2020) conducted a comparative analysis for air cooling and liquid cooling, highlighting the limitations of air cooling. As air has a low heat capacity, large flowrates of air must be directed to the battery, which aligns with the significant fan power finding from Sabbah et al. (2008). Additionally, air cooling necessitates the exposure of battery surfaces to air, potentially requiring infrastructure modifications and additional ductwork. Furthermore, conditioning and filtering of the air may be necessary to prevent corrosion effects. Sundin & Sponholtz (2020) also noted that the evolving demands of applications, including faster charge/discharge cycles, faster battery cycling, extended service life, higher battery voltages, and enhanced stabilization of voltage output, pose challenges to the effectiveness of air cooling.

PCMs

Passive thermal management solutions have gained interest in commercial applications to avoid the drawbacks of overdesigned and unnecessarily complicated systems. One such solution is the utilization of phase change materials (PCMs). PCMs are substances that undergo a phase transition, typically from solid to liquid and back, during the process of absorbing or releasing heat. PCMs utilize the latent heat associated with their phase change.

Numerous studies have been conducted to evaluate the suitability of PCMs for thermal management systems, some specifically for the application of electric vehicles, such as the study conducted by Ramandi et al. (2011) in which passive thermal management systems with PCMs were examined.
These developments led to the testing and evaluation of various PCM materials. Rao & Wang (2011) have defined specific criteria for selection of PCM for battery thermal management:

- The PCM melting point must be in the desired operating temperature range
- Thermal properties: high latent heat, high thermal conductivity, high specific heat
- Small volume changes during the phase transition
- No or little subcooling during freezing
- Stable material, non-poisonous, non-flammable, and non-explosive
- Low cost and available in large quantities

Furthermore, Agyenim et al. (2010) have conducted a review of a large range of PCM's, providing an overview of the melting temperature of each PCM. Building upon this overview, Rao & Wang (2011) have compiled a list of ideal PCMs for battery thermal management. They found that a single PCM is not sufficient for high heat fluxes, however, composite PCM's can be used instead. Wang et al. (2016) reviewed such composite PCMs that have been studied for vehicle applications.

While the use of PCMs offers several advantages, it is important to acknowledge certain limitations compared to other cooling methods. PCM-based cooling has been found to exhibit lower thermal conductivity, increased weight, and potential leakage issues (Zhao, et al., 2021) (Rao & Wang, 2011). The increased likelihood of leakage in PCM systems is caused by the PCM volume changes as a result of phase changes (Lu, et al., 2020).

While PCMs alone exhibit low thermal conductivity and passive heat rates, efforts have been made to increase heat transfer by attaching heat fins to the battery modules (Khateeb, et al., 2004). The study revealed that PCM alone is insufficient for Li-ion thermal management, but that aluminum heat fins proved effective for thermal management when used for three cycles of an electric scooter. In applications with larger battery packs such and higher charging rates, it may be that PCMs with heat fins is not sufficient. Chen et al. (2016) mention the PCMs need to release the heat absorbed from the battery, which can be a challenge during continuous charge- and discharge cycles. However, PCMs can aid preventing maximum temperature situations.

An important consideration with PCMs is that after absorbing heat and transitioning from a solid to a liquid state, their effectiveness in absorbing heat diminishes, leading to a potential significant rise in battery temperature (Khateeb, et al., 2004) (Khateeb, et al., 2005). The cause of this has been indicated in thermal management system studies by Choudhari, et al. (2020) and Wang et al. (2016), who stated that fully melted PCM introduces an additional thermal resistance between the battery and the PCM cooling medium, essentially acting as an insulator. This poses a challenge in utilizing PCMs since fully melted PCM provides inferior cooling compared to direct-air cooling (Wang, et al., 2016). Consequently, PCM-based solutions are less suitable for long-term and long-distance operations (Shen & Gao, 2020).

To overcome these challenges, Choudhari, et al. (2020) proposed installation of heat fins to increase PCM melting time and enhance heat transfer. However, this approach has not been widely implemented in battery thermal management systems and has primarily been explored in solar-based systems thus far.

Liquid cooling

The majority of modern electric vehicles use a liquid-based battery thermal management system, which has a high heat transfer efficiency and can provide cooling or heating (Wu, et al., 2019).

Liquid cooling can be classified as either direct liquid cooling or indirect liquid cooling. In direct liquid cooling, battery modules are submerged in a dielectric thermal fluid. This is referred to in literature as Single-phase Liquid Immersion Cooling (SLIC) (Sundin & Sponholtz, 2020). In indirect liquid cooling, a fluid flows through cooling plates or through tubes around the battery modules.

For both direct and indirect liquid cooling, a number of characteristics should be considered when selecting for thermal management type. Indirect liquid cooling faces a higher thermal resistance than direct liquid cooling because of the plate or tube material that the heat flow must pass through which reduces the cooling efficiency (Liu, et al., 2017) (Sundin & Sponholtz, 2020). Furthermore, Sundin & Sponholtz (2020) highlighted that for an indirect liquid cooling system, it is important that any air gaps between battery cells and cold plate/jacket are avoided by ensuring proper contact or by filling any air gaps with dielectric thermal grease or bonding agents, to avoid rapidly degrading thermal management system cooling efficiency. However, Liu et al. (2017) mention that the higher viscosity of dielectric fluid used in direct liquid cooling results in high power consumption if high rates of forced flow are needed. Therefore, both types of liquid cooling have their own advantages and disadvantages.

Chacko & Charmer (2011) mentioned that indirect liquid cooling or heating system would be one of the most promising methods for battery thermal management (Chen, et al., 2016).

Sundin & Sponholtz (2020) stated in their review of thermal management methods that direct liquid cooling theoretically delivers the best thermal management performance and at the lowest cost and complexity of the system, as this system does not require a cooling plate/jacket framework and thermal bonding requirements, contrary to indirect liquid cooling. Sundin & Sponholtz (2020) mentioned that at the same volumetric flow rate, direct cooling fluids have higher heat transfer than air, as the fluid has a higher thermal conductivity and a thinner boundary layer. Roe et al. (2022) also reviewed direct liquid cooling and discussed its performance, describing their excellent heat transfer compared to air-cooled system. However, they indicated a research gap on direct cooling systems' lifetime, stability of fluid, safety, and material compatibility.
Larrañaga-Ezeiza, et al. (2022) conducted research on direct liquid cooling (with mineral oil as dielectric fluid) and compared the effectivity to indirect liquid cooling (with 50/50 volumetric percent glycol/water). The study found that the order of magnitude of the thermal resistance between the thermal fluid and the battery cell was significantly lower for direct liquid cooling, which is advantageous for thermal management.

In addition to evaluating the characteristics and performance of liquid thermal management systems, design considerations have been highlighted in literature. Choudhari, et al. (2020) mentioned that in liquid cooled thermal management systems, the coolant flow rate and number of channels are an important factor in the thermal management system design. Higher flow rates are more effective in maintaining maximum temperature and temperature uniformity but consume more power. Furthermore, it is crucial that the liquid used in a direct liquid cooling system is compatible with the battery material Sundin & Sponholtz (2020).
Additionally, differences can be observed in the lifetime of different liquid thermal management systems. Abdelkareem et al. (2022) mention that the lifetime of a direct liquid cooling system (immersed cooling) has an expected lifetime of 3-5 years, where the indirect liquid cooling has a lifetime expectancy of about 20 years.

Single-circuit and dual-circuit liquid TMS
The direct and indirect liquid thermal management systems discussed in previous section apply to a TMS utilizing a coolant circuit. This is a circuit containing liquid that is directed to the battery to remove heat. In order to remove this heat from the coolant, a chiller (type of heat exchanger) is used that absorbs the heat from the coolant circuit and exchanges it with a refrigerant circuit. Due to the use of both a coolant circuit and a refrigeration circuit, these systems can be called a dual-circuit liquid cooling system (Yang, et al., 2019).

Contrary to dual-circuit liquid cooling systems for battery thermal management, single-circuit refrigerant-based systems exist in which the refrigerant that regulates thermal comfort of the cabin (HVAC system) also has the objective to directly cool or heat the battery through heat exchange with its refrigerant circuit. These systems do not have an extra loop with a chiller heat exchanger (Wang, et al., 2016).
Several studies have been done for single-circuit cooling systems. Guo & Jiang (2021) proposed a refrigerant-based thermal management system for EVs that can regulate the temperature of both the vehicle cabin air and the battery pack. The results of the study indicated that the temperatures can be controlled well by this system. The temperatures of the cabin and battery can be adjusted independently and preheating of the battery to 20 °C at 0 °C ambient

temperature can be completed in about 15 minutes. Tete et al. (2021) and Park et al. (2019) also found that this type of system is effective in both mild and demanding conditions (charging rates and ambient temperatures). However, they stated that a refrigeration cooling system's effectivity is strongly related to ambient temperature (Tete, et al., 2021). Wang et al. (2022) evaluated various studies on single-phase cooling systems and summarized that they can provide a greater heat transfer coefficient. Furthermore, these systems are less complex and lighter weight, as there is no chiller used. Instead of using cooling plates with channels that circulate the refrigerant, the batteries could be directly submerged in refrigerant liquid, such as studied by Al-Zareer et al. (2020). However, the storage of large amounts of refrigerant increases system weight and might lack the space to integrate it in the vehicle.

Figure 4 visualizes the difference between such a refrigerant based cooling system and a coolant loop system.

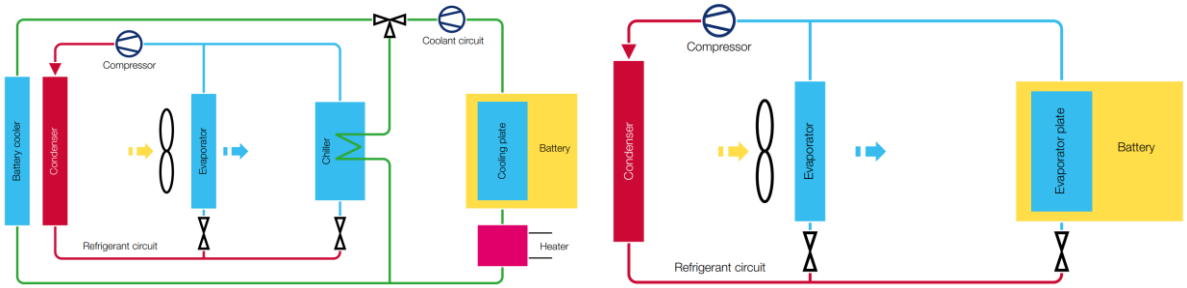

Figure 4: Battery thermal management by dual-circuit (left) and refrigerant-based single-circuit (right). Adapted from (Wang, et al., 2016) and (Mahle Behr, 2021)

An advantage of using a separate refrigerant loop and coolant loop such as in the dual-circuit cooling system allows independent control over the battery system and the cabin, in a way that the coolant loop ensures the battery temperature can be maintained in its optimal temperature range, while the refrigerant loop provides comfortable cabin temperatures. Furthermore, having these two loops enables further optimization of thermal management. While the coolant loop can be designed to remove the majority of the battery heat generated, the refrigerant loop can be used in combination with the coolant loop in situations such as fast charging for additional cooling.

2.3.6 Comparison of methods

This section aims to evaluate the differences between the thermal management strategies discussed in previous sessions and compare their effectiveness for the application of MHDEV's utilizing Megawatt charging.

In summary, when considering the different types of thermal management techniques that can be implemented, it is evident that these strategies vary in their ability to effectively maintain an optimal battery temperature. While most literature is dedicated to development and performance of a specific type of thermal management, several studies evaluated the differences between the thermal management types, such as Tete et al. (2021) who reviewed and listed numerical and experimental results found between 2011 and 2020 for the battery thermal management systems discussed in this study.
Other examples are Rao & Wang (2011) who performed a trade-off analysis on several battery thermal management methods and Choudhari, et al. (2020) who evaluated different liquid

cooling thermal management systems and listed the resulting maximum battery temperature and temperature difference for various types and conditions. Wang et al. (2016) listed strengths and weaknesses of air cooled and liquid cooled (for single-circuit and dual-circuit) battery thermal management systems.
Rao & Wang (2011) described that traditional air-cooled and liquid-cooled battery thermal management systems make the system too bulky, complex, and expensive, and state that a novel use of pulsating heat pipes or PCM's may be more effective when well designed. However, the study itself focusses on the effectiveness of PCM's in TMS's for hybrid electric vehicles. While the claimed disadvantages mentioned are discussed in the study for air-cooled methods, it lacks substantiated evidence and references for liquid-cooled thermal management systems. Furthermore, Liu et al. (2017) compared different Li-ion battery cooling methods and listed advantages and disadvantages for each.
Other scholars such as Buidin & Mariasiu (2021) analyzed studies and research that has been conducted on battery TMS's and they discussed advantages and disadvantages of the individual components and the system itself.

As MHDEV's face high charge rates during operation, it is of significant importance to evaluate the effectiveness of the battery thermal management strategies at these high charge rates. De Vita et al. (2017) compared various thermal management methods at several charge- and discharge rates up to 8C. During the study, Li-ion batteries were subjected to 8C charging and discharging for 225 seconds each, and the temperature increase for forced- and natural convection by air have been determined. While forced air convection was able to reach lower average temperatures of the battery pack, the natural convection method presented a more homogeneous temperature distribution.
Comparing the findings with a method using indirect liquid cooling in which water flows through cooling plates that are located in the battery pack, resulted in even lower average battery temperatures.
This study aligns with the consensus among scholars that that despite its simplicity and low-cost, air-cooled systems are not sufficient for thermal management in demanding conditions such as during high charge rates. Akinlabi & Solyali (2020) further emphasize that despite its extreme simplicity, low costs, ease of implementation, it is almost impossible for air cooled battery TMS systems to provide adequate cooling for Lithium-ion batteries in electric vehicles.

While various studies demonstrated a favorable performance of liquid thermal management types compared to air or PCM thermal management, concerns about all traditional approaches were highlighted by Rao & Wang (2011). They found that traditional battery thermal management systems such as air- and liquid cooling might not meet requirements at stressful and abuse conditions, especially at high battery discharge rates and at high operating or ambient temperatures. At high charge- and discharge rates at high currents, batteries generate much more heat (Rao & Wang, 2011).
Hence, when it comes to applications like MHDEV fleets, the design of thermal management systems must be approached with utmost care. This is due to the fact that traditional methods are nearing their technical limits in terms of performance.
However, when considering traditional thermal management types, liquid cooling is found to be the most suitable method for large-scale battery applications at high discharging and

charging C-rates, as well as in high-temperature environments (An, et al., 2017) (Zhao, et al., 2021).

Another point of evaluation is the power consumption of the various thermal management strategies. Chen et al. (2016) conducted a study in which the effectiveness of liquid cooling (direct and indirect), air cooling, and fin cooling are assessed for EVs. The parasitic power of an air-cooled system was found to be about 2 to 3 times higher than the other methods in order to reach the same battery temperatures. Furthermore, systems where fins have been added in attempt to improve thermal performance resulted in the heaviest option of all systems. Indirect liquid cooling was stated to be a more practical form of cooling than direct liquid cooling. Additionally, costs have been identified as an important factor for deciding which thermal management system to implement (Tete, et al., 2021).

Furthermore, for selecting the optimal thermal management strategy, optimization techniques have to be considered that might significantly change a specific thermal management strategy's effectiveness compared to another one.
Various designs for each battery thermal management system can be found in Tete et al. (2021). For liquid cooling systems, different configurations can be made of cold plates, microchannels, and tube cooling. For air cooled system, different airflow ducts can be designed for a thermal management system.

2.3.7 Heating

While battery cooling has received much more attention in scientific literature, battery heating is also required when operating in sub-zero conditions (Liu, et al., 2017). Along with electrochemical effects, cold environmental temperatures (close to or below 0 °C) temporarily increase the battery internal resistance which decreases the capacity of the battery and decrease the charging speed and efficiency (Choudhari, et al., 2020) (Yang, et al., 2019). Therefore, it is necessary to preheat the Li-ion batteries before the start of the operation in colder environmental conditions.

Liu et al. (2017) listed 4 criteria for the selection of a battery heating system:

- The power consumption for heating
- The time to heat the battery
- The total system costs (purchasing, energy expenses, maintenance)
- The complexity addition (extra components, weight, and space)

Scholars distinguish between external heating methods and internal heating methods (Li, et al., 2021) (Qin, et al., 2020). Examples of external heating methods include positive temperature coefficient (PTC) heating, PCM heat storage, or hot fluid methods in combination with heating plates or fans. Internal heating method examples are self-heating batteries containing an internal heat generator in the battery pack, or heating methods using a battery's own current to generate heat (including AC, DC, and pulse heating) (Qin, et al., 2020).

Nelson et al. (2002) found that during cold ambient temperatures, batteries in EV's cannot heat themselves sufficiently rapid with internal Ohmic heating ($I^2 * R$) as cited by (Rao & Wang, 2011).

Solutions proposed by Nelson et al. (2002) to deliver the heat are either by utilizing electric heaters (PTC) within the battery or by transferring the heat through the battery coolant. The latter approach involves the battery coolant receiving heat from an engine coolant loop. However, it is worth noting that this study specifically focused on hybrid electric vehicles that still incorporate an internal combustion engine. As a result, in the case of electric vehicles (EVs) which lack an internal combustion engine, alternative heat sources need to be considered for effectively providing heat to the EV battery.
Literature also provided insights regarding these EVs with batteries that receive both cooling and heating from one loop of the thermal management system. One notable finding is that the temperature change of the fluid flowing through the battery pack varies significantly when comparing cooling and heating processes. Consequently, to address this effect, it may be necessary to consider increasing the cooling channel size and/or the coolant flow rate, as suggested by Nelson et al. (2002). This adjustment can help effectively mitigate the temperature fluctuations during both cooling and heating operations.

Furthermore, thermal management can be strategically set to prevent the battery- and cabin temperature from rising towards or above the maximum operating temperature during standby (or non-extreme conditions), because once the battery heat generation or ambient temperatures rise, maintaining desired temperatures can become more challenging (Nelson, et al., 2002).

2.3.8 HVAC

The Heating Ventilation and Air Conditioning (HVAC) system in electric vehicles is required for providing seasonal thermal comfort and is one of the major power consumers in EV's (Poal, et al., 2021). A regularly used component in the HVAC system is a Positive Temperature Coefficient (PTC) electric heater which provides heating to the cabin of the vehicle (Poal, et al., 2021).

Wu et al. (2019) emphasize the significant energy-saving potential and efficiency improvement by connecting the battery thermal management system with other subsystems, such as the HVAC system, through the utilization of liquid circulation. Several scholars have developed such integrated systems, including Yokoyama et al. (2011) who propose a TMS that incorporates waste heat recovery for interior heating. Additionally, Kelly et al. (2002) described an integration of cabin TMS and battery TMS in the Toyota Prius and Honda Insight, where fans force cabin air towards the battery modules. These novel approaches demonstrate the potential for efficient coordination between different subsystems to optimize thermal management and enhance overall vehicle performance.

2.4 Thermal Fluids in Electric Vehicles

A thermal fluid or heat transfer fluid is a fluid used for the transfer of heat from one location to another. Thermal fluids are specifically designed to have excellent heat transfer properties. This section explores the various thermal fluids that are commonly used in battery thermal management systems in electric vehicles. To emphasize the importance a thermal fluid in a TMS, Tete et al. (2021) highlighted that one of the primary considerations for any battery thermal management system is the selection of an appropriate cooling medium.

2.4.1 Coolants and refrigerants

Thermal fluids used for undergoing a phase transition and used for achieving below-ambient temperatures are called refrigerants and are often applied in HVAC systems, where thermal fluids used for battery thermal management and remain in single phase are called coolants.

When considering coolants, certain coolants such as dielectric liquids are designed for the use in direct liquid (immersion) cooling systems, where other coolants such as ethylene-glycol are designed for indirect liquid cooling. This distinction is necessary as both fluid types have significantly different characteristics, which would strongly reduce thermal performance when used in the other system and can lead to material incompatibility issues between the fluid and battery when used incorrectly.

Refrigerants are more regulated than coolants due to their contribution to global warming, toxicity, and flammability. Developments in legislation prohibit the use of certain refrigerants that were commonly used in the past, such as R134a, also known as 1,1,1,2-Tetrafluoroethane. The 2006/40/EC directive introduced by the European Commission prohibits the use of these refrigerants in new vehicles due to their high Global Warming Potential (GWP) (European Parliament, 2006). Consequently, refrigerants for the use in electric have to be selected carefully.

2.4.2 Glycols

In the category coolants, synthetic organic and silicone fluid can be used for heat transfer applications with maximum temperatures above 175 ˚C. For systems with maximum temperature requirements below 175 ˚C and freeze protection, glycol-based fluids can be used (Dow, 2020).

Glycols have characteristics that include low viscosity, low volatility, low electrical conductivity, high heat transfer, and low cost (Santambrogio, et al., 2016). Furthermore, ethylene glycol specifically is the most common fluid used for the purpose of freeze protection (Madera, et al., 2003). It is colorless and odorless and completely miscible with polar solvents such as water (Yue, et al., 2012).

Electric vehicles that use a cooling circuit typically use a mixture of this ethylene-glycol/water as coolant.

A big advantage of using this mixture of ethylene-glycol and water, contrary to pure ethylene-glycol or pure water, is the increased temperature operating range. While the freezing point of pure ethylene glycol is -12 ˚C and that of water 0 ˚C, a 60/40 mixture of both has a freezing point of -45 ˚C. The mixture also has an elevated boiling point compared to both pure fluids.

However, as glycols are corrosive, corrosion inhibitors such as nitrite and molybdate must be added to the fluid protect the thermal management system (Madera, et al., 2003).

As stated before, a coolant such as an ethylene-glycol/water mixture should not be implemented in an immersion cooled system. The reason for this is that aqueous glycol fluids such as ethylene-glycol/water are highly electrically conductive, which limits the use of these fluids to indirect cooling methods where the fluid does not come in contact with the battery (Sundin & Sponholtz, 2020).

A safety hazard of indirect liquid fluids such as glycol/water mixtures is that when there is leakage in the TMS or any other cause that results in fluid contact with the battery, electronics short circuit and shock hazards can occur (Sundin & Sponholtz, 2020).

When evaluating the toxicity of ethylene glycol, it is important to note that the compound itself has a low toxicity, however, produces toxic metabolites that can result in damage to multiple organs when ingested, absorbed by skin, or inhaled (Yue, et al., 2012). Ethylene glycol can be fatal to humans in relatively small amounts of approximately 100ml or 1.6 g/kg body weight (Hess, et al., 2004). Consequently, the fluid should be treated with caution and preferably stay in a closed system without the need for direct human interaction. A non-toxic alternative of ethylene glycol is propylene glycol, however, as it is more viscous and has a lower heat capacity, it is not optimal for implementation in a TMS.

When comparing these coolants to dielectric fluids used in immersion cooling, they have a high heat transfer coefficient. Wang et al. (2016) reviewed scientific literature on thermal fluids used for battery thermal management and found that a TMS using a water/glycol mixture cooling system has a more than 3 times higher heat transfer coefficient compared to that of air. Using dielectric oils achieves a 1.5 to 3 times higher heat transfer coefficient compared to air.

2.4.3 Dielectric fluids

Dielectric fluids can be used for immersion cooling applications. These oils are typically based on mineral oils, but alternative formulations exist. Dielectric fluids for direct liquid cooling exist that are biodegradable, non-toxic, and food grade rated, which avoids most safety and environmental issues (Sundin & Sponholtz, 2020).
Contrary to the safety risks involved with indirect cooling fluids when coming in contact with batteries, dielectric fluids have the advantage of being not electrically conductive and therefore avoid this safety hazard.
When comparing dielectric fluids for immersion cooling to water-glycol coolants, dielectric fluids perform worse on most thermal aspects. The thermal conductivity, specific heat capacity, and convective heat transfer coefficient are typically all lower (Roe, et al., 2022).

2.4.4 Nanofluids

A novel type of fluids described in literature that can be used for thermal management are nanofluids. These are water- or oil-based thermal cooling liquids containing dispersed solid particles (such as ZnO, Al_2O_3, TiO_2, CuO) with a size between 20 and 60 nm (Tung, et al., 2020) (Abdelkareem, et al., 2022).

The extremely small size of the particles enables a large total surface area of the material and enhances the thermal cooling properties of the fluid by increasing the heat conductivity and heat transfer coefficient (Tung, et al., 2020). However, Abdelkareem et al. (2022) explained that a number of critical difficulties exist for application of nanofluids in battery thermal management systems in EV's. Some examples of this are sedimentation of the nanofluid particles, fluid stability, and erosion. There are only a few studies on the impact of using nanofluids in battery thermal management systems and the majority of these studies used numerical modeling of the thermal management system (Abdelkareem, et al., 2022).

Literature and testing results have a mixed view on the potential of nanofluids in EV's thermal management. Testing results from Tung et al. (2020) claim high potential and high thermal conductivity for application in EV's, however other literature finds significant practical disadvantages of nanofluids for thermal management. Lee & Mudawar (2007) also assessed the effectiveness of nanofluids in both single-phase and two-phase heat transfer. Despite the

enhancement in heat transfer coefficient in some flow regions, the overall cooling effectiveness appeared to be very small as there was a large axial temperature rise compared to a regular fluid. Tete et al. (2021) has similar findings and found that while the addition of nanofluids increases the thermal conductivity of the base fluid, the cooling efficiency is not increased significantly.
For two-phase heat transfer, catastrophic failure was found as the nanofluid deposited into large clusters due to localized evaporation (Lee & Mudawar, 2007). However, the study of Lee & Mudawar is done in microchannels and therefore the disadvantages might be less when using larger sized channels.

2.4.5 Degradation

Over time and under certain conditions, thermal fluids can degrade, resulting in a deterioration of their thermal properties.
A consequence of thermal fluid degradation can be corrosion to the components of a thermal management system. An example is the fact that glycols such as ethylene-glycol are susceptible to thermal oxidative reactions (Clifton, et al., 1985). Consequently, heating of the fluid will slowly degrade the solution and decreases the pH of the solution due to acidic by-products (mainly carboxylic acids), resulting in corrosion and foaming problems (Madera, et al., 2003) (Ranjbar & Abasi, 2013). Therefore, it is important that there is a possibility for fluid replacement and monitoring when designing a thermal management system.
Buffers known as corrosion inhibitors can be added to the solution to mitigate decreasing pH, however, corrosive conditions can still develop if the liquids are not rebuffered or replaced regularly, as the buffers are gradually being consumed (Clifton, et al., 1985). To quantify the speed of depletion of the corrosion inhibitors, Madera et al. (2003) studied the degradation products of ethylene glycol using chromatography. It was found that a nitrite-based inhibitor (added for corrosion protection) depleted in 1 month from 300 ppm to 10 ppm. However, the heat exchanger system used in the study had a hot- and cold side temperature of 110 ˚C and 70 ˚C respectively, which might be higher temperatures (and thus faster degradation) than most battery thermal management systems encounter.
Another corrosion mitigation option might be implementing a higher concentration ethylene-glycol when using ethylene-glycol/water mixtures, as Danaee et al. (2012) studied the corrosion behavior of ethylene-glycol/water mixtures on steel alloy and found that corrosion rate was decreased with increasing concentrations of ethylene glycol.

2.5 Battery Thermal Modeling Efforts

Preceding the design of a thermal management system, it is essential to determine the heat generation of a battery in response to specific current loads. While the heat generation rate is related to batteries' characteristics and heat generation rate changes as electric current changes, a battery electro-thermal model can be used to evaluate battery heat generation in a range of conditions. These outcomes can then be used as an input for the design of a thermal management system.

Extensive research has been conducted on the subject of heat generation of lithium-ion batteries.
Zadeh et al. (2022) described that two main method categories exist for determining battery heat generation, which are experimentally by using calibration calorimetry, and by using

numerical methods. Wang et al. (2016) reviewed studies that used a heat generation method. These methods included using experimental data, accelerated rate calorimetry, and using open-circuit potential.
During calorimetry, an accelerating rate calorimeter (ARC) is used which measures the cell material thermal response to increasing temperature in an adiabatic environment (Doughty, et al., 2002) (Eddahech, et al., 2013). This means no heat is lost to the surroundings during experiments and is therefore an effective method for determining the heat generation process in a battery. Determining battery heat generation from the caloric method also requires cell parameters such as dimensions, materials, heat capacity, and thermal conductivity (Doughty, et al., 2002).
The majority of Li-ion heat generation studies used calorimetry methods with the objective to characterize the thermal behavior of the battery cells and obtain heat generation values (Sabbah, et al., 2008) (Eddahech, et al., 2013).

In addition to caloric methods, numerical methods exist. As part of the development of a thermal management system, a model based on numerical methods can be made to predict the behavior and response of the designed system in various conditions. Scholars have used various modeling relations for their thermal modelling work, including equivalent circuit models, Reduced-Order Models (ROM), thermal resistance models, lumped capacitance thermal models, and electrochemical models (Tete, et al., 2021) (Gan, et al., 2020). Zadeh et al. (2022) also reviewed numerical modelling studies on batteries and their heat generation, which are electrochemical, electro-thermal, and lumped thermal models. Electrochemical-thermal coupled models have been used extensively and primarily at cell level and are effective in gaining understanding of battery operation (Nieto, et al., 2014).

For batteries in EVs, electro-thermal models are often used due to their relatively low complexity and less detailed required battery data. Figure 5 showcases an example of an electrical model, a thermal model, and the integrated electro-thermal model, as described by Chen et al. (2020), which are further described in chapter 2.5.1 and 2.5.2. An electro-thermal model consists of 2 parts: an electrical/electrochemical model, and a thermal model.
When combining an electrical model and a thermal model, the resulting electro-thermal model can be either coupled or uncoupled (Wang, et al., 2016). In coupled electro-thermal models, the electrical and thermal model are interconnected. Changes in electrical behavior of the system will influence the thermal behavior and vice versa. In an uncoupled model, the models are not interconnected, and the electrical behavior of the system has no effect on the heat generation rate in the thermal model and uses a fixed heat generation rate.

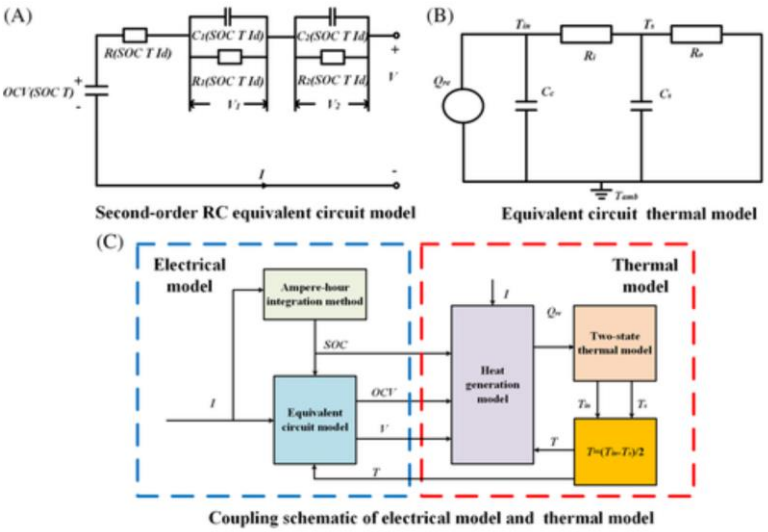

Figure 5: Schematic of (A) equivalent circuit model, (B) thermal model, (C) electro-thermal model. Adapted from (Chen, Hu, Cao, et al. 2020)

Literature reports various simulation studies that have been done for air- and liquid cooling systems based on electro-thermal models, using commercial computational fluid software such as MATLAB Simulink, ANSYS Fluent, and COMSOL Multiphysics (Tete, et al., 2021).
An example of this is Vikram et al. (2022) who developed an electro-thermal model in MATLAB Simulink to model an EV battery pack and a thermal management system consisting of cooling plates.
While the models can prove to be very valuable for describing system behavior, Nieto et al. (2014) mention that previous work on modeling and numerical simulations of thermal management systems had limited experimental validation, which restricted the model's reliability. Therefore, the reliability of the models should be taken into consideration when utilizing or developing models.

2.5.1 Electrical model

An electrical model is tool that simulates the electrical behaviour of a battery during its operation. A type of numerical model that is classified as an electrical model is an equivalent circuit model (ECM). An ECM is an electrochemical analogy which aims to describe a battery cell's behaviour in response to a certain current load. The analogy consists of an electrical circuit which includes voltage sources, resistances, and capacitors.
Equivalent circuit models can be used to obtain the electrical current and potential and are used to estimate the heat generation term in the energy conservation equations (Effat, et al., 2016) (Wang, et al., 2016). ECMs are especially suitable for modelling at system-level and manage to capture nonlinear electrochemical phenomena while avoiding complex electrochemical process calculations (Huria, et al., 2012). Determining the characteristic parameters of an equivalent circuit can be done by parameter estimation, in which simulation results are compared with experimental data with as many iterations until equal values are found.
Examples of scholars that used ECMs for modelling Li-ion batteries in electric vehicles are Baghdadi et al. (2015), Andreev et al. (2015), and Vikram et al. (2022).
Yang et al. (2019), Madani et al. (2018), and Wang et al. (2016) defined various equivalent circuit models (ECM) that are typically used for batteries in electric vehicles, such as the RC model, Thevenin model, PNGV (partnership for a new generation of vehicles) model, and dual polarization model.

2.5.2 Thermal model

Thermal models are developed to describe temperature profiles and temperature changes over time. A battery thermal model takes into account heat generation, heat accumulation, conduction and convection (Wang, et al., 2016).
Scholars highlighted that the equations of a battery thermal model should always be based on (Rao & Wang, 2011):

- The energy balance equation
- The heat generation equation (simplified or complex)
- The boundary condition equation (linear/non-linear, conductive/convective/radiated)

Iraola et al. (2013) distinguished analytical models and behavioural models for thermal modelling of battery cells. Analytical models solve the battery's energy balance differential equations, such as done in finite element analysis. On the other hand, behavioural models can predict battery cell temperatures by using equivalent circuit models.

For thermal modelling of batteries, a lumped thermal model is often used as an analytical method (Wang, et al., 2016). If a battery is assumed to be a lumped body, it is assumed that the temperature of the battery is uniformly distributed in all directions at all times during transient heat transfer.
The validity of the assumption of uniform temperature in a battery cell is done through the dimensionless Biot number. The Biot number describes the ratio of heat transfer by convection on the outside of a body and the heat transfer on the inside of the body by conduction (Ismail, et al., 2013). The lumped thermal model applies when the dimensionless Biot number is much smaller than 1:

$$Bi = \frac{h_c L}{\lambda} \ll 1 \tag{2.3}$$

Where λ is the thermal conductivity of the object, h_c the convective heat transfer coefficient at the surface of the object, and L the characteristic length of the object.

The Biot number is often much smaller than 1 when battery cells have a small thickness. A small Biot number implies that transfer of heat inside the object takes place much faster than the transfer of heat at the surface of the object.

If the uniform temperature assumption is valid, heat transfer inside a battery cell using a lumped thermal model can be written as the following equation:

$$\frac{d(\rho * c_p * T)}{dt} = h_c * A_s * (T - T_\infty) + q \tag{2.4}$$

In the lumped thermal model, heat accumulation, convective heat transfer, and heat generation are balanced.
Therefore, it can be written in the form:

$$m * c_p \frac{dT}{dt} = Q_{irrev} + Q_{rev} + Q_{conv} \tag{2.5}$$

A multitude of studies such as Bai et al. (2019), Mahamud & Park (2011), Liu et al. (2017), Liu et al. (2021), and Sato (2001) investigated heat generation in a battery cell, which consists of the terms Q_{irrev} and Q_{rev} that represent the irreversible heat generation and reversible heat generation respectively in a battery cell.
The equation for internal heat generation in a battery cell used in all of these studies is derived from Bernardi et al. (1984), which created the following relation:

$$q = I(U_{OC} - V) - I\left(T\frac{dU_{OC}}{dT}\right) \tag{2.6}$$

The first term in the equation represents the Joule/Ohmic heating as a result of a battery's internal resistance (irreversible heat), and the second term represents the heating from entropy changes that occur in the battery (reversible heat).
The equation can be rewritten and expressed in the equivalent internal resistance R_i as done by Ma et al. (2010) in the form:

$$q = I^2 * R_i - I\left(T\frac{dU_{OC}}{dT}\right) \tag{2.7}$$

The heat generation model described by Liu et al. (2021) that utilized this Bernardi equation was found to describe a battery heat generation rate with a high accuracy of 7% and was found to be valid for prediction of heat generation in battery packs in practice.

When implementing the equation for battery heat generation in the heat balance equation described earlier in this section, a new rewritten form of the heat balance equation is created. For modeling heat transfer inside an EV battery cell, Ismail et al. (2013) used this rewritten equation which is:

$$m_{cell} * c_{cell} * \frac{dT_{cell}}{dt} = I^2R + T_{cell}\,\Delta S\frac{I}{nF} + Ah_c(T_{cell} - T_{amb}) \tag{2.8}$$

Where the first term on the right side of the equal sign represents the irreversible heat generation in the battery, the second term represents the reversible heat, and the third term represents the heat convection to the batteries' surroundings.

2.6 Conclusion

In conclusion, the literature review highlighted key findings of research conducted in the field of thermal management systems. Overall, the literature review provided a comprehensive overview of the current state of knowledge in the field and demonstrated the importance of having a well-designed thermal management system in an electric vehicle, especially in demanding conditions.

Key findings addressed in the literature review are the high demand for reduced charging times, in order to keep the Total Cost of Ownership (TCO) for medium- and heavy-duty electric vehicles as low as possible. Furthermore, the literature review found which physical phenomena cause Li-ion battery heat generation and found which battery temperature range is optimal according to scholars.

The literature highlighted that a large number of studies have investigated the various thermal management types and their performance. HVAC systems can be integrated with the battery thermal management system, and heating of the battery can be done by pulse heating. Furthermore, it was found that the use of certain heat transfer fluids is limited to certain types of thermal management. Lastly, the literature review created an overview of the electro-thermal modeling that can be used for describing the behavior of batteries under various conditions.

The literature review also identified the existing knowledge gaps in literature. While it has been found that various thermal management types are used in various EV models over several years, it remains unknown which type of battery thermal management system would fit best to the requirements and objectives of medium- and heavy-duty electric vehicles in demanding conditions such as Megawatt Charging. Furthermore, there is a lack of experiments or models that describe how such a thermal management system behaves in medium- and heavy-duty electric vehicles under various conditions, as the implementation of these vehicles is still in a very early phase.

A scientific contribution containing the information of how to design a thermal management system for medium- and heavy-duty electric vehicles utilizing Megawatt Charging Systems will be very valuable for the mobility sector, energy industry, and the academic sector. The literature review set the foundation for the research that will be conducted in this study, providing a framework for identifying research questions, selecting appropriate research methods, and contributing to the advancement of knowledge in the field.

3

Research Methodology

As it is currently unknown which type of battery thermal management system will fit best to the requirements and objectives of medium- and heavy-duty electric vehicles in the demanding conditions of Megawatt Charging and how such a system should be designed, the objective of this study is to describe how the battery thermal management system should be designed for MHDEV's utilizing Megawatt Charging and explore which design is optimal. The design methodology does not only aid in deciding which battery thermal management strategy from existing methods is most optimal, but also aids in assessment of novel battery thermal management strategies.

The main research question and sub-research questions addressed in this study are therefore formulated as follows:
How should the battery thermal management system be designed for medium- and heavy-duty electric vehicles utilizing Megawatt Charging Systems (MCS)?

SRQ1: *What are the specific requirements for a MHDEV BTMS?*
SRQ2: *What is the battery heat generation quantity for Megawatt charging MHDEV's based on typical battery specifications?*
SRQ3: *Which BTMS strategy and heat transfer medium is most advantageous for Megawatt Charging MHDEV's?*
SRQ4: *What is an optimal configuration of the BTMS components and what should the dimensions be?*
SRQ5: *How does the BTMS design affect driving range of MHDEV's?*

This chapter outlines the research process, tools, and techniques utilized during the study.
The study utilizes a system engineering approach to design, create, and operate a thermal management system for medium- and heavy-duty electric vehicles. This approach as described by Ramadesigan et al. (2012) consists of the identification and quantification of system objectives, creation of system design concepts, evaluation of design trade-offs, selection and implementation of design, verification of design, and post-implementation assessment to test whether the system meets the set objectives.

For the high-level design of the BTMS, methodological steps obtained from Pesaran (2001) and Pesaran et al. (1999) as earlier described in chapter 2.2.3 in the literature review of this study, are employed in this study. However, the step of predicting detailed battery module and

pack temperature behavior before designing a preliminary BTMS is omitted, as computational fluid dynamics (CFD) and finite element analysis (FEA) is required for this step that aims to enhance optimization of the BTMS.
An overview of these steps utilized in this study is shown in Figure 6.

Figure 6: High-level overview of the methodology used in this study

A more detailed explanation of the methodology used in each section of the study is described in chapters 3.1-3.6.

3.1 BTMS requirements

3.1.1 Battery- and operating temperature requirements

To be able to assess various battery thermal management system options and propose one for the application of Megawatt charging, determining the system's requirements is a crucial part. One of the main requirements is to meet the temperature objective of the system. The temperature objective in this study for any given BTMS is based on literature findings, and is used for calculations and modelling in this study.
Literature previously analyzed in this study indicated an optimal battery temperature in the range of 15-35 ℃. Therefore, the objective of the BTMS strategy assessment and subsequent proposed design is also set to maintain the battery temperature in this temperature range.
If it appears unavoidable that this optimal temperature range is slightly exceeded for a short duration, for example during startup of the cooling system, the consequences for the battery health might be limited. However, as the lithium-ion onset temperature of self-heating is about 90 ℃, another requirement is that the battery temperature should never reach this temperature, as exothermic reactions in the battery are then taking place at an increased rate and battery heat generation increases (Mao, et al., 2020).
Furthermore, the requirement of a less than 5 ℃ temperature difference between any two battery cells in the pack is used in this study, which ensures sufficient battery pack temperature uniformity (Mahamud & Park, 2011) (Park & Jaura, 2003) (Rao, et al., 2017).

In addition to the battery temperature requirements, the ambient temperatures under which the vehicles operate play an important role which adds requirements to the BTMS to be designed. The required battery thermal management system ambient temperature operating range selected for this study is from -10 ℃ to 40 ℃.
The motivation for this is as follows. For the BTMS, it is a requirement that the system is able to operate in a various range of locations and conditions. For this reason, some typical locations of MHDEV's have been analyzed to gain an understanding of the temperatures the system will face.
While it is known that trucks and buses operate almost everywhere around the globe, mining sites and thus the location of operation of mining haul trucks is also very widespread. When analyzing the location data of mines, Figure 21 in Appendix I indicates that the locations are widespread over the globe and spatial agglomeration can be seen in certain areas. When

assuming future electric mining trucks will be operating and charging at the locations of the mines highlighted in the figure, it is understandable that the temperatures that an electric mining truck and its BTMS face can become extreme. Furthermore, Figure 22 in Appendix I illustrates current stop locations of trucks in Europe. Assuming current and future electric trucks will mostly be charging at these locations as well, it can be concluded that most activity is around densely populated areas, however, very widespread and facing various climates. Taking into account the operations of electric trucks in other parts around the globe, the temperature conditions can take even more extreme shapes.
To summarize; to be able to operate the MHDEV's and their BTMS, the BTMS has to be designed for a wide temperature operating range.

Furthermore, additional requirements exist that relate to the practical considerations of a BTMS and will be used for the assessment of various BTMS'. This is described in further detail in chapter 3.3.

3.1.2 Battery requirements

Another requirement that dictates the BTMS design is the required battery pack capacity in kWh, as the battery capacity required influences the number of battery cells and the battery heat generation. To determine which battery pack capacity would be required for a typical MHDEV, a database from organization CALSTART with medium- and heavy-duty electric vehicles has been analyzed (CALSTART, 2023). The database contains 856 medium- and heavy-duty vehicle models, with over 90% of the vehicles in the database being electric. All vehicles have a market introduction anywhere between 2016 and 2023. Based on the range of energy capacity values, a value of 500 kWh is used in the study as a requirement for the battery.

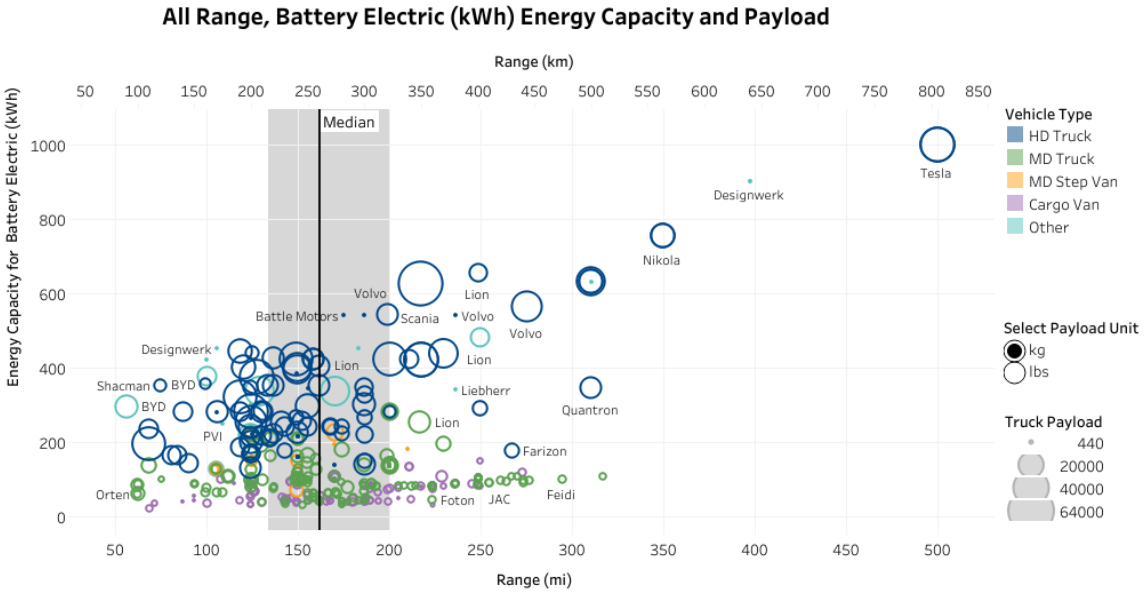

Figure 7: Electric truck data (CALSTART, 2023)

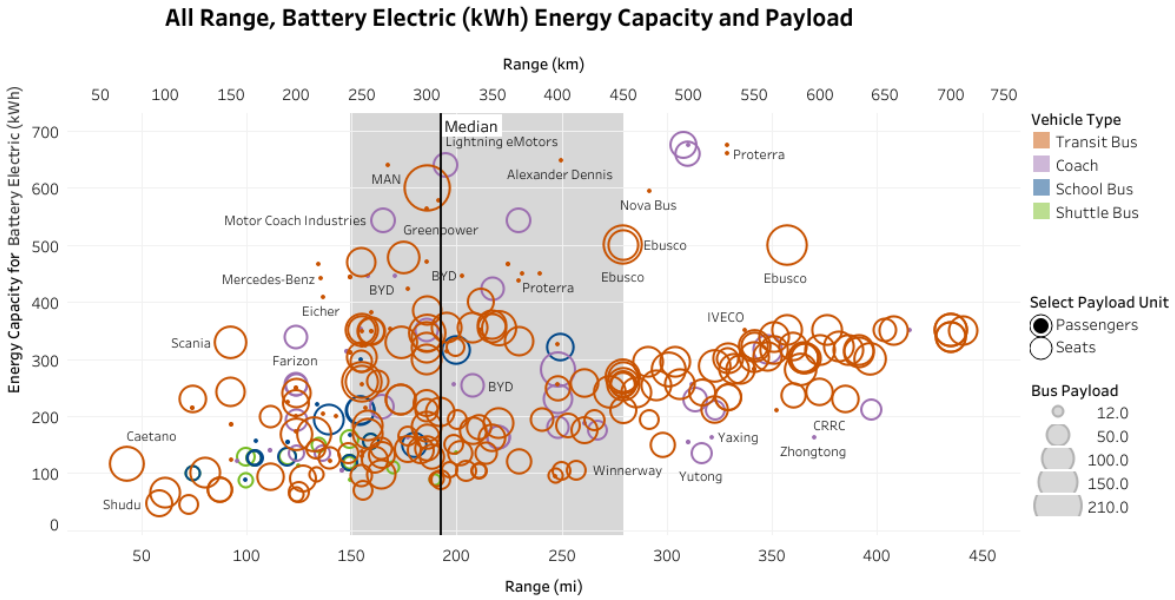

Figure 8: Electric bus data (CALSTART, 2023)

3.2 Battery heat generation

3.2.1 Battery cell selection and pack configuration

In order to model the battery pack and its heat generation, a battery cell type has to be selected. To ensure that the results of the study are as generalizable as possible, criteria for battery selection are that the chemistry, cell type, and capacity, is typical for most batteries. To assess this aspect, an analysis has been done on a large dataset originating from the 'BetterBat' research project, which is a battery research project done by the German Fraunhofer institute and partners (Fraunhofer, 2023). The dataset contains 393 different batteries from various manufactures with a wide range of specifications. The information from this dataset indicated an NMC/NCA chemistry, less than 10Ah capacity, and pouch or prismatic cell type, are the most frequently found. The study therefore utilized a battery that falls in these categories.

Aside from cell chemistry, type, and capacity, more detailed battery cell specifications are typically proprietary data and therefore difficult to obtain. This limits the choice of battery cells to study. In order to investigate a battery's specifications including cell capacity, internal resistance, nominal voltage, and dimensions, the set of battery cell models available in MATLAB Simulink has been assessed which are shown in Appendix II. The battery cell model chosen for the study's calculations is the cell model with the highest energy density in mAh/g from the cells that met the typical battery capacity, chemistry, and cell type found in the 'BetterBat' database. This cell is the Panasonic NCA 973450 battery, whose specifications are shown in Table 3 and Appendix III.

Variable	Quantity
Capacity	1515 mAh
Nominal Voltage	3.6 V
Weight	24.7 g
Dimensions	40.25 x 35.1 x 7.95 mm

Table 3: Specifications of Panasonic NCA 793450

Other battery-related parameters used for the study include the charging specifications. A charging rate of 4.5 MW at 1500 V and 3000 A is used in the study for modeling the rate at which the battery is charged, as this is the upper limit of the MCS SAE J3271 and ISO 5474-3 charging rate standards under development (SAE, 2021) (CharIN, 2022) (Meintz, et al., 2021) (Bohn, 2020).
Based on the MCS voltage specification, the nominal voltage of the battery pack model utilized in the study is also set at 1500 V. The total number of battery cells required in the battery pack, the number of battery groups in series, and groups in parallel, have been calculated based on the previously mentioned battery capacity and power specifications.

The number of battery cells required in series is defined as:

$$\#\ series\ groups = \frac{V_{total}}{V_{cell}} \tag{3.1}$$

- Where V_{total} is the total voltage of the pack which is 1500 Volt
- V_{cell} is the cell voltage specified in Appendix III

The number of parallel groups are defined as:

$$\#\ parallel\ groups = C_{pack} * \frac{1000}{V_{total}} * \frac{1}{A_{h_{cell}}} \tag{3.2}$$

- Where C_{pack} is the energy capacity of the battery pack which is 500 kWh
- $A_{h_{cell}}$ is the Amp-hour rating of the battery cell as specified in Appendix III

Multiplication of the groups gives the number of cells required:

$$n_{cellls} = \#\ series\ groups * \#\ parallel\ groups \tag{3.3}$$

- Where n_{cells} is the required number of cells in the battery pack

The number of cells in the pack are then used to determine the total weight of the cells:

$$total\ pack\ weight = n_{cells} * m_{cell} \tag{3.4}$$

- Where m_{cell} is the mass of the battery cell as specified in Appendix III

3.2.2 Quantification of battery heat generation

Modelling the heat generation in the battery is important as it dictates the required heat duty of the BTMS.
The study considers irreversible heat generation by Ohmic heating and does not include the heat generation phenomena resulting from reversible heat, as at high C-rates irreversible heat generation is the dominating heat generating phenomenon (Nazari & Farhad, 2017) (Jeon & Baek, 2011) (Ye, et al., 2012) (Liu, et al., 2021).

To determine the quantity of heat generation in the battery cells, a MATLAB calculation tool is used. The specifications of the selected battery are given to the model, as well as the charging rate specifications and configuration of the battery cells. For determining the heat generation in a single cell, the current and voltage applied to each single cell is determined. The current through each cell is calculated by dividing the total battery pack current of 3000 A by the number of parallel battery groups. The voltage through each cell is calculated by dividing the total battery pack voltage of 1500 V by the number of series battery groups.
The heat generation for each cell is then calculated with the following equation:

$$\dot{Q}_{cell} = I_{cell}^2 * R_{cell} \tag{3.5}$$

- Where $\dot{Q}_{cell}$ is the heat generation rate of a single battery cell in W.
- I_{cell} represents the current flowing through a single cell in Amps. This cell current should not be confused with the total battery pack current.
- R_{cell} is the internal resistance of the battery cell in Ohm.

The total heat generation rate in the battery pack is then calculated using the Ohmic heating equation again and multiplying by the number of cells in the battery pack:

$$\dot{Q}_{pack} = I_{cell}^2 * R_{cell} * n_{cells} \tag{3.6}$$

While the heat generation can fluctuate in practice as a result of the internal resistance dependence on battery temperature and State of Charge (SOC), quantification of battery heat generation in this stage of the study is performed at a fixed internal resistance.
For the internal resistance of the battery cells, a value of 0.02 Ohm has been adopted in the study, as that has been found typical and in the right order of magnitude for Li-ion battery cells (Ismail, et al., 2013) (Novak, 2013) (Culcu, et al., 2009) (Razi, et al., 2022) (Schindler, et al., 2021) (Steger, et al., 2022).

3.3 Assessment BTMS strategies & heat transfer media

The BTMS strategies assessed in the study are forced air cooling, forced immersion cooling, cooling plates with coolant, cooling plates with refrigerant, and phase-change materials (PCM). The motivation of this choice is the history of these thermal management strategies for various applications including battery thermal management, while still offering enough novelty as some of the strategies have not been implemented commercially in an electric vehicle before. Furthermore, the chosen BTMS strategies offer sufficient technological maturity to be able to thoroughly assess the feasibility of each strategy for Megawatt charging for MHDEV's.

For immersion cooling, the properties of Shell Immersion Cooling Fluid S5 X have been used for the calculations. The motivation for selecting the immersion cooling fluid is for its advantage of being dielectric and therefore being able to submerge battery cells in the fluid. For cooling plates with a coolant, the coolant water ethylene glycol (WEG) in a 70/30%

volumetric ratio from the brand Dowtherm SR-1 has been selected. The motivation for selecting this coolant is that water has some of the best thermal properties, however, the addition of some ethylene-glycol is needed to reduce the mixture's freezing point and to avoid bacterial growth.
For the use of refrigerants in the BTMS, an investigation of the thermophysical properties of refrigerants R134a, R1234yf, and R717 has been conducted. R134a and R1234yf are known for their use in automotive- and battery thermal management and therefore included in the study, and R717 is included as it has a very high heat of vaporization which is indicated in Appendix VI. The properties of the refrigerants and their logarithmic pressure-enthalpy (log-ph) diagrams have been retrieved through software Coolselector 2. As evaporation and condensing temperature, temperatures of -10 ℃ and 40 ℃ respectively have been used for modelling the refrigeration cycle.

The heat transfer medium used must be able to absorb all generated battery heat, as pointed out in the literature review (Sundin & Sponholtz, 2020), which is implemented in the calculations for BTMS assessment by equating the battery heat generation and the heat removal by the heat transfer medium.

The first part of this section of the study's approach is assessing whether each battery cell can be modelled as having a uniform temperature, known as a 'lumped capacitance model'. This is described in chapter 3.3.1. If the lumped capacitance condition is not satisfied, the temperature gradient through a battery cell is calculated based on its maximum allowable temperature of 35 ℃, its internal heat generation rate, and its thermal conductivity in each direction. This enables determining the maximum allowable battery cell surface temperature which is the input for calculations for the BTMS strategies.

Subsequent to the battery temperature gradient assessment, two assessment stages are proposed to assess the feasibility of various BTMS', where both assessment stages have to be completed before successful implementation of the BTMS strategy in the MHDEV can take place:

1. Assessment of BTMS required heat transfer area: based on convective heat transfer coefficient and heat transfer medium temperature.
2. Assessment of BTMS required heat transfer medium mass flow rate: based on heat transfer medium's specific heat and allowable heat transfer medium temperature increase.

These assessments are used to investigate which design requirements are needed when implementing each of the BTMS strategies in a MHDEV.

3.3.1 Lumped capacitance validation and battery temperature gradient

Lumped capacitance validation
As the maximum allowable battery temperature is 35 ℃ and occurs at the core of the battery cells during cooling, the dimensionless Biot number is determined to validate whether the assumption of a uniform temperature through the battery cells is valid and if a lumped capacitance model can be used to represent each battery cell.

The Biot number describes the ratio of heat transfer by convection on the outside of a body and the heat transfer on the inside of the body by conduction (Ismail, et al., 2013). The lumped thermal model applies when the dimensionless Biot number is significantly smaller than 1:

$$Bi = \frac{h_c L_{cell}}{\lambda} \ll 1 \tag{3.7}$$

- Where λ is the thermal conductivity of the object in W/mK
- h_c is the convective heat transfer coefficient at the surface of the object W/m^2K
- L_{cell} is the characteristic length of the object, which is the volume of the battery divided by its total surface area in m

In this study, the assumption of a uniform cell temperature is seen as validated when $Bi < 0.1$. When this condition is met, the temperature at the surface of the battery cell will then not differ more than 5% from the temperature at the core of the battery (Mills, 2014).

The Biot equation is determined for two cases in this study: For battery cell in-plane heat transfer, and for cross-plane heat transfer. For both cases, it is determined what the maximum convective heat transfer coefficient is while still meeting the condition of $Bi < 0.1$. This gives insight for which BTMS methods, if for any, the lumped capacitance model can be used.

The variables used are:

	In-plane	Cross-plane
Bi	0.1	0.1
λ	20	0.5
L_{cell}	0.0056	0.0056

Table 4: Overview of values used for battery cell thermal properties

The thermal conductivities selected for the study are based on literature findings that indicated a range of 20-30 W/mK for in-plane conductivity, and a significantly lower range of 0.14 -1.40 W/mK for cross-plane conductivity (Zeng, et al., 2021).

Battery cell temperature gradient

In the case the heat transfer through in-plane or cross-plane does not meet the Biot number criteria and the lumped capacitance model assumption, the battery cell temperature gradient is calculated.

For this approach it is assumed that the battery length ranges from x = -L to x = L, where L represents half of the total length of the battery cell dimension through which the thermal conduction takes place. Furthermore, it is assumed that steady-state heat transfer occurs, that the thermal conductivity of the battery cell λ is constant and that the volumetric internal heat generation of the battery cell $\dot{Q}_v$ in W/m^3 is uniform within the battery.

The temperature profile is determined by utilizing the heat equation:

$$\frac{d}{dx}\left(\lambda\frac{dT}{dx}\right)+\dot{Q}_v=0 \tag{3.8}$$

$$\frac{d^2T}{dx^2}+\frac{\dot{Q}_v}{\lambda}=0 \tag{3.9}$$

Where $\dot{Q}_v$ is the battery cell internal heat generation in W/m^3
The value of $\dot{Q}_v$ is determined by dividing the heat generation of a single battery cell by its cell volume, based on the dimensions given in Appendix III.

The general solution to the heat equation is:

$$T(x)=-\frac{\dot{Q}_v}{2\lambda}x^2+C_1x+C_2 \tag{3.10}$$

Differentiating once gives:

$$\frac{dT}{dx}=\frac{\dot{Q}_vx}{\lambda}+C_1 \tag{3.11}$$

The first boundary condition applied is a Neumann boundary condition:

$$\frac{dT}{dx}\Big|_{x\,=\,0}=0$$

This boundary condition is chosen as the temperature is at maximum at the core of the battery cell and therefore, the temperature gradient at that location is equal to zero.

Implementing this in equation 3.11 results in $C_1=0$

Applying a Dirichlet boundary condition as the second boundary condition:

$$T(\pm L)=T_s$$

Filling in into equation 3.10 gives:

$$T(L)=-\frac{\dot{Q}_v}{2\lambda}L^2+C_2=T_s \tag{3.12}$$

Solving C_2 gives:

$$C_2=T_s+\frac{\dot{Q}_v}{2\lambda}L^2 \tag{3.13}$$

The final equation for the temperature distribution then becomes:

$$T(x)=T_s+(\frac{\dot{Q}_v}{2\lambda})(L^2-x^2) \tag{3.14}$$

This temperature distribution equation based on a 1-dimensional approach is applied to the battery in both of its in-plane configurations, as well as its cross-plane configuration, to determine the temperature gradients encountered in each direction. $\dot{Q}_v$ is determined by

dividing the heat generation rate of a battery cell by its volume, based on the dimensions given in Appendix III.

3.3.2 Assessment 1

For the first assessment, the required total battery cell surface area is determined for various BTMS targeting possibilities. The targeting possibilities refer to which surfaces of a battery cell are subject to heat transfer from a BTMS.

First, the heat transfer coefficients ranges have been obtained from literature and are shown in Figure 9. These ranges have been used to determine a typical heat transfer coefficient value for each BTMS strategy.

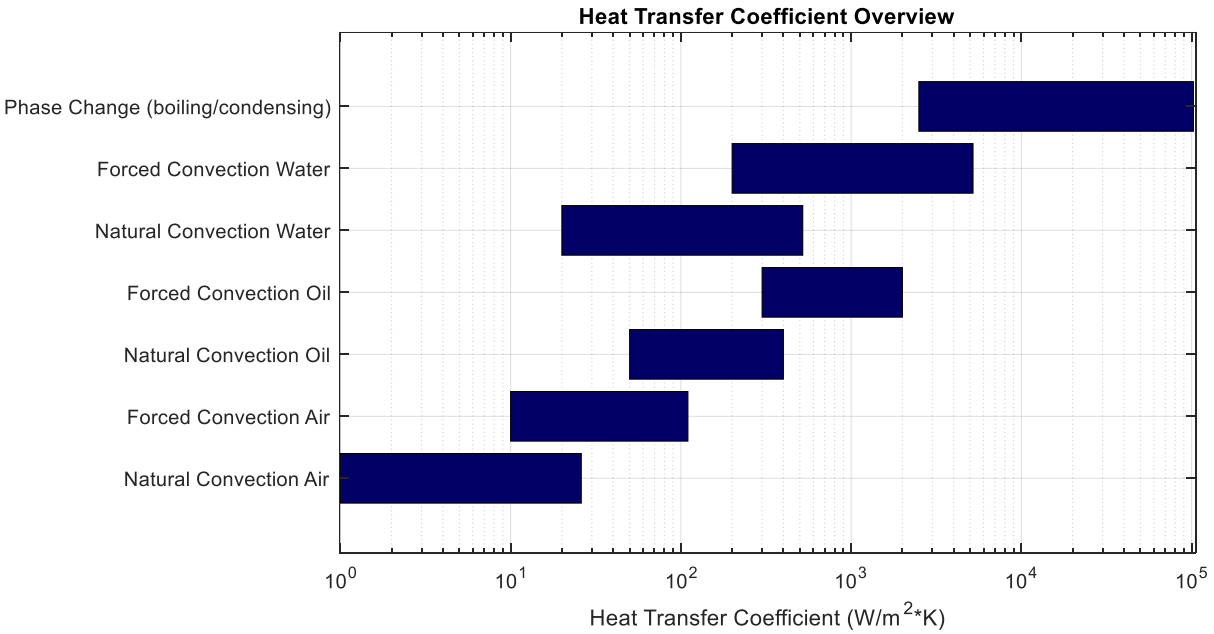

Figure 9: Overview of cooling strategy heat transfer coefficient for convection (Aamir, et al., 2016) (Sridhar, 2013) (Vargas, et al., 2018) (Moran, et al., 2012)

The selected heat transfer coefficient for convection for each BTMS assessed in the study is shown in Table 5.

BTMS strategy	Heat transfer coefficient value used $[W/m^2K]$
Forced air cooling	100
Forced immersion cooling	500
Cooling plates with coolant	1000
Cooling plates with refrigerant	4000

Table 5: Overview of heat transfer coefficient values used in the study

For each BTMS strategy, the heat transfer surface area required is determined using Newton's law of cooling:

$$\dot{Q}_{pack} = \dot{Q}_{abs} = h_c * A * \Delta T \quad (3.15)$$

- Where $\dot{Q}_{pack}$ is the heat generated per unit time by all battery cells in W
- $\dot{Q}_{abs}$ is the heat per unit time in W that is absorbed by the heat transfer medium
- h_c is the heat transfer coefficient for convection for the specific BTMS strategy
- A is the surface area at which the convective heat transfer takes place

- ΔT is the temperature difference between the battery surface and the heat transfer medium

Which is then rewritten in the form:

$$A = \frac{\dot{Q}_{abs}}{h_c \, \Delta T} \tag{3.16}$$

For each BTMS strategy, the process is done for a heat transfer medium temperature ranging from 0 °C to 20 °C. The motivation for these heat transfer medium temperatures is to investigate the outcome over a range of possible heat transfer medium temperatures, that at the same time seem achievable from a practical perspective as well as providing a sufficiently low temperature to the battery cells.

Subsequently, the resulting required heat transfer area is compared with the available surface area in the battery pack. An overview of these surface areas is given in Table 6. For air cooling and immersion cooling it is assumed that heat transfer by convection takes place at the four sides of each battery cell. The top and the bottom of each battery cell are assumed to not exchange heat as these could be used for mounting the battery cells to the pack casing or used for stacking battery cells.

For cooling plates with either a coolant or refrigerant, the surface at which convective heat transfer takes place is at the wall of the cooling channels in the cooling plate, and can be increased by e.g. increasing the number of channels. Therefore, this table which is part of the verification whether the required surface area is already available in the battery pack only applies to air cooling and immersion cooling.

Heat-exchanging surface area available	Quantity [m^2]
All surface area available	369.13
Top or bottom area	25.59
Small long side	29.36
All sides	317.93

Table 6: Overview of total battery cell surface area for various targeting modes

Lastly, by using Newton's law of cooling for the cooling plate BTMS strategies, it is assumed that the cooling plate is sufficiently thin and thermally conductive to be able to impose the condition that the cooling channel tube surface area temperature is equal to the battery cell surface temperature. This is validated by determining the temperature gradient through the cooling plate by using Fourier's law, which is shown in Appendix XI.

3.3.3 Assessment 2

The methods in the previous assessment stage assumed a constant heat transfer medium temperature at every location in the battery pack. However, in practice, the heat transfer medium increases in temperature between its battery pack inlet and outlet which reduces the BTMS effectiveness at the battery cells closer to the outlet. In this assessment of required mass flow, the maximum allowable heat transfer medium temperature increase is taken into account, which is 5 °C. The motivation for this is as follows.

In this study it is assumed that the heat transfer coefficient and surface area stay constant while each BTMS thermal medium flows along the battery cells, and that the battery internal heat generation stays constant, while the heat transfer medium increases in temperature. Therefore, Newton's cooling law states that the temperature difference between the heat transfer medium and the battery surface area stays constant. This means that in a scenario where a heat transfer medium increases 10 ℃ in temperature after absorbing a fraction of the total battery heat, the battery cells that come into contact with this temperature-elevated heat transfer medium reach a surface temperature of 10 ℃ higher as well once in steady-state, compared to battery cells with the colder heat transfer medium.
Therefore, when utilizing a heat transfer medium with an inlet temperature close to the battery surface temperature and designing the thermal management system to maintain the battery cell surface temperature at its maximum allowed temperature, it is evident that the maximum allowed cell surface temperature and thus the cell core temperature will be exceeded at some places in the battery pack, as the BTMS strategy loses its effectiveness when increasing in temperature.

To counteract this unavoidable effect with any sensible type of heat transfer medium, the heat transfer medium inlet temperature has to be lowered. A temperature increase in the heat transfer medium still results in a battery surface temperature increase, however, this can be designed such that the cells remain in the optimal temperature range of 15-35 ℃.
Based on the requirement that the temperature variation between any two battery cells may not differ more than 5 ℃, the temperature increase of the BTMS strategies in this step are modelled for a temperature increase of 5 ℃, to avoid larger temperature differences in the battery pack. The maximum allowable outlet temperature of any BTMS strategy is dictated by the maximum allowable battery surface temperature. In the case that a lumped capacitance model is valid based on section 3.4.1, this temperature is at 35 ℃, however, when there are significant temperature gradients found than this temperature gradient lowers the maximum allowed cell surface temperature with the found value below 35 ℃.

In addition to heat transfer media temperature increments while travelling across the battery cells, there can also be heat transfer media temperature increments over time. Therefore, another critical aspect in the design of the thermal management system is ensuring the heat transfer medium used is able to reject its absorbed heat to be able to sustain longer periods of heat transfer. This is included in chapter 3.4.

The required mass flow rate for each BTMS is determined through the following approach.
Based on the first law of thermodynamics, the energy conservation principle is given as (Mills, 2014):

$$\rho V c \frac{dT}{dt} = \dot{Q} + \dot{Q}_v \tag{3.17}$$

Rewriting this equation for e.g. battery cells cooled by air gives:

$$\dot{Q} = \frac{dm}{dt} * c_p * \frac{dT}{dt} = \dot{m}_{air} * c_{p_{air}} * \Delta T_{air} \tag{3.18}$$

Rewriting this enables the mass flows to be calculated:

$$\dot{m} = \frac{\dot{Q}}{c_{p_{air}} * \Delta T_{air}} \tag{3.19}$$

- Where $\dot{m}$ is the required mass flow rate of air
- $\dot{Q}$ is the heat generated per unit time by all battery cells in W
- $c_{p_{air}}$ is the specific heat capacity of air in kJ/kgK
- ΔT_{air} is the temperature increase of the air

The specific heat values c_p used in equation 3.19 for each heat transfer medium are 1.006 kJ/kgK for air, 3.633 kJ/kgK for water ethylene glycol, and 2.274 kJ/kgK for immersion coolant, as shown in Appendix VIII and described in references (Wang, et al., 2020) (Dow, 2020) (Shell, 2021).

3.4 Concept development

The objective of the concept development is to explore the required dimensions and configuration of concepts in a higher level of detail. Furthermore, contrary to the focus on heat removal from the battery cells in previous section, this section focuses on the rejection and storage of battery-generated heat from/in the heat transfer medium. One aspect is the exploration of storing the heat generated by the batteries in a phase change material, which could be feasible as the charging cycle is a discontinuous process. Another aspect included is exploring the requirements for the heat exchanger through which a refrigerant releases its heat, after which it can be circulated back to the battery pack for reuse.

To conclude, this section develops the concepts for two types of BTMS systems:

- A Thermal Energy Storage (TES) system located in the battery pack, utilizing a Phase Change Material (PCM).
- The BTMS strategy for cooling plates with refrigerant.

3.4.1 TES development

This section explores the utilization of a Thermal Energy Storage (TES) system in the battery pack. Through a TES system which refers to the storage of thermal energy, the heat generated by battery cells during a charging session can be stored in the energy storage material. The heat transfer media assessed in this study are immersion oil (Shell Immersion Cooling Fluid S5 X), paraffin PCM, and hydrated salt PCM (commercial type S27). The properties and references of these materials can be found in Table 7. The motivation for selecting paraffin and the hydrated salt as PCM is their relatively high latent heat and melting temperatures of 32 °C and 27 °C which are close to typical battery temperatures. The immersion oil is selected for comparison with PCM's.

As Megawatt charging sessions generate relatively large amounts of heat in a relatively short duration, the possibility of storing this heat could be very advantageous. Therefore, it is determined how the BTMS should be dimensioned when storing the battery-generated heat.

The first step is to determine the duration of one charging session.
During a Megawatt charging session, the theoretical power supply rate is a constant 4.5 MW. However, as charging losses occur in practice or charging power is downscaled for any reason, it is assumed for the calculation of charging time duration that the average charging rate over a charging session is 3.5 MW. Furthermore, it is assumed that during a charging session, the 500 kWh pack is charged from 20% to 80% SOC (State-of-Charge) to prevent battery damage. This means that 300 kWh will be supplied to the battery in one charging session.

The duration of one charging session is thus calculated as:

$$t_{charge} = \frac{C_{battery}}{P_{charge}} \tag{3.20}$$

- Where t_{charge} is the duration of the charging session in s
- $C_{battery}$ is the battery pack capacity that is refilled in kWh
- P_{charge} is the average charging power supplied in W

Based on the battery pack capacity of 300 kWh and the average charging power the charging time used is 308.57 seconds.

Considering the total battery heat calculated in section 3.2, the total amount of heat to be absorbed by the TES system is determined as:

$$Q_{TES} = t_{charge} * \dot{Q}_{pack} \tag{3.21}$$

- Where Q_{TES} is the required heat storage in J
- $\dot{Q}_{pack}$ is the total amount of heat generated per unit time by the battery in W

For sensible heat transfer media such as immersion oil, the required total mass is determined by:

$$m = \frac{Q_{TES}}{c_{p_{oil}} * \Delta T_{oil}} \tag{3.22}$$

- Where m is the total mass required in kg
- $c_{p_{oil}}$ is the specific heat capacity of the immersion fluid in kJ/kgK
- ΔT_{oil} is the temperature increase of the immersion fluid in K

The ΔT_{oil} used in this study is 5 °C to minimize the reduction in heat transfer between the battery cells and heat transfer fluid as the heat transfer fluid increases in temperature.

For PCMs which contain latent heat that is utilized, the total mass required is determined by:

$$m = \frac{Q_{TES}}{\lambda_{fusion}} \tag{3.23}$$

- Where λ_{fusion} is the latent heat of fusion of the PCM in kJ/kg

Table 7 provides an overview of the specific properties used the aforementioned equations.

Property	Immersion oil	Paraffin	Hydrated salt
Density	806 kg/m^3	830 kg/m^3	1530 kg/m^3
Specific heat	2274 kJ/kgK	-	-
λ_{fusion}	-	251 kJ/kg	185 kJ/kg

Table 7: Values used for TES calculations (Shell, 2021) (Agyenim, et al., 2010) (Nair, et al., 2022)

3.4.2 Active BTMS development

Heat exchanger dimensioning

This section describes the heat exchanger dimensioning requirements for the heat exchanger that has the objective of rejecting the heat absorbed by the battery refrigerant. When considering a sensible heat transfer medium this heat exchanger is typically referred to as a radiator and when considering a 2-phase heat transfer medium, it is referred to as the condenser. The motivation for development of this BMTS strategy from all BTMS strategies assessed is that refrigerants offer the highest heat transfer coefficient from the strategies assessed and are therefore expected to result in the lowest required heat transfer surface area, as well as the high latent heat that reduces required mass flow. The heat exchanger dimensioning is conducted for refrigerant R717, also known as ammonia. The full cycle is referred to as a vapor-compression refrigeration system. The vapor-compression refrigeration system modelled in the study has an evaporation temperature of -10 ℃ and a condensing temperature of 40 ℃, which have been selected to be sufficiently below battery temperature and above typical ambient temperatures respectively. Furthermore, 8 ℃ superheating and 2 ℃ subcooling is used to ensure the refrigerant is fully vaporized before compression and fully condensed before passing the expansion valve.

Prior to the design of the heat exchanger, it is required to select a heat transfer medium that acts as heat sink and will be positioned on the opposite side of the heat exchanger in contrast to the higher temperature refrigerant. This to be selected heat transfer medium is the medium that absorbs heat rejected by the battery refrigerant through the heat exchanger.
Given the outdoor operation of MHDEV's, the most practical and straightforward choice for heat transfer medium is air, as this is readily available in large quantities. Consequently, the heat exchanger dimensioning presented in this section is for an air-cooled heat exchanger. The design of this heat exchanger follows a crossflow configuration, with air flowing perpendicularly across tubes containing the battery refrigerant, as visually depicted in Figure 10.

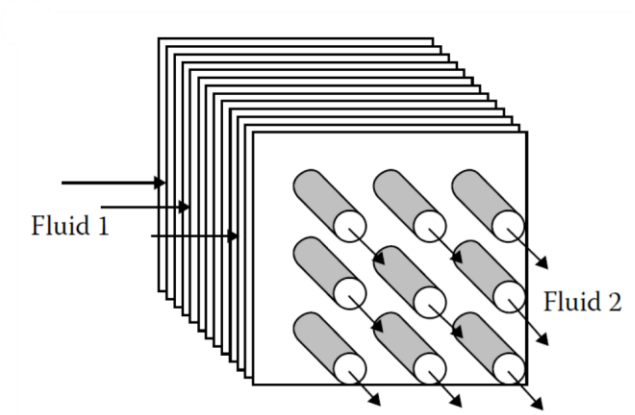

Figure 10: Crossflow heat exchanger (B. Noshirvani University of Technology, 2023)

In this step of the methodology, the overall heat transfer coefficient in a refrigerant-air heat exchanger is determined, as well as the required surface area.
First, the heat exchanger is modelled for ambient air with an inlet temperature of 15 °C and an outlet temperature of 35 °C, such that the pinch temperature difference between the refrigerant and air is 5 °C to ensure heat transfer at every point in the heat exchanger. Additionally, the dimensioning is done for an ambient air inlet temperature at -10 °C and 30 °C to investigate the requirements at different temperature extremes.

The heat transfer through the heat exchanger is calculated by the following equation (Sinnott & Towler, 2020):

$$\dot{Q}_{rej} = UAFT_{lm} \tag{3.24}$$

- $\dot{Q}_{rej}$ is the heat rejected from the battery refrigerant to the ambient air in W
- U is the overall heat transfer coefficient in W/m^2K
- Where ΔT_{lm} is the logarithmic mean temperature difference between the two fluids in the heat exchanger in K
- F is a correction factor that is specific to the type of heat exchanger.

The value for U is obtained through a coefficient table for air-cooled heat exchangers which can be found in Appendix X, where the value for U used for the ammonia-air heat exchanger in the study is 624.61 W/m^2K. However, it is expected that similar overall heat transfer coefficients exist for other refrigerants, which results in similar required heat transfer areas for other refrigerants. The effect of fouling of the heat exchanger tubes is assumed to be negligible in this study.
The variable F is a correction factor that is used as a crossflow heat exchanger is modelled, as this does not require a closed system for the air flow and air can flow perpendicular to the refrigerant pipes. Variable F is added to account for deviations counter-current flow that the equation above is representing. However, when the battery heat transfer fluid's temperate change is negligible, such as during condensation, F is simply equal to 1 (Tarawneh, 2006).
Notably, $\dot{Q}_{rej}$ is not the same value as $\dot{Q}_{pack}$ or $\dot{Q}_{abs}$ earlier mentioned in the study, as $\dot{Q}_{rej}$ includes the compressor power that is added to the refrigerant. The calculation for the compressor power is shown in the next section of this chapter.

$\dot{Q}_{rej}$ is calculated as:

$$\dot{Q}_{rej} = \dot{Q}_{abs} + W_{compressor} \tag{3.25}$$

Moreover, the logarithmic mean temperature difference is calculated as:

$$\Delta T_{lm} = \frac{\Delta T_1 - \Delta T_2}{\ln \frac{\Delta T_1}{\Delta T_2}} \tag{3.26}$$

Where ΔT_1 is the temperature difference between the air inlet and battery heat transfer medium outlet, and ΔT_2 the temperature difference between the air outlet and battery heat transfer medium inlet.

Rewriting equation 3.24 for the required surface area gives:

$$A = \frac{\dot{Q}_{rej}}{UF\Delta T_{lm}} \tag{3.27}$$

Based on the results of this required surface area, Appendix XIII which contains a specification sheet of an air-cooled heat exchanger is used to find what the size and weight requirement is. The largest available heat exchanger is used for the relation between surface area and size as well as the relation between surface area and weight.

Energy requirements and COP

This section describes the methods used to determine the BTMS energy requirements.
The reason why determining the BTMS's required energy consumption is important is that the power consumed by the operation of a BTMS directly impacts the available power of the battery pack left for driving.

For the vapor-compression refrigeration system, the mass flow rates of R717, R134a, and R1234yf have been determined by:

$$\dot{m} = \frac{\dot{Q}_{pack}}{\Delta h_{vap}} \tag{3.28}$$

- Where $\dot{m}$ is the required refrigerant mass flow rate in kg/s
- $\dot{Q}_{pack}$ is the battery pack generated heat per unit time absorbed by the refrigerant in W
- Δh_{vap} is the latent heat of vaporization of the refrigerant in kJ/kg

Subsequently, the required compressor power is determined from the following equation:

$$W_{compressor} = \dot{m} * \Delta h_{compression} \tag{3.29}$$

- Where $W_{compressor}$ is the required compressor power in W
- $\dot{m}$ is the required refrigerant mass flow rate in kg/s
- $\Delta h_{compression}$ enthalpy change during compression in kJ/kg

For the deviation of $\Delta h_{compression}$ from an ideal compression, a compressor isentropic efficiency of 85% has been used. This isentropic efficiency is defined as:

$$\eta = \frac{h_{2s} - h_1}{h_{2r} - h_1} * 100\% \tag{3.30}$$

- Where η is the isentropic efficiency of the compressor
- $h_1, h_{2r},$ and h_{2s} are the specific enthalpy at the compressor entrance, compressor exit for the real process, and compressor exit at the isentropic process respectively.

Lastly, the coefficient of performance (COP) of the vapor-compression refrigeration cycle is determined by:

$$COP = \frac{\dot{Q}_{pack}}{W_{compressor}} \tag{3.31}$$

The coefficient of performance is a dimensionless value and displays the ratio between useful cooling done by the vapor-compression refrigeration system and the energy required by the compressor. A higher COP value indicates a more efficient refrigeration system.

3.5 BTMS simulation model

In order to analyze the dynamic behavior of a battery pack whilst using a BTMS and Megawatt charging, a BTMS model is created in MATLAB – Simulink.
An advantage such of a battery thermal management system model is its flexibility. The model can be used to simulate several scenarios and adjust parameters as required. Practical experiments have limited flexibility due to the constraints of the physical environment.
Time and costs as part of the development of a battery thermal management system can be significantly reduced by using a good simulation tool (Kiss, et al., 2015). Furthermore, the dynamic system simulation environment MATLAB-Simulink is widely used in the automotive sector and can effectively co-simulate with vehicle simulations and evaluate various control algorithms (Kiss, et al., 2015). Using experimental methods instead to investigate system operating modes and outcomes is much more time consuming.

In this model, the battery cells in the battery pack are represented as a one-RC branch equivalent circuit model (ECM). An equivalent circuit model is a simplification of a battery cell, in which the operational characteristics of the battery are mimicked by representing the battery as an electrical circuit with capacitors and resistors. Furthermore, a lumped capacitance model approach is used for the battery cells.

A digital twin of the battery cell used in the study is built in MATLAB, as displayed in Figure 11. This is done by using the BatteryBuilder function. The battery cell has been created in MATLAB with the same properties and dimensions as used earlier in this study. However, for large battery packs such as in this study, limitations are encountered in the software when modelling a pack where more than 150 cell groups are either in series or parallel configuration, as this is not supported.

Therefore, a standard Simulink battery pack model of a smaller battery pack has been chosen for this part of the study. The specifications of this battery pack can be found in Appendix XVII.

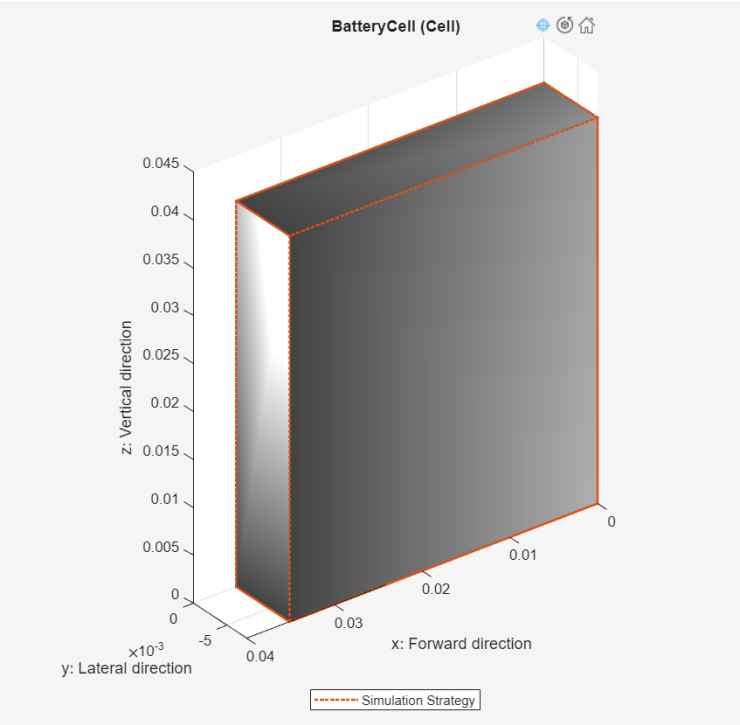

Figure 11: Battery cell model of Panasonic NCA cell

The BTMS Simulink model represents a charging session with a battery pack cooled by cooling plates with a 70/30 volumetric percent water ethylene glycol mixture, which releases its heat through an air-cooled heat exchanger. An overview of this model is shown in Appendix V.
The flow rate of the coolant is controlled by a pump that circulates the coolant through the BTMS system. A control strategy implemented to the pump is that as soon as the measured battery temperature increases 1 ℃ above the battery temperature setpoint, the coolant pump is switched on and stays on until the battery temperature is equal or below the temperature setpoint. The temperature setpoint used in the model is 30 ℃, as this is in the optimal temperature range for battery cells and does not require as much pumping power as with lower temperature setpoints. Furthermore, the 1 ℃ offset from the temperature setpoint reduces the number of times the coolant pump has to switch on and off, which would be much higher if the pump switches on and off at every slight deviation from the temperature set point.
The ambient temperature used in the model is 25 ℃. The model is simulated over a period of 600 seconds.
The standard cells in the battery model have a capacity of 28 Ah and the pack is charged at a current of 100 A, which is lower than MCS, however as the pack is also smaller than the pack earlier discussed in the study this ensures the model can still run. Although it does not represent the earlier selected battery cells and charging conditions in this study, the model will still provide valuable dynamic phenomena that occur during battery thermal management.

The standard values and equations used in the study's remaining BTMS component blocks are documented by MathWorks, the developer of MATLAB – Simulink, which are the Pipe (thermal liquid) component for the cooling plates (MathWorks, 2023d), Heat Exchanger (thermal liquid – moist air) (MathWorks, 2023a), Moist Air Properties block (MathWorks, 2023c), and Fixed-Displacement Pump (MathWorks, 2023a).

3.6 BTMS effect on MHDEV driving range

An analysis is made of the impact of extra weight on the driving range of a MHDEV. This is done by a thorough analysis of an electric truck dataset shown in Table 8.
The battery pack capacity of the vehicles and the listed range have been used to calculate their energy consumption in kWh/km. This energy consumption is plotted against the weight of the vehicles. The plot contains a collection of data points that show a correlation between vehicle weight and energy consumption. From this information, the impact of each additional weight unit, for example from the BTMS and its components, on the vehicle driving range is determined and visualized. An analysis of the impact of adding additional weight on vehicle range is done for the lightest vehicle in the dataset, the heaviest one, and for the mean weight value. The information can aid in BTMS design decisions such that battery operating requirements are met, while at the same time keeping the impact on driving range as little as possible.

Manufacturer	Model	Type	Weight (tonne GVW)	Battery capacity (kWh)	Range (km)	Energy consumption (kWh/km)	Charging power (kW)	Battery chemistry
BYD	T7	Medium-duty	11.00	175	200	0.88	100/150	
BYD	T9	Semi	36.00	350	200	1.75	100/150	LiFEPo4
Cummins	AEOS	Semi	28.10	140	160	0.88	-	-
DAF/VDL	CF electric VDL E-Power	Semi	40.00	170	100	1.70	-	Li-ion
E-Force One	E18 (18t)	Rigid	18.00	240	200	1.20	-	LiFEPo4
E-Force One	E44	Semi		310	180	1.72	-	Li-ion (NMC- C)
E-FUSO	Vision ONE	Rigid	23.30	300	350	0.86	-	-
Einride	T-Pod	Rigid	20.00	200	200	1.00	-	-
eMoss	EMS 18	Rigid	18.00	120-240	100-250	1.00	22/44	-
eMoss	EMS 1820	Rigid	18.00	200	190	1.05	-	LiFEPo4
Freightliner	eM2 106	Rigid	12.00	325	370	0.88	260	
Freightliner	eCascadia	Semi	40.00	550	400	1.38	260	
Hytruck	C18e	Rigid	19.00	120	150	0.80	-	Li-ion
MAN	eTruck	Rigid	18.00	-	200		-	Li-ion

Mercedes-Benz		Rigid	26.00	212	200	1.06	-	
Mercedes-Benz	eActross	Rigid	25.00	240	200	1.20	-	Li-ion
Mitsubishi	eCanter	Medium-duty	7.50	82.8	120	0.69		
Renault	DZE.	Rigid	16.00	200-300	300	1.00	22/150	
Renault	D WIDE Z.E.	Rigid	26.00	200	200	1.00	22/150	
Tesla	Semi	Semi	36.00		480-800	1.25		
Tesla	Semi (500 mile)	Semi	36.30	1000	805	1.24		-
Thor	ET-One	Semi	36.30	-	480			Li-ion
US hybrid	eTruck	Semi	29.50	240	160	1.50		Li-ion
Volvo	FL electric	Rigid	16.00	300	300	1.00	22/150	Li-ion
Volvo	FE Electric	Rigid	27.00	300	200	1.50		Li-ion

Table 8: Overview of electric trucks and specifications (Verbruggen, et al., 2018) (Arora, et al., 2021)

4

Results

This chapter presents the results derived from the research conducted. First, the results of the battery heat generation are discussed. Then the findings of possible temperature gradients are discussed. Subsequently, the results of BTMS strategies that have been assessed in the study are displayed as well as the developed concepts. Furthermore, the results of the BTMS MATLAB Simulink model are shown. Lastly, the effect of the BTMS on the MHDEV driving range is addressed.

4.1 Battery Heat Generation

Results for the calculations of the battery pack model are shown in Table 9. The electrical current through each cell is found to be 13.6 A, which correlates with about 9C charge rate. The table shows the required number of battery cells in series and parallel, as well as the total number of cells required, to meet the battery pack requirements.

Variable	Result
$series\ groups$	417
$parallel\ groups$	220
n_{cells}	91740 cells
Total pack weight	2266 kg

Table 9: Battery configuration results

Furthermore, simulating a charging session with 4.5MW resulted in a cell heat generation of 3.72 W. For the total number of battery cells, charging at this rate resulted in 341 kW of heat generation.

The relation between charging power supplied to the battery pack and the resulting heat generation in a single cell is shown in Figure 12. It can be seen that the heat generation in a cell increases quadratically with increasing charging power, as a result of the current to the second power in the Ohmic Heating equation.

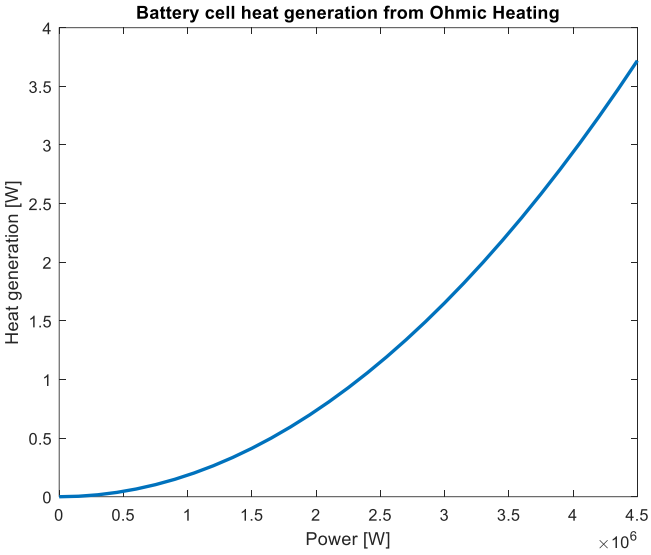

Figure 12: Battery cell heat generation from Ohmic Heating at various charging rates

For all battery cells in the pack, a 4.5 MW charging correlates with a 7.58% power loss as a result of heat generation during the charging session. This result for power loss and how the power loss is affected by charging rate is shown in Figure 13.

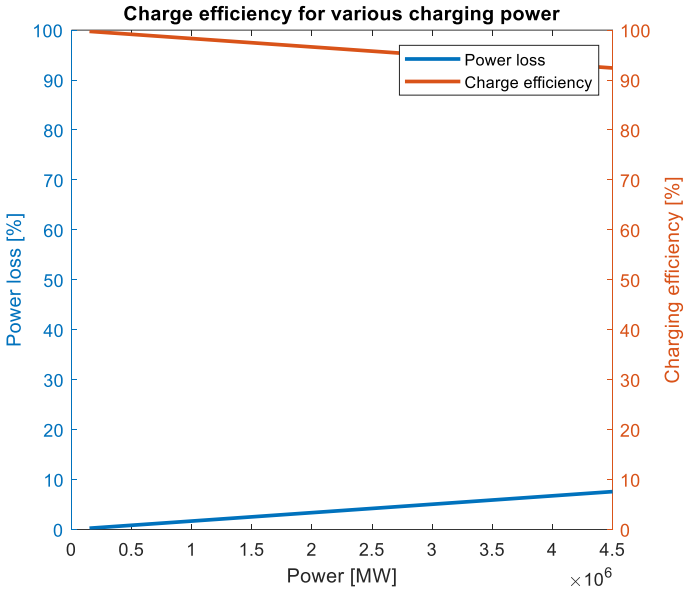

Figure 13: Power loss due to resistive heating at various charging rates

4.2 Battery temperature gradient

Lumped capacitance model

The results indicate that when considering in-plane heat transfer, BMTS strategies with a convective heat transfer coefficient below 357 W/m^2K can be modelled using a battery lumped capacitance model, as this still satisfies the condition $Bi < 0.1$. For cross-plane heat transfer, BMTS strategies with a convective heat transfer coefficient below 8.9 W/m^2K can be modelled using a battery lumped capacitance model.

The previously described results for in-plane heat transfer demonstrate that all BTMS strategies except forced air cooling result in a battery cell temperature gradient too large for the lumped

capacitance model to be valid. For cross-plane heat transfer, the result obtained is much lower which means that when cooling the battery in the cross-plane direction, all BTMS strategies result in a temperature too large for the lumped capacitance model to be valid. The implication of the results is that a temperature gradient occurs in each battery cell that should be determined and taken into account when determining the requirements of each BTMS strategy.

Battery cell temperature gradient

For the battery cell temperature gradient, the results indicate that there is a temperature gradient through the battery when considering its internal heat generation and when imposing a fixed temperature at 2 of its sides. Such a fixed temperature is imposed through a thermal management strategy, where the battery surface temperature and core temperature are maintained at a temperature below the maximum allowed battery temperature. When considering heat conduction in-plane through the battery's short dimension, a temperature difference between the battery core and the battery surface of 2.55 °C is found (shown in Figure 14 (a)), while heat conduction through the battery's long dimension results in a temperature difference of 3.35 °C (shown in Figure 14 (b)).

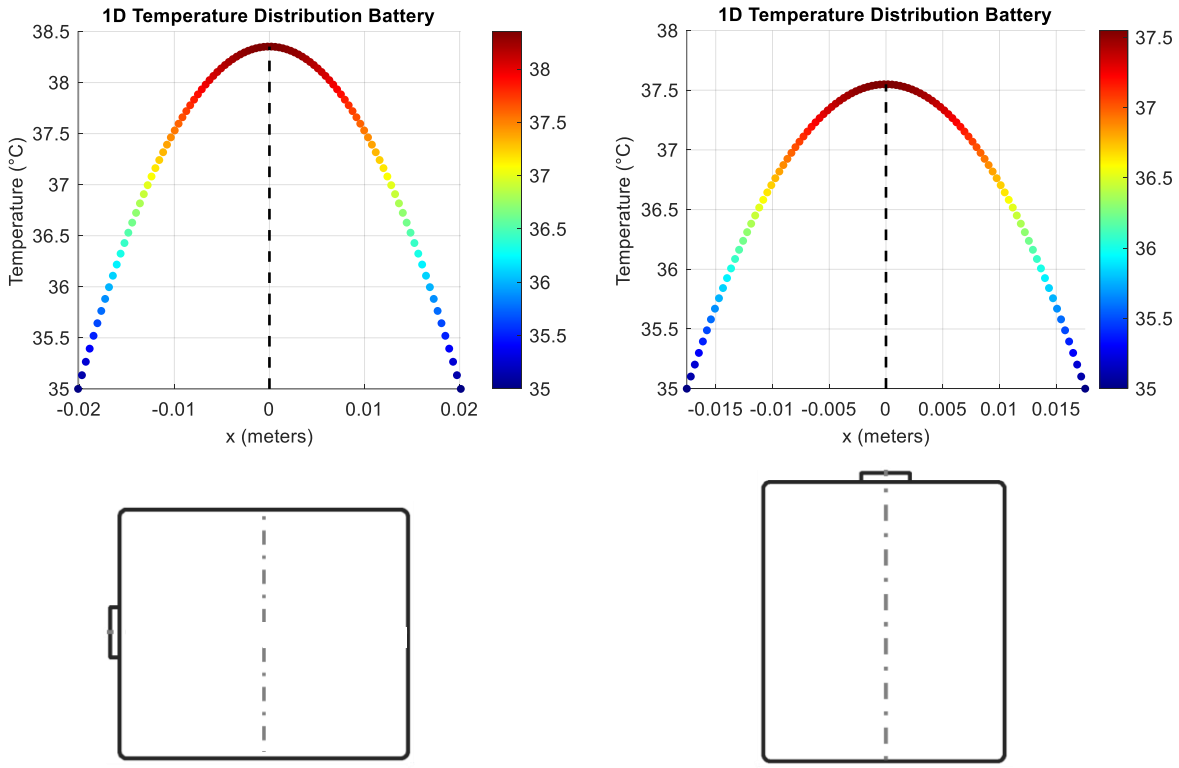

Figure 14: 1-dimensional in-plane conductive heat transfer through battery cell's (a) long dimension and (b) short dimension

When considering conduction in the cross-plane direction, contrary to the previously investigated in-plane directions, results show that the temperature gradient is much more significant, as a result of the lower effective thermal conductivity, even though the thickness of the material that the heat dissipates through is much smaller than the in-plane situations. This is visualized in Figure 15. The temperature difference found is 5.23 °C.

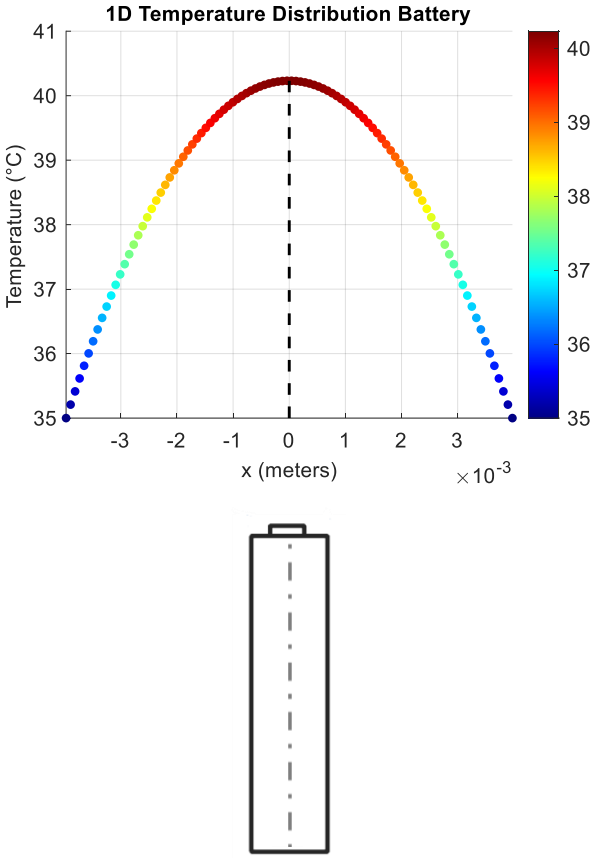

Figure 15: 1-dimensional cross-plane conductive heat transfer through battery cell

4.3 BTMS Assessment

4.3.1 Assessment 1

As part of the required heat transfer area assessment, results show that the larger the heat transfer coefficient of a BTMS and heat transfer medium is, the smaller the required heat transfer surface area is. This effect is displayed in Figure 16. While the figure on the left displays the relation between heat transfer coefficient and surface area over a surface area ranging from 10^0 to 10^3, the right figure zooms in on the range between 10^2 and 10^3 to display the relation for relatively small heat transfer coefficients. The figures indicate that for lower heat transfer medium temperatures, a smaller surface area is required to absorb the battery heat.

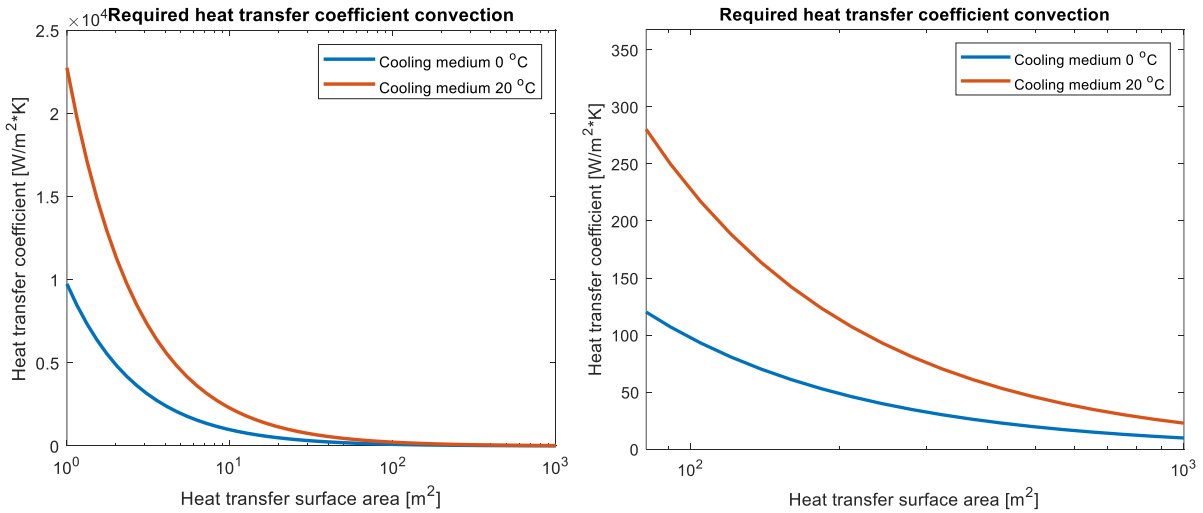

Figure 16: Required heat transfer coefficient for various surface area quantities at a battery surface temperature of 35 ℃

As the cross-plane heat transfer results in the previous chapter indicated a battery temperature gradient of 5.23 ℃, the resulting maximum allowable cell surface temperature is 29.77 ℃ in order to ensure the core temperature does not exceed 35 ℃. This holds for BTMS strategies with air and immersion cooling that target the battery cross-plane. For BTMS strategies with cooling plates, the temperature gradient of 2.55 ℃, results in a maximum cell surface temperature of 32.45 ℃.
Based on these cell surface temperatures, the results obtained for the various BTMS strategies are shown in Table 10.

Thermal medium inlet temperature	Forced air	Forced immersion cooling	Cooling plates with coolant	Cooling plates with refrigerant
0 ℃	117.57 m^2	23.51 m^2	10.79 m^2	2.69 m^2
20 ℃	358.24 m^2	71.65 m^2	28.11 m^2	7.03 m^2

Table 10: Results overview of BTMS surface area requirements

The assessment of the temperature gradient in a cooling plate indicated a temperature gradient of 0.0495 ℃.
This result indicates that for each additional millimeter of cooling plate wall thickness, the difference between the battery surface temperature and the cooling plate channel wall temperature increases by 0.0495 ℃. This value indicates that the battery cell surface area is almost equal to the wall temperature of the cooling plate's channels.

Inspection of the results shown in Table 10 and comparison with the available surface area shown in Table 6 of chapter 3.3.2 learns that aside from forced convection by air at an inlet temperature of 20 ℃, all BTMS strategies require a surface area that is available in the battery pack. For forced convection by air at an inlet temperature of 20 ℃, a sufficient amount of heat can only be absorbed from the battery when all surface area from each battery cell is targeted. When targeting e.g. only the sides of all cells, the surface area utilized is not sufficient and thus the heat transfer will not be sufficient.

4.3.2 Assessment 2

Based on the maximum allowable cell difference and thus also maximum allowable thermal medium temperature increase of 5 ℃, the required mass flow results for the BMTS' is shown in Table 11. For clarity, the results for cooling plates with refrigerant are included in section 4.4.2.

Thermal medium temperature increase	Forced air	Forced immersion cooling	Cooling plates with coolant
5 ℃	69.58 kg/s	30.78 kg/s	19.27 kg/s

Table 11: Results overview of BTMS mass flow rate requirements

4.4 BTMS Developed Concepts

4.4.1 TES

Based on the thermal energy storage for a Megawatt charging session with a charging duration of 308.57 seconds, it was found that the heat storage requirement is 107.99 MJ.

Using immersion cooling oil resulted in a required mass of 9497.8 kg to store the charging session's generated heat. Based on the oil's density of 806 kg/m^3, the resulting mass needed equals a volume of 11.78 m^3.

	Forced immersion oil	PCM paraffin	PCM hydrated salt
Required mass	9497.80 kg	430.24 kg	583.73 kg
Required volume	11.78 m^3	0.52 m^3	0.38 m^3

Table 12: Results of TES calculations

The results show that PCM's require a significantly smaller amount of material in both mass and volume to absorb a charging session its heat. When comparing paraffin with hydrated salt, the results show that even though the hydrated salt requires more mass (as a result of the lower latent heat compared with paraffin), the required volume is less (as a result of the higher density compared with paraffin).

4.4.2 Active BTMS

For the vapor-compression refrigeration cycle with a -10 ℃ evaporation temperature and 40 ℃ condensing temperature, the results obtained are as follows.

Utilizing ambient air that increases in temperature from 15 ℃ to 35 ℃, the logarithmic mean temperature difference found is 12.42 ℃. For refrigerant ammonia, the required surface area for the condenser to be able to reject the battery-generated heat is found to be 57.4 m^2.
However, varying the ambient air inlet temperature from -10 ℃ to 30 ℃, while maintaining an air outlet temperature of 35 ℃, the required condenser surface area varies from 36.5 m^2 to 98.8 m^2. This indicates that the required condenser surface area is very dependent on the temperature of ambient air.

Considering the air-cooled heat exchanger specifications in Appendix XIII that provides 4.2 m^2 of heat transfer area for the largest model, a total of 14 heat exchanger equivalents are necessary for an ambient air inlet temperature of 15 ℃. Based on the specifications, the weight will equal 102.2 kg and requires a frontal area of 1.7 m^2.

The resulting operating conditions of the vapor-compression refrigeration cycle are shown in Figure 17 and Table 13. The numbers shown in the figure and table indicate the location in the refrigeration process for which the refrigerant properties are specified.

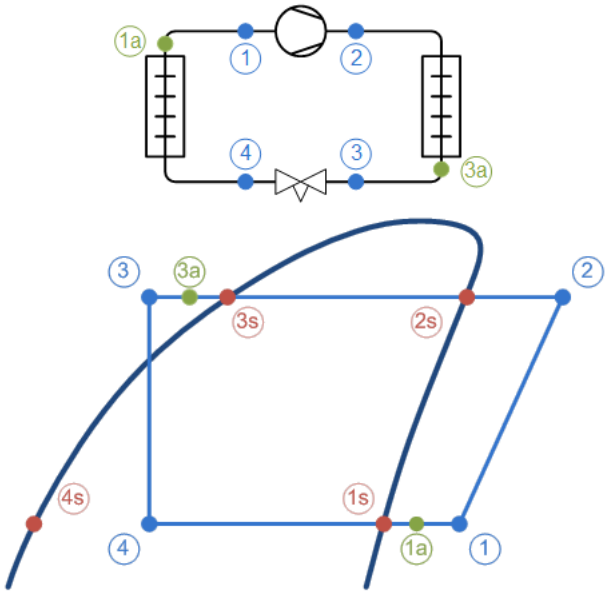

Figure 17: Schematic representation of the vapor-compression cycle (Danfoss, 2023)

		Temperature	Pressure	Density	Enthalpy	Entropy
Point	Description	[°C]	[bar]	[kg/m^3]	[kJ/kg]	[J/(kg-K)]
1	Compressor suction	-2.0	2.906	2.303	1471	5834
2	Compressor discharge (estimated)	140.0	15.55	8.102	1769	5933
2s	Condensation dew point	40.0	15.55	12.02	1490	5155
3s	Condensation bubble point	40.0	15.55	579.6	390.4	1644
3a	Condenser out	38.0	15.55	582.9	380.6	1612
3	Including additional subcooling	38.0	15.55	582.9	380.6	1612
4	After expansion valve	-10.0	2.906	13.45	380.6	1690
4s	Evaporation bubble point	-10.0	2.906	652	154.1	829.5
1s	Evaporation dew point	-10.0	2.906	2.391	1450	5755
1a	Evaporator out	-2.0	2.906	2.303	1471	5834

Table 13: Operating conditions of the vapor-compression refrigeration cycle

The obtained results for the required refrigerant mass flow rate are displayed in Table 14. The results show a significant difference in mass flow rate between refrigerants. Compared to R134a and R1234yf, R717 (ammonia) requires an 86.69% and 89.75% lower mass flow rate respectively.

Refrigerant	Required mass flow rate	Required compressor power
R717	0.32 kg/s	99.59 kW
R134a	2.41 kg/s	117.37 kW
R1234yf	3.13 kg/s	122.97 kW

Table 14: Required refrigerant mass flow rate and compressor power

For using R717 as refrigerant, the required compressor power is found to be 99.59 kW. Comparing this with R134a where the resulting compressor power is 117.37 kW, the use of ammonia reduces required compressor power consumption with 15.15 %. Comparing with R1234yf, the use of R717 results in a 19.01 % power consumption reduction.

Based on the resulting compressor power required for each refrigerant, the COP value found for each is displayed in Table 15.

Refrigerant	COP
R717	3.51
R134a	2.98
R1234yf	2.84

Table 15: Overview of COPs for the refrigerants assessed in the study

4.5 Simulink BTMS

The results of the MATLAB Simulink BTMS model are displayed in Figure 18. It can be seen that for a constant charging current, dynamic effects occur in the BTMS. This is shown by the pump that is not constantly turned on, but only switched on as battery temperature exceeds the temperature setpoint. The model results show that the battery temperature fluctuates, as the BTMS aims to maintain the battery temperature at the setpoint of 30 °C. However, the BTMS that is modeled manages to keep the battery temperature in close proximity to the set temperature. Additionally, the results indicate a gradual rise in the minimum temperature of the battery cells over the course of a charging session.

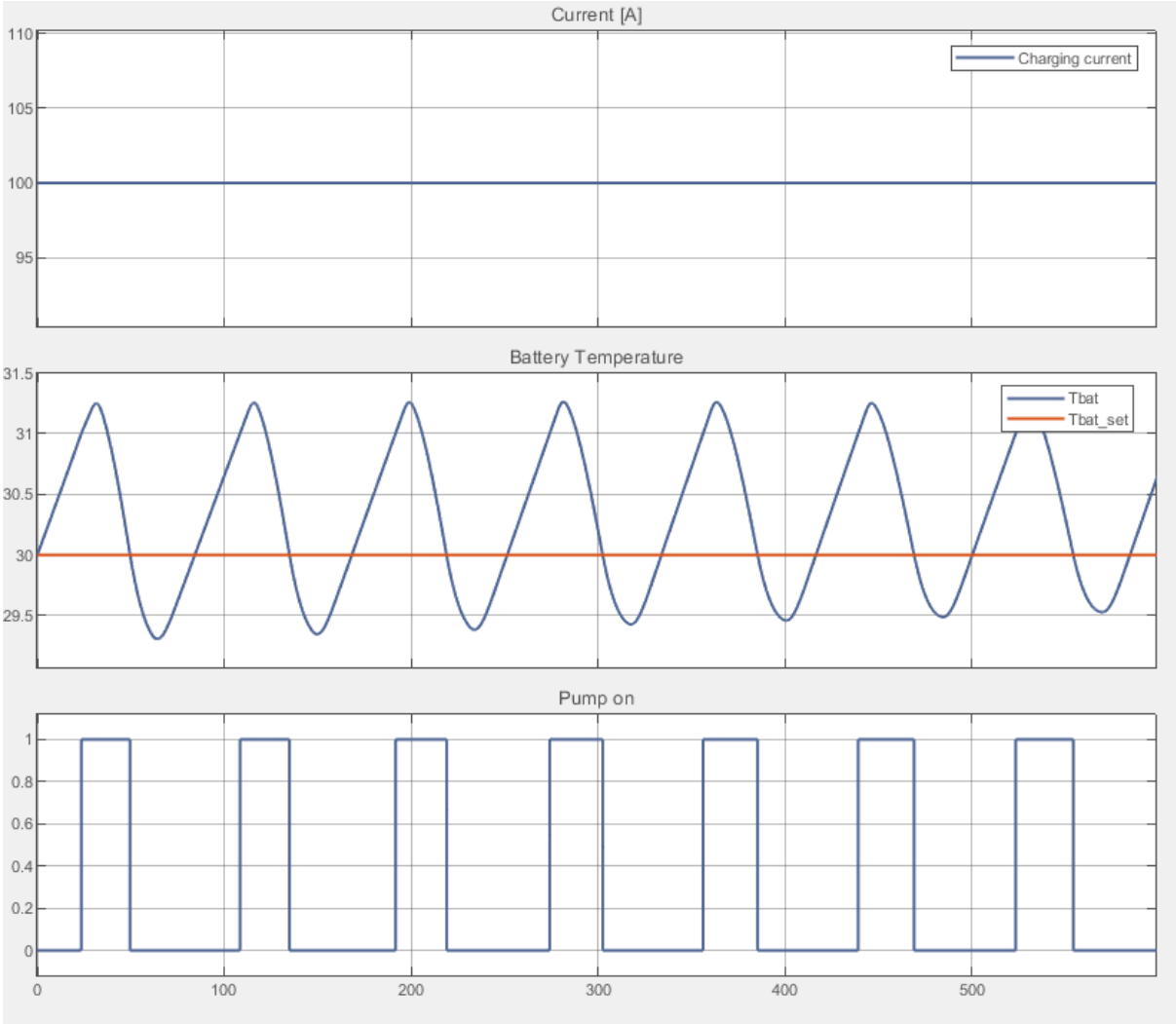

Figure 18: MATLAB Simulink BTMS results

4.6 BTMS effect on MHDEV driving range

The resulting data points indicating the weight and energy consumption of each truck in the dataset have been plotted and are presented in Figure 19. The data points indicate a correlation between these two variables, from which it can be concluded that increasing vehicle weight increases vehicle consumption.

Utilizing this correlation to assess the impact of additional weight on the vehicle, gives the results shown in Figure 20, which demonstrates a linear relationship. These findings highlight that, particularly for lighter e-Trucks, the impact of each additional unit of weight on driving range is more significant when compared to heavier e-Trucks. For the mean case, the results show that for each tonne of weight added by the BTMS, the vehicle's range is reduced by approximately 2%.

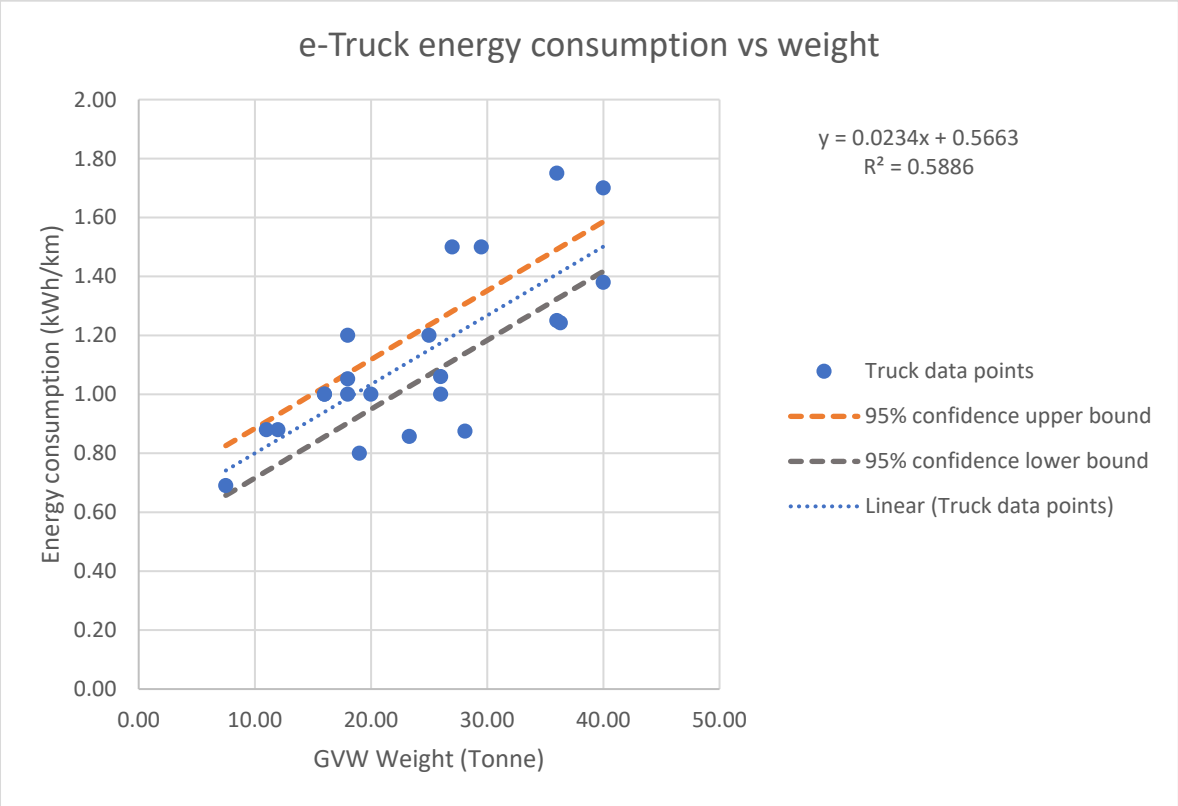

Figure 19: Relation between e-Truck energy consumption and weight

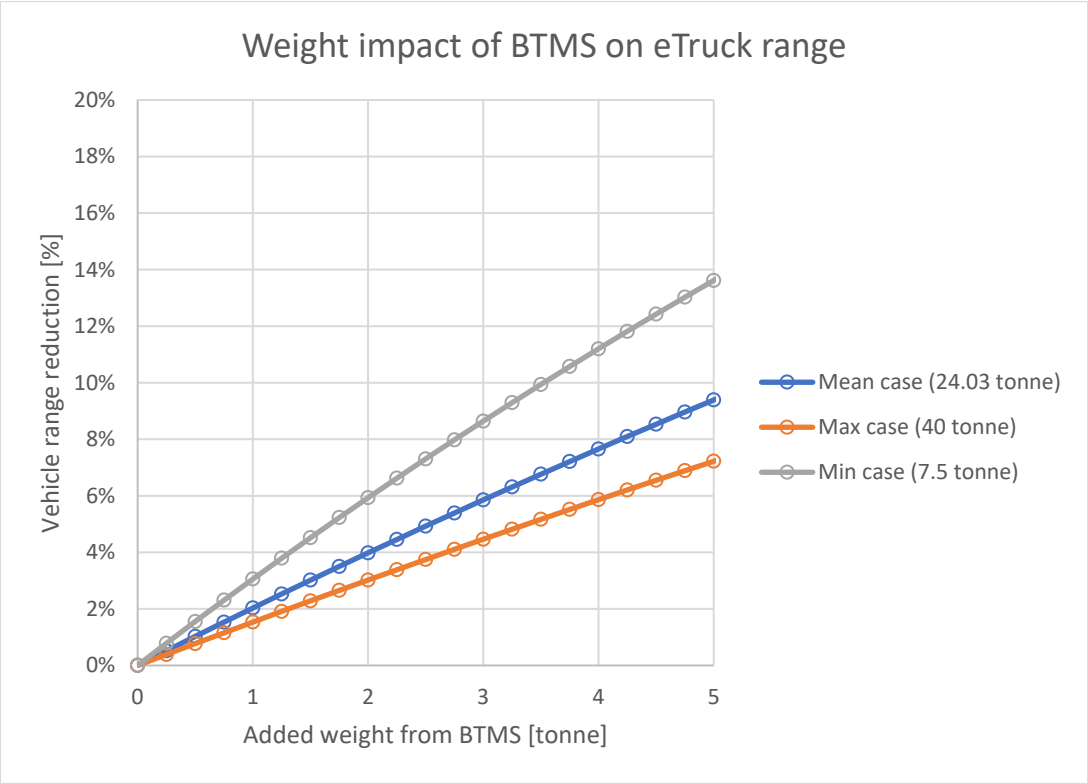

Figure 20: Relation between e-Truck added weight and driving range reduction

5

Discussion

This chapter describes the analysis, interpretation, and significance of the study's results.

5.1 Battery Heat Generation & Temperature Gradient

The study discussed the main requirements for a battery pack that affect the BTMS design. However, additional practical requirements for batteries exist with the objective of further improving safety, reliability, and battery longevity, all of which can influence design choices for BTMS's. These additional standards are governed in the SAE battery pack standards that are shown in Appendix XV.
Furthermore, the results indicated that a large number of 91740 battery cells is required. This large number is caused by the combination of the requirement of a 500 kWh battery pack which is relatively large, the requirement to meet a 1000 V voltage, and the fact that the battery cells selected for the study are relatively small and therefore have a relatively low energy capacity in Ah. Opting for larger battery cell types with greater capacity would result in a lower number of battery cells, however, the cells will be subject to a higher electric current as a lower number of cell groups in parallel are required.
To accommodate the high number of battery cells, it is not practical to assemble all cells in a single battery pack. Therefore, it is suggested that the battery set of 500 kWh is divided over five smaller battery packs of 100 kWh each, with each pack containing 18348 battery cells. A suggested configuration for this is shown in Appendix XIV.

Regarding the battery cell heat generation, results with similar order of magnitude of heat generation, however, typically at lower C-rates and therefore lower heat generation, can be found in literature (Peng, Ma, Garg, et al. 2019) (Pesaran, et al., 1999). However, as charging rates and battery specifications differ in each study, specific results can only be compared if all conditions are the same.
In the calculation approach of the battery heat generation, it is evident that the heat generation outcome is very sensitive to the internal resistance factor. A battery with a twice as high internal resistance will also generate twice the amount of heat, ceteris paribus.
Considering the high C-rate of charging during Megawatt charging, the result of 7.58% charging losses at 4.5 MW appears to be relatively low. However, it should be considered that this only accounts for the resistive losses in the battery cells and does not include other inefficiencies anywhere else in the charging process. In practice, it is therefore expected that total charging inefficiencies are higher.

It is important to acknowledge that the calculation approach in this study for determining battery heat generation is limited to Ohmic Heating and therefore does not take into account heat generated from chemical reactions taking place in the battery cells. A more accurate prediction of battery heat generation will result in improved BTMS equipment dimensioning.
Moreover, the heat generation calculation approach used in this study is limited to Megawatt charging scenarios and other situations with very high C-rates. During charging with significantly lower C-rates, the accuracy of the approach used in this study decreases, as the share of reversible heat generation is larger and can be a significant share in the total heat generation.
Lastly, the model does not consider heat generation from battery components such as the cables and electric terminals, contrary to some other research in the field (Gozdur et al., 2021).

As the results indicated a difference in battery cell temperature gradients based on the direction of heat transfer, it underscores the importance of designing a BTMS such that the battery temperature gradient is kept as small as possible.
The battery temperature gradient that is calculated in the study is a result of its material specifications and the heat transfer strategy applied to the battery. Selecting smaller batteries can to some extend decrease the temperature gradient in battery cells, which will make maintaining battery cell core temperatures less challenging. However, the low thermal conductivity still remains a contributor to temperature gradients.

5.2 BTMS Strategies

In the study, a relatively small battery cell model has been used. The significance of this is that in situations where a larger battery cell is used, a lower total battery surface area is available (assuming the total battery energy capacity is dictated by total battery volume, and remains equal), which requires larger BTMS heat transfer coefficients to be able to absorb the same amount of heat from the battery cells.

The results indicated that a relatively large surface area is required for forced air heat transfer. The required surface area for other BMTS strategies is significantly lower, which means that a lower temperature difference between the battery cells and heat transfer medium is needed to remove the heat from the battery cells. However, aside from forced air heat transfer with inlet temperatures around 20 °C, all BMTS strategies can be applied to Megawatt charging in theory based on this first assessment. The practical barrier remaining for heat transfer by forced air, is how the required air inlet temperature is kept sufficiently below 20 °C at all times. When ambient air temperatures are high it is not feasible anymore to use forced air cooling.
Furthermore, the required mass flows shown in the study indicate high required mass flow rates for sensible heat transfer media. This is largely explained by their limitation of 5 °C temperature increase in order to avoid temperature non-uniformity of the battery cells, as well as due to the heat transfer media their limited specific heat capacity. Such high mass flow rates might be difficult to achieve on a vehicle where space is limited and weight should be minimized, contrary to large industrial installations. Utilizing refrigerants instead for the battery thermal management showed significantly smaller required mass flow rates and therefore appear to be much more feasible for the application of Megawatt charging.

Furthermore, the required surface area calculated for BMTS methods using cooling plates is accomplished through the cooling channel surface area. As a result, for relatively large surface areas required, it might be required to use a high number of small diameter channels.
When using a BTMS with cooling plates, it has to be considered how many cooling plates are implemented in the battery pack and in which configuration the battery cells make contact with the cooling plates. With a high number of battery cells, the battery cells might have to be divided in banks where each bank has a cooling plate above, beneath, or both, making contact with the battery cells. Stacking multiple battery cells without a cooling plate in between can result in temperature hot spots in some battery cells.
While the study assumed that the cooling plate and the battery make contact, there might be air gaps in between the battery cells and cooling plates which reduces heat transfer. Therefore, thermal pads can be placed between battery cells and cooling plates to ensure proper contact. However, the thermal pads should be as thin as possible, to minimize the effect of increased thermal resistance from adding the thermal pads.

5.3 BTMS Developed Concepts

Compared with the BMTS strategies' results and significance in previous chapter, the TES and vapor-compression refrigeration BTMS systems show to be more optimal systems for the application of MHDEVs that use MCS, as these BTMS' are able to absorb all generated battery heat during a charging session without temperature increments, with no- or the lowest required mass flows, and effective over a wide range of ambient temperatures.

Regarding the implementation of the thermal energy storage system concept, the results indicated that PCM is much more favorable than immersion oil as both the required mass and volume of the PCM are lower than when using immersion oil, which minimizes weight and volume in the MHDEV's. While paraffin has a lower required mass than hydrated salt, the hydrated salt requires less volume. Therefore, the decision of which PCM is most optimal depends on the specific requirements of fleet owners and charging point operators. As the total battery cell volume accounts for 1.03 m^3, implementing the required 0.38 m^3 of hydrated salt around each cell results in a 36.8% increase in size occupied by each cell with its PCM, which seems feasible. While it is expected that achieving a low BTMS weight is of higher importance than achieving a low volume as long as the system still fits in the vehicle, due to vehicle weight limitations, selecting paraffin over hydrated salt also comes with certain safety considerations such as paraffin's flammability. Implementing this in a MHDEV can create risks for vehicle personnel. Furthermore, as hydrated salts are corrosive to metals, direct contact with batteries should be avoided. A solution for this could be to implement a thin protective membrane between the battery cells and the PCM. Therefore, implementation of hydrated salt appears to be more feasible compared to paraffin.
As the thermal conductivity of PCM's is typically low and around 0.5 W/mK, the PCM might encounter 'slow charging', meaning that the melting process of the PCM does not take place evenly through the material and the latent heat usage is limited. This could be improved by adding thermally conductive materials in the PCM to increase its overall thermal conductivity.

For the vapor-compression refrigeration system, it is disadvantageous that a heat exchanger (condenser) is required to reject the heat from the refrigerant, as this increases system complexity, weight, and volume. While thermal energy storage will also need a way for heat release once the charging session is over, using passive cooling by ambient air might be sufficient, depending on the conditions of the vehicle and the duration until a next charging session is initiated. Furthermore, the need for cooling plates as part of the vapor-compression refrigeration is disadvantageous, as this results in additional battery pack weight, however, it is expected that the additional weight of implementing the cooling plates is less than the weight that is added by implementing an immersion coolant or a PCM as energy storage in the battery pack.

While heavy duty vehicles such as mining haul trucks might have sufficient available space for a large condenser, the vapor-compression refrigeration might be favorable for this vehicle, as the BTMS can be used for the driving cycle as well.

As the condenser temperature is selected to be 40 ℃, the system will be able to operate in ambient temperatures up to this temperature.

The COP results found for the refrigerants analyzed in this study are around 3, which implies that for every kW of compressor power, approximately 3 kW of heat can be removed by the vapor-compression refrigeration system, depending on the specific refrigerant used. The COP can be increased by reducing the difference between the heat source and heat sink, which are the evaporation temperature in the battery pack and the condenser temperature in the condenser. However, selecting a lower condenser temperature with the objective to increase the system's COP imposes a risk for operations when ambient temperatures approach- or increase beyond condenser temperatures, as the BMTS may not longer be capable to reject all absorbed heat, resulting in reduced heat absorption capacity from the battery.

Moreover, the total required compressor power determined in the study can be reduced by dividing the full compression in two compression steps with intercooling after the first compression. However, the drawback of this is increased system complexity and that the available cooling from the intercooler comes at the cost of decreased battery cooling or increased refrigerant mass flow rate.

When comparing the environmental effects of the refrigerants used in the study, an advantage of ammonia over other refrigerants is the GWP of 0, which is shown in Appendix VII. Furthermore, the ability to create ammonia without carbon emissions through the Haber-Bosch process, as shown in Appendix XVI is an advantage for this refrigerant. At industrial sites or charging hubs where MHDEV's are charging, locally generated electricity and electrolyzers can be used to produce ammonia on-site for use as refrigerant in the MHDEV's. Creating such a production facility on a small scale powered by renewable energy has been proven feasible already by (The Royal Society, 2020).

While results indicated R717 to be advantageous compared to R134a and R1234yf when assessing COP, required mass flow rate, and required compressor power, its flammability and toxicity introduce challenges and risk to its implementation in a BTMS. If these risks can not be eliminated, another refrigerant should be selected for the BTMS of MHDEV's. As R134a faces regulatory challenges in several countries due to its large GWP (European Parliament, 2006), large-scale BTMS implementation of R1234yf appears to be the most feasible of the refrigerants assessed in the study. However, the relatively large mass flow rates required, especially when selecting R1234yf over R717, are paired with relatively large- and heavy

BTMS compressors as indicated in Appendix XII. Therefore, implementation of PCM as BTMS strategy might be more favorable, depending on the specific future sector requirements.

5.4 Simulink BTMS

The results of the Simulink BTMS model indicated some of the dynamic phenomena that occur when implementing a BTMS. However, due to limitations in the modeling software the opportunities to create an as much as similar digital twin of the battery pack and BTMS' in this study were limited. Therefore, the model should be considered a high-level supplement to the other work displayed in this study. Furthermore, the transparency of the blocks in Simulink is limited, which does not make it fully clear how the outcome of the subcomponents are determined in the software. An example of this is the state of charge of the batteries used in the model. It is not fully clear if the battery block used in the model adjusts the internal resistance values of the battery accordingly when charging takes place and state of charge of the batteries increases. The specific results should therefore be used with caution, however, can still be used to display BTMS effects that are likely to happen when using MCS with MHDEV's.
Lastly, the observed rise in minimum temperature over time can be attributed to either an increase in heat generation from the battery cells or a decrease in the heat removal capacity of the coolant during the later stages of the charging session.
It is unlikely that the increased battery heat generation is the primary cause of this effect, given that the charging current remains constant and the internal resistance values in Appendix XVII suggest a decrease as state of charge or battery temperature increases.
Therefore, it is anticipated that a gradual increase in coolant temperature is responsible for this trend. This underscores the importance of a well-designed heat exchanger, as it plays a pivotal role in enabling the coolant to reject heat, thereby ensuring effective thermal management of the battery over extended periods.

5.5 Driving range impact

The results for the relation between vehicle energy consumption and vehicle weight showed data points with a relatively low coefficient of determination (R^2), which means the linear prediction is not very accurate. A cause of this can be that the eTrucks in the dataset have different years of market introduction. As typically the energy density of batteries increases as a result of technical developments, newer eTrucks might have battery packs with higher energy density cells and therefore can have a higher driving range with the same vehicle weight as a similar older eTruck.
Furthermore, as the results indicate a reduction in driving range as the weight of the BTMS increases, the importance of designing the BTMS such that weight is minimized is emphasized. The results also showed that MHDEV's that are lighter in weight are more significantly impacted by a fixed added weight to the vehicle. The implication of this is that a certain BTMS design reduces the range of lighter MHDEV's more significantly than heavier ones if no adaptions are made. As the lighter vehicles are likely to have smaller battery packs and therefore also less total heat generation than heavier ones, it is optimal to adapt the BTMS design to the specific vehicles, instead of implementing a one-size-fits-all approach, to avoid unnecessary reductions in driving range.

6

Conclusions

The study investigated how a battery thermal management system should be designed for MHDEV's utilizing Megawatt Charging Systems, and which BTMS is most optimal for this application. This conclusion chapter summarizes the key findings and contributions of this research.
The sub-research questions addressed in the study are covered in this chapter, after which the main research question is answered.

SRQ1: *What are the specific requirements for a MHDEV BTMS?*

The requirements identified for the study and proposed for any MHDEV BTMS can be categorized into battery- and operating temperature requirements and battery-related requirements.
Important temperature requirements are that the battery cells should maintain in their optimal temperature operating range of 15 ℃ to 35 ℃. Additionally, the battery cell temperature difference should not be more than 5 ℃ at any two points in the battery pack, to ensure adequate temperature uniformity.
Battery requirements which play a pivotal role in BTMS design for the application of MHDEV MCS, encompass two criteria. Firstly, the battery pack capacity must meet the typical capacity, which is found to be 500 kWh. Secondly, compliance with the MCS standard is essential, which encompasses accommodating charging rates of up to 4.5 MW and adhering to a voltage specification of 1500 V.

SRQ2: *What is the battery heat generation quantity for Megawatt charging MHDEV's based on typical battery specifications?*

As Megawatt charging takes place at high C-rates, the predominant heat generation phenomenon is Ohmic Heating, which has been used in the study to model battery heat generation.
The study's calculations for battery heat generation, based on the cell specifications employed in the study, indicate that the MCS battery generates approximately 3.72 W per cell, resulting in a total heat generation of 341 kW.

SRQ3: *Which BTMS strategy and heat transfer medium is most advantageous for Megawatt Charging MHDEV's?*

The study assessed four distinct BTMS strategies, namely forced air BTMS, forced immersion BTMS, cooling plates with coolant BMTS, and cooling plates with refrigerant BTMS. For each BTMS strategy, the required surface area for heat transfer has been determined as well as the required mass flow of heat transfer medium. Based on the required heat transfer surface area and required mass flow, either a BTMS system with refrigerant through cooling plates or phase change materials to store the heat are found to be the most advantageous among these assessed BTMS strategies. For the first system, refrigerant R717 demonstrated a higher COP, lower required mass flow, and reduced compressor power demand, compared to R134a and R1234yf. Nevertheless, considerations related to safety and regulatory compliance lean in favor of R1234yf. For the second system, hydrated salt emerged as the most favorable phase change material based on the study's analysis on thermal energy storage.

SRQ4: *What is an optimal configuration of the BTMS components and what should the dimensions be?*

The BTMS can be configured as an active system in which a heat transfer medium absorbs the generated battery heat and rejects the heat through a heat exchanger or can be configured such that the heat generated during the charging session is stored in a heat transfer medium.
The required dimensions for both systems have been determined, which are carried out trough dimensioning of a heat exchanger for the vapor-compression refrigeration cycle using refrigerant and determining the required compressor power, as well as determining the required mass and volume for thermal energy storage of the generated heat during a charging session by utilizing immersion coolant and phase change materials.

SRQ5: *How does the BTMS design affect driving range of MHDEV's?*

Analysis of eTruck data showed that for an average weighing eTruck, each additional tonne of BTMS weight results in about 2% reduction in driving range. Therefore, the weight of the components as part of the BTMS directly impacts the driving range of the MHDEV which emphasizes the importance of weight reduction in BTMS design.

The main research question that has been guiding this study is formulated as follows:
How should the battery thermal management system be designed for medium- and heavy-duty electric vehicles utilizing Megawatt Charging Systems (MCS)?

The methodology employed in the study is based on a system engineering approach and is proposed to be used for the design of any BTMS for MHDEV's using MCS, while following the specific requirements for MHDEV BTMS's that have been addressed in the study.
Based on the requirements found for implementing existing BTMS strategies for the application of Megawatt charging of MHDEV's and exploring their configuration and dimensions more in-depth through concept development, implementing a PCM material as heat storage during the charging session appears to be the most optimal BTMS strategy. Utilizing a hydrated salt as PCM is the most advantageous for this. When requiring one BTMS for both driving as well as Megawatt charging, a vapor-compression refrigeration system is found to be more beneficial, as it can operate continuously compared to the discontinuous PCM thermal storage. However, the large dimensions might require placing some of the BTMS components offboard. When handling refrigerants, this introduces safety risks that should be considered.

7

Recommendations

Several recommendations for future research are discussed below, based on the findings of this study.

- Based on this study, it is recommended that researchers who design novel heat transfer equipment that can potentially be used for battery thermal management, adopt the design approach used in this study to assess the novel heat transfer strategy for the use of MHDEV MCS.
- Moreover, it is recommended that computational fluid dynamics analysis is used to assess battery temperatures, battery temperature gradients, and battery pack temperature uniformity, as part of the MHDEV MCS BTMS design process and prior to actual implementation of such a BTMS in practice.
- It is advised to conduct experiments with battery cells during which the battery heat generation is measured with calorimetry, to obtain more accurate battery heat generation results. This will in turn result in a more accurate prediction for the required heat duty of the BTMS.
- To maximize the overall efficiency of MHDEV's, research should be conducted on how to strategically combine the BTMS with the HVAC and the thermal management of the power electronics in the vehicles.
- As the results of the study show a significant impact of battery internal resistance on battery heat generation and thus temperature, it is for this application recommended to battery OEM's to select battery cells with an as low as possible internal resistance for battery packs that will be used in MHDEV that utilize MCS, while still maintaining a high battery energy density.
- Based on the optimal battery temperature range identified in this study, it is valuable to know what the positive effect is on battery longevity as a result of reduced battery degradation, compared with battery temperatures above this optimal temperature range. This work should specifically investigate the degradation effects of battery cells exposed to the MCS charging rates. This requires analysis of battery degradation for the specific battery cells used in MHDEV's for MCS.
- As the MATLAB Simulink model that has been discussed in the study is a high-level BTMS model that simplified some of the subsystems in the BTMS, it is recommended

that subcomponents of the model are made with a higher level of fidelity to create a more realistic and accurate BTMS model. Creating a more detailed battery model will result in more accurate results for its heat generation and thermal behavior.

References

Aamir, M. et al., 2016. Study on Ultra-fast Cooling Behaviors of Water Spray Cooled Stainless Steel Plates. *Experimental Heat Transfer*, 5, 29(3), pp. 299-321.

Abdelkareem, M. A. et al., 2022. Battery thermal management systems based on nanofluids for electric vehicles. *Journal of Energy Storage*, 6, Volume 50, p. 104385.

ACEA, 2021. *Heavy-duty vehicles: Charging and refuelling infrastructure requirements.* [Online]
Available at: https://www.acea.auto/files/ACEA_Position_Paper-Heavy-duty_vehicles-Charging_and_refuelling_infrastructure.pdf

Agyenim, F., Hewitt, N., Eames, P. & Smyth, M., 2010. A review of materials, heat transfer and phase change problem formulation for latent heat thermal energy storage systems (LHTESS). *Renewable and Sustainable Energy Reviews*, 2, 14(2), pp. 615-628.

Akinlabi, A. A. & Solyali, D., 2020. Configuration, design, and optimization of air-cooled battery thermal management system for electric vehicles: A review. *Renewable and Sustainable Energy Reviews*, 6, Volume 125, p. 109815.

Al-Hanahi, B., Ahmad, I., Habibi, D. & Masoum, M. A., 2021. Charging Infrastructure for Commercial Electric Vehicles: Challenges and Future Works. *IEEE Access*, Volume 9, pp. 121476-121492.

Ally, M. R., Sharma, V. & Nawaz, K., 2019. Options for low-global-warming-potential and natural refrigerants part I: Constrains of the shape of the P–T and T–S saturation phase boundaries. *International Journal of Refrigeration*, 10, Volume 106, pp. 144-152.

Al-Saadi, M. et al., 2022. Fast Charging Impact on the Lithium-Ion Batteries' Lifetime and Cost-Effective Battery Sizing in Heavy-Duty Electric Vehicles Applications. *Energies*, 2, 15(4), p. 1278.

Al-Zareer, M., Dincer, I. & Rosen, M. A., 2018. A review of novel thermal management systems for batteries. *International Journal of Energy Research*, 8, 42(10), pp. 3182-3205.

Al-Zareer, M., Dincer, I. & Rosen, M. A., 2020. A thermal performance management system for lithium-ion battery packs. *Applied Thermal Engineering*, 1, Volume 165, p. 114378.

Andreev, A. A., Vozmilov, A. G. & Kalmakov, V. A., 2015. Simulation of Lithium Battery Operation Under Severe Temperature Conditions. *Procedia Engineering*, 1, Volume 129, pp. 201-206.

An, Z. et al., 2017. A review on lithium-ion power battery thermal management technologies and thermal safety. *Journal of Thermal Science 2017 26:5*, 9, 26(5), pp. 391-412.

Arora, S., 2017. Design of a Modular Battery Pack for Electric Vehicles.

Arora, S., Abkenar, A. T., Jayasinge, S. G. & Tammi, K., 2021. *Heavy-Duty Electric Vehicles: From Concept to Reality.* s.l.:Butterworth-Heinemann.

B. Noshirvani University of Technology, 2023. *Basic Design Methods of Heat Exchangers.* [Online]
Available at: https://ostad.nit.ac.ir/payaidea/ospic/file8494.pdf

Baghdadi, I. et al., 2015. Electro-thermal model of lithium-ion batteries for electrified vehicles applications. *IEEE International Symposium on Industrial Electronics,* 9, Volume 2015-September, pp. 1248-1252.

Bai, Y. et al., 2019. Reversible and irreversible heat generation of NCA/Si–C pouch cell during electrochemical energy-storage process. *Journal of Energy Chemistry,* 2, Volume 29, pp. 95-102.

Bandhauer, T. M., Garimella, S. & Fuller, T. F., 2011. A Critical Review of Thermal Issues in Lithium-Ion Batteries. *Journal of The Electrochemical Society,* 1, 158(3), p. R1.

Barkh, H. et al., 2022. Vehicle fleet electrification and its effects on the global warming potential of highway pavements in the United States. *Resources, Conservation and Recycling,* 10, Volume 185, p. 106440.

Belharouak, I., Koenig Jr., G. M. & Amine, K., 2011. Electrochemistry and safety of Li4Ti5O12 and graphite anodes paired with LiMn2O4 for hybrid electric vehicle Li-ion battery applications. *Journal of Power Sources,* 196(23), pp. 10344-10350.

Bernardi, D., Pawlikowski, E. & Newman, J., 1984. A General Energy Balance for Battery Systems. *Electrochemical Society Extended Abstracts,* 1, 84-2(1), pp. 164-165.

Bernard, M. R., Tankou, A., Cui, H. & Ragon, P.-L., 2022. *Charging Solutions for Battery-Electric Trucks.* [Online]
Available at: www.theicct.orgcommunications@theicct.org

Bohn, T., 2020. Multi-port, 1+MW Charging System for Medium-and Heavy-Duty EVs: What We Know and What Is on the Horizon?.

Buidin, T. I. C. & Mariasiu, F., 2021. Battery Thermal Management Systems: Current Status and Design Approach of Cooling Technologies. *Energies 2021, Vol. 14, Page 4879,* 8, 14(16), p. 4879.

CALSTART, 2023. Global Commercial Drive To Zero Program — ZETI Data Explorer.

Carballo, A. & Sahla, S., 2022. What does the energy transition mean for the mining sector?. *Transparency International Australia.*

Chacko, S. & Charmer, S., 2011. Lithium-ion pack thermal modeling and evaluation of indirect liquid cooling for electric vehicle battery thermal management. *Institution of Mechanical Engineers - Innovations in Fuel Economy and Sustainable Road Transport,* 1.pp. 13-21.

ChargeOn, 2023. *Charge On Innovation Challenge: Electrifying Mining.* [Online]
Available at: https://chargeoninnovation.com/

CharIN, 2022. *How to prepare for the Megawatt Charging System.* [Online] Available at: https://www.charin.global/news/how-to-prepare-for-the-megawatt-charging-system/

CharIN, 2023. *Megawatt Charging System (MCS).* [Online] Available at: https://www.charin.global/technology/mcs/

Chen, D. et al., 2016. Comparison of different cooling methods for lithium ion battery cells. *Applied Thermal Engineering,* 2, Volume 94, pp. 846-854.

Chen, L. et al., 2020. Core temperature estimation based on electro-thermal model of lithium-ion batteries. *International Journal of Energy Research,* 6, 44(7), pp. 5320-5333.

Choudhari, V. G., Dhoble, D. A. & Sathe, T. M., 2020. A review on effect of heat generation and various thermal management systems for lithium ion battery used for electric vehicle. *Journal of Energy Storage,* 12, Volume 32, p. 101729.

Chu, S., Cui, Y. & Liu, N., 2016. The path towards sustainable energy. *Nature Materials 2017 16:1,* 12, 16(1), pp. 16-22.

Clifton, J. R., Rossiter, W. J. & Brown, P. W., 1985. Degraded aqueous glycol solutions: pH values and the effects of common ions on suppressing pH decreases. *Solar Energy Materials,* 3, 12(1), pp. 77-86.

Culcu, H. et al., 2009. Internal resistance of cells of lithium battery modules with FreedomCAR model. *World Electric Vehicle Journal,* 3(4), pp. 702-710.

Danaee, I., Niknejad Khomami, M. & Attar, A. A., 2012. Corrosion behavior of AISI 4130 steel alloy in ethylene glycol–water mixture in presence of molybdate. *Materials Chemistry and Physics,* 8, 135(2-3), pp. 658-667.

Danfoss, 2023. Coolselector 2.

De Vita, A. et al., 2017. Transient thermal analysis of a lithium-ion battery pack comparing different cooling solutions for automotive applications. *Applied Energy,* 11, Volume 206, pp. 101-112.

Doughty, D. H., Butler, P. C., Jungst, R. G. & Roth, E. P., 2002. Lithium battery thermal models. *Journal of Power Sources,* 8, 110(2), pp. 357-363.

Dow, 2020. *High-temperature heat transfer fluids - Dowtherm and Syltherm.* [Online] Available at: https://www.dow.com/content/dam/dcc/documents/en-us/catalog-selguide/176/176-01638-01-high-temperature-heat-transfer-fluids-dowtherm-sylthern-selection-guide.pdf

Drive to Zero, 2022. Memorandum of Understanding on Zero-Emission Medium-and Heavy-Duty Vehicles.

Eddahech, A., Briat, O. & Vinassa, J. M., 2013. Thermal characterization of a high-power lithium-ion battery: Potentiometric and calorimetric measurement of entropy changes. *Energy,* 11, Volume 61, pp. 432-439.

Effat, M. B., Wu, C. & Ciucci, F., 2016. Modeling efforts in the key areas of thermal management and safety of lithium ion battery cells: a mini review. *Asia-Pacific Journal of Chemical Engineering,* 5, 11(3), pp. 399-406.

Ertugrul, N. et al., 2020. Status of mine electrification and future potentials. *Proceedings - 2020 International Conference on Smart Grids and Energy Systems, SGES 2020,* 11.pp. 151-156.

European Parliament, 2006. 2006/40/EC Directive. *EUR-Lex.*

Feng, X. et al., 2018. Thermal runaway mechanism of lithium ion battery for electric vehicles: A review. *Energy Storage Materials,* 1, Volume 10, pp. 246-267.

Feng, X. et al., 2015. Characterization of penetration induced thermal runaway propagation process within a large format lithium ion battery module. *Journal of Power Sources,* 2, Volume 275, pp. 261-273.

Feng, Y. et al., 2022. Energy efficiency and CO2 emission comparison of alternative powertrain solutions for mining haul truck using integrated design and control optimization. *Journal of Cleaner Production,* 10, Volume 370, p. 133568.

Fineprint, 2023. *An open source database on global coal and metal mine production.* [Online] Available at: https://www.fineprint.global/publications/briefs/open-database-global-coal-and-metal-mine-production/

Fraunhofer, 2021. *Truck Stop Locations in Europe - Final Report.* [Online] Available at: https://www.isi.fraunhofer.de/content/dam/isi/dokumente/cce/2021/ACEA_truckstop_report_update.pdf

Fraunhofer, 2023. *Open-source database for lithium-ion batteries released.* [Online] Available at: https://www.isi.fraunhofer.de/en/blog/themen/batterie-update/lithium-ionen-batterien-open-source-datenbank-veroeffentlicht.html

Gan, Y. et al., 2020. Development of thermal equivalent circuit model of heat pipe-based thermal management system for a battery module with cylindrical cells. *Applied Thermal Engineering,* 1, Volume 164, p. 114523.

GEA, 2021. *Screw Compressor Package - Product Information.* [Online] Available at: https://www.gea.com/fr/binaries/grasso-screw-compressor-package-pi_tcm29-38504.pdf

GEA, 2023. *GEA Grasso M Packages.* [Online] Available at: https://www.gea.com/en/products/refrigeration-heating/packaged-compressors/packaged-screw-compressor/m-series-packaged-screw-compressor.jsp

Greco, A., Jiang, X. & Cao, D., 2015. An investigation of lithium-ion battery thermal management using paraffin/porous-graphite-matrix composite. *Journal of Power Sources,* 3, Volume 278, pp. 50-68.

Green, D. & Southard, M., 2019. *Perry's Chemical Engineers' Handbook.* s.l.:McGraw Hill.

Guo, J. & Jiang, F., 2021. A novel electric vehicle thermal management system based on cooling and heating of batteries by refrigerant. *Energy Conversion and Management,* 6, Volume 237, p. 114145.

Heiskanen, S. K., Kim, J. & Lucht, B. L., 2019. Generation and Evolution of the Solid Electrolyte Interphase of Lithium-Ion Batteries. *Joule,* 10, 3(10), pp. 2322-2333.

Heredia, F., Martinez, A. L. & Urtubey, V. S., 2022. The Important Role of Mining Within the Energy Transition: The Case of the Lithium Sector in Argentina. pp. 137-151.

Hess, R., Bartels, M. J. & Pottenger, L. H., 2004. Ethylene glycol: an estimate of tolerable levels of exposure based on a review of animal and human data. *Archives of toxicology*, 12, 78(12), pp. 671-680.

Huang, Q., Yan, M. & Jiang, Z., 2006. Thermal study on single electrodes in lithium-ion battery. *Journal of Power Sources,* Volume 156, pp. 541-546.

Huria, T., Ceraolo, M., Gazzarri, J. & Jackey, R., 2012. High fidelity electrical model with thermal dependence for characterization and simulation of high power lithium battery cells. *2012 IEEE International Electric Vehicle Conference, IEVC 2012.*

IEA, 2023. Global EV Outlook 2023: Catching up with climate ambitions.

IEA, 2023. Trucks & buses - IEA.

International Energy Agency, 2022. The Role of Critical Minerals in Clean Energy Transitions. *World Energy Outlook Special Report,* 3.p. 5.

Iraola, U. et al., 2013. Methodology for thermal modelling of lithium-ion batteries. *ieeexplore.ieee.org*, pp. 6752-6757.

Ismail, N. H. F. et al., 2013. Simplified Heat Generation Model for Lithium ion battery used in Electric Vehicle. *IOP Conference Series: Materials Science and Engineering*, 12, 53(1), p. 012014.

ISO, 2019. ISO 6469-1:2019 - Electrically propelled road vehicles - Safety specifications.

Jeon, D. H. & Baek, S. M., 2011. Thermal modeling of cylindrical lithium ion battery during discharge cycle. *Energy Conversion and Management*, 52(8-9), pp. 2973-2981.

Jilte, R., Afzal, A. & Panchal, S., 2021. A novel battery thermal management system using nano-enhanced phase change materials. *Energy*, 3, Volume 219, p. 119564.

Kalaf, O. et al., 2021. Experimental and simulation study of liquid coolant battery thermal management system for electric vehicles: A review. *International Journal of Energy Research*, 4, 45(5), pp. 6495-6517.

Keklikcioglu, O., Ozceyhan, V., Keklikcioglu, O. & Ozceyhan, V., 2018. A Review of Heat Transfer Enhancement Methods Using Coiled Wire and Twisted Tape Inserts. *Heat Transfer - Models, Methods and Applications*, 6.

Kelly, K. J., Mihalic, M. & Zolot, M., 2002. Battery usage and thermal performance of the Toyota Prius and Honda Insight during chassis dynamometer testing. *Proceedings of the Annual Battery Conference on Applications and Advances,* Volume 2002-January, pp. 247-252.

Khateeb, S. A. et al., 2005. Thermal management of Li-ion battery with phase change material for electric scooters: experimental validation. *Journal of Power Sources*, 3, 142(1-2), pp. 345-353.

Khateeb, S. A., Farid, M. M., Selman, J. R. & Al-Hallaj, S., 2004. Design and simulation of a lithium-ion battery with a phase change material thermal management system for an electric scooter. *Journal of Power Sources*, 4, 128(2), pp. 292-307.

Kim, J., Oh, J. & Lee, H., 2019. Review on battery thermal management system for electric vehicles. *Applied Thermal Engineering,* 2, Volume 149, pp. 192-212.

Kiss, T., Lustbader, J. & Leighton, D., 2015. Modeling of an Electric Vehicle Thermal Management System in MATLAB/Simulink.

Koellner, W. G. et al., 2004. Recent advances in mining haul trucks. *IEEE Transactions on Industrial Electronics,* 4, 51(2), pp. 321-329.

KPMG, 2021. Decarbonizing the mining industry: Achieving 2030 and 2050 goals. 11.

Lai, X. et al., 2022. Remaining discharge energy estimation for lithium-ion batteries based on future load prediction considering temperature and ageing effects. *Energy,* 1, Volume 238, p. 121754.

Larrañaga-Ezeiza, M. et al., 2022. A novel direct liquid cooling strategy for electric vehicles focused on pouch type battery cells. *Applied Thermal Engineering,* 11, Volume 216, p. 118869.

Lee, J. & Mudawar, I., 2007. Assessment of the effectiveness of nanofluids for single-phase and two-phase heat transfer in micro-channels. *International Journal of Heat and Mass Transfer,* 2, 50(3-4), pp. 452-463.

Leonida, C., 2022. Powering Trucks for the Long Haul. *Engineering and Mining Journal,* 5.

Liang, K. et al., 2021. Advances and challenges of integrated thermal management technologies for pure electric vehicles. *Sustainable Energy Technologies and Assessments,* 8, Volume 46, p. 101319.

Lindgren, L., Grauers, A., Ranggård, J. & Mäki, R., 2022. Drive-Cycle Simulations of Battery-Electric Large Haul Trucks for Open-Pit Mining with Electric Roads. *Energies,* 7, 15(13), p. 4871.

Lin, J. et al., 2021. A review on recent progress, challenges and perspective of battery thermal management system. *International Journal of Heat and Mass Transfer,* 3, Volume 167, p. 120834.

Liu, H., Wei, Z., He, W. & Zhao, J., 2017. Thermal issues about Li-ion batteries and recent progress in battery thermal management systems: A review. *Energy Conversion and Management,* 10, Volume 150, pp. 304-330.

Liu, S. et al., 2014. Research on applicability of lithium titanate battery for low-floor vehicles. *Lecture Notes in Electrical Engineering,* 288 LNEE(VOL. 2), pp. 115-125.

Liu, S., Zhang, H. & Xu, X., 2021. A study on the transient heat generation rate of lithium-ion battery based on full matrix orthogonal experimental design with mixed levels. *Journal of Energy Storage,* 4, Volume 36, p. 102446.

Li, Y. et al., 2021. *Drive circuitry of an electric vehicle enabling rapid heating of the battery pack at low temperatures.* [Online].

Lopez, C. F., Jeevarajan, J. A. & Mukherjee, P. P., 2015. Experimental Analysis of Thermal Runaway and Propagation in Lithium-Ion Battery Modules. *Journal of The Electrochemical Society,* 7, 162(9), pp. A1905-A1915.

Lu, L. et al., 2013. A review on the key issues for lithium-ion battery management in electric vehicles. *Journal of Power Sources,* 3, Volume 226, pp. 272-288.

Lu, M. et al., 2020. Research progress on power battery cooling technology for electric vehicles. *Journal of Energy Storage,* 2, Volume 27, p. 101155.

Lyu, Y. et al., 2019. Electric vehicle battery thermal management system with thermoelectric cooling. *Energy Reports,* 11, Volume 5, pp. 822-827.

Madani, S. S., Schaltz, E. & Kær, S. K., 2018. A Review of Different Electric Equivalent Circuit Models and Parameter Identification Methods of Lithium-Ion Batteries. *ECS Transactions,* 11, 87(1), pp. 23-37.

Madera, M., Höflinger, W. & Kadnar, R., 2003. Ion chromatographic identification and quantification of glycol degradation products. *Journal of chromatography. A,* 5, 997(1-2), pp. 279-284.

Mahamud, R. & Park, C., 2011. Reciprocating air flow for Li-ion battery thermal management to improve temperature uniformity. *Journal of Power Sources,* 7, 196(13), pp. 5685-5696.

Mahle Behr, 2021. *Thermal management in electric and hybrid vehicles.* [Online] Available at: https://www.mahle-aftermarket.com/media/homepage/facelift/media-center/klima/2-4-broschu-re-thermomanagement-fu-r-e-mobilita-t-210712-en-lay.pdf

Mali, V. et al., 2021. Review on battery thermal management systems for energy-efficient electric vehicles. *Renewable and Sustainable Energy Reviews,* 11, Volume 151, p. 111611.

Mao, B. et al., 2020. Self-heating reaction and thermal runaway criticality of the lithium ion battery. *International Journal of Heat and Mass Transfer,* Volume 149, p. 119178.

Marín, A. & Goya, D., 2021. Mining—The dark side of the energy transition. *Environmental Innovation and Societal Transitions,* 12, Volume 41, pp. 86-88.

MathWorks, 2023a. *Fixed-Displacement Pump (TL) documentation.* [Online] Available at: https://nl.mathworks.com/help/hydro/ref/fixeddisplacementpumptl.html

MathWorks, 2023b. *Heat Exchanger (TL-MA) documentation.* [Online] Available at: https://nl.mathworks.com/help/hydro/ref/heatexchangertlma.html

MathWorks, 2023c. *Moist Air Properties (MA) documentation.* [Online] Available at: https://nl.mathworks.com/help/simscape/ref/moistairpropertiesma.html

MathWorks, 2023d. *Pipe (TL) documentation.* [Online] Available at: https://nl.mathworks.com/help/hydro/ref/pipetl.html

Ma, Y., Teng, H. & Thelliez, M., 2010. Electro-Thermal Modeling of a Lithium-ion Battery System. *SAE International Journal of Engines,* 3(2), pp. 306-317.

Mazumdar, J., 2013. All electric operation of ultraclass mining haul trucks. *Conference Record - IAS Annual Meeting (IEEE Industry Applications Society).*

McKinsey, 2021. Creating the zero-carbon mine. *McKinsey Metals and Mining,* 6.

Meintz, A., Starke, M. & Bohn, T., 2021. Charging Infrastructure Technologies: Development of a Multiport, >1 MW Charging System for Medium-and Heavy-Duty Electric VehiclesMeeting.

Mills, A., 2014. *Basic Heat and Mass Transfer.* 2 ed. s.l.:Pearson.

Modine, 2023. *Commercial Coolers - General Catalogue.* [Online]
Available at: www.modinecoolers.com

Moran, M. J., Shapiro, H. N., Boettner, D. D. & Bailey, M. B., 2012. *Principles of Engineering Thermodynamics.* 8 ed. s.l.:Wiley.

Moreno, G. et al., 2022. Electric-Drive Vehicle Power Electronics Thermal Management: Current Status, Challenges, and Future Directions. *Journal of Electronic Packaging, Transactions of the ASME,* 3.144(1).

Muralidharan, R., Kirk, T. & Koch Blank, T., 2019. Pulling the Weight of Heavy Truck Decarbonization: Exploring Pathways to Decarbonize Bulk Material Hauling in Mining. *Rocky Mountain Institute.*

Nair, A. M. et al., 2022. Phase change materials in building integrated space heating and domestic hot water applications: A review. *Journal of Energy Storage,* 10, Volume 54, p. 105227.

Nazari, A. & Farhad, S., 2017. Heat generation in lithium-ion batteries with different nominal capacities and chemistries. *Applied Thermal Engineering,* 10, Volume 125, pp. 1501-1517.

Nelson, P., Dees, D., Amine, K. & Henriksen, G., 2002. Modeling thermal management of lithium-ion PNGV batteries. *Journal of Power Sources.*

Nieto, N. et al., 2014. Novel thermal management system design methodology for power lithium-ion battery. *Journal of Power Sources,* 12, Volume 272, pp. 291-302.

Novak, P., 2013. Elevated Recharge of Electrochemical Cells.

O'Brien, J., 2020. The Path to Decarbonization: Miner's role in reducing emissions. *Deloitte Insights,* 2.

Olabi, A. G. et al., 2022. Battery thermal management systems: Recent progress and challenges. *International Journal of Thermofluids,* 8, Volume 15, p. 100171.

Park, C. & Jaura, A. K., 2003. Dynamic Thermal Model of Li-Ion Battery for Predictive Behavior in Hybrid and Fuel Cell Vehicles. *SAE Technical Papers,* 6.

Park, S. et al., 2019. Simulation on cooling performance characteristics of a refrigerant-cooled active thermal management system for lithium ion batteries. *International Journal of Heat and Mass Transfer,* Volume 135, pp. 131-141.

Pesaran, A., 2001. Battery thermal management in EV and HEVs: issues and solutions. *Advanced Automotive Battery Conference,* 2.

Pesaran, A. A., 2002. Battery thermal models for hybrid vehicle simulations. *Journal of Power Sources,* 8, 110(2), pp. 377-382.

Pesaran, A. A., Burch, S. & Keyser, M., 1999. An Approach for Designing Thermal Management Systems for Electric and Hybrid Vehicle Battery Packs Preprint.

Pesaran, A. et al., 2013. Tools for Designing Thermal Management of Batteries in Electric Drive Vehicles. *Technical Report National Renewable Energy Laboratory,* 2.

Poal, V., Panchare, D. & Mehta, B., 2021. Balancing of HVAC System Energy Consumption in Electric Vehicles. *SAE Technical Papers*, 9.Issue 2021.

Qin, Y. et al., 2020. *A rapid lithium-ion battery heating method based on bidirectional pulsed current: Heating effect and impact on battery life.* [Online].

Rafi, M. A. H., Rennie, R., Larsen, J. & Bauman, J., 2020. Investigation of fast charging and battery swapping options for electric haul trucks in underground mines. *2020 IEEE Transportation Electrification Conference and Expo, ITEC 2020,* 6.pp. 1081-1087.

Raijmakers, L. H., Danilov, D. L., Eichel, R. A. & Notten, P. H., 2019. A review on various temperature-indication methods for Li-ion batteries. *Applied Energy*, 4, Volume 240, pp. 918-945.

Ramadesigan, V. et al., 2012. Modeling and Simulation of Lithium-Ion Batteries from a Systems Engineering Perspective. *Journal of Electrochemical Society*, 159(3).

Ramandi, M. Y., Dincer, I. & Naterer, G. F., 2011. Heat transfer and thermal management of electric vehicle batteries with phase change materials. *Heat and Mass Transfer/Waerme- und Stoffuebertragung,* 7, 47(7), pp. 777-788.

Ranjbar, K. & Abasi, A., 2013. Failure assessment of crude oil preheating tubes in mono ethylene glycol–water mixture solution. *Engineering Failure Analysis*, 7, Volume 31, pp. 161-167.

Rao, Z., Qian, Z., Kuang, Y. & Li, Y., 2017. Thermal performance of liquid cooling based thermal management system for cylindrical lithium-ion battery module with variable contact surface. *Applied Thermal Engineering,* 8, Volume 123, pp. 1514-1522.

Rao, Z. & Wang, S., 2011. A review of power battery thermal energy management. *Renewable and Sustainable Energy Reviews,* Volume 15, pp. 4554-4571.

Rao, Z. et al., 2013. Experimental investigation on thermal management of electric vehicle battery with heat pipe. *Energy Conversion and Management,* 1, Volume 65, pp. 92-97.

Razi, M. F. I. M. et al., 2022. Li-NMC Battery Internal Resistance at Wide Range of Temperature. *Journal of Advanced Research in Fluid Mechanics and Thermal Sciences,* 8, 99(1), pp. 9-16.

Rizzo, G., Santis, A., Held, M. & Bachofen, M., 2018. World's Largest Electric Vehicle Operation in Mines. *ATZoffhighway worldwide,* 10, 11(4), pp. 12-19.

Roe, C. et al., 2022. Immersion cooling for lithium-ion batteries – A review. *Journal of Power Sources,* 3, Volume 525, p. 231094.

Sabbah, R., Kizilel, R., Selman, J. R. & Al-Hallaj, S., 2008. Active (air-cooled) vs. passive (phase change material) thermal management of high power lithium-ion packs:

Limitation of temperature rise and uniformity of temperature distribution. *Journal of Power Sources,* Volume 182, pp. 630-638.

SAE, 2021. *SAE J3271: Megawatt Charging System for Electric Vehicles.* [Online] Available at: https://www.sae.org/standards/content/j3271/

Santambrogio, M. et al., 2016. Effect of major degradation products of ethylene glycol aqueous solutions on steel corrosion. *Electrochimica Acta,* 6, Volume 203, pp. 439-450.

Sato, N., 2001. Thermal behavior analysis of lithium-ion batteries for electric and hybrid vehicles. *Journal of Power Sources,* 8, 99(1-2), pp. 70-77.

Schindler, M. et al., 2021. Evolution of initial cell-to-cell variations during a three-year production cycle. *eTransportation,* 5, Volume 8, p. 100102.

Schmidt, M., Staudt, P. & Weinhardt, C., 2021. Decision support and strategies for the electrification of commercial fleets. *Transportation Research Part D: Transport and Environment,* 8, Volume 97, p. 102894.

Schmitt, J. et al., 2017. Impedance change and capacity fade of lithium nickel manganese cobalt oxide-based batteries during calendar aging. *Journal of Power Sources,* 6, Volume 353, pp. 183-194.

Shell, 2021. *Shell Immersion Cooling Fluid S5 X,* [Online] Available at: https://www.shell-livedocs.com/data/published/en/615128f8-db18-4709-bb03-10bf668eb6eb.pdf

Shen, M. & Gao, Q., 2020. System simulation on refrigerant-based battery thermal management technology for electric vehicles. *Energy Conversion and Management,* 1, Volume 203, p. 112176.

Sinnott, R. & Towler, G., 2020. *Chemical Engineering Design - Sixth Edition.* s.l.:Butterworth-Heinemann.

Smith, J., Singh, R., Hinterberger, M. & Mochizuki, M., 2018. Battery thermal management system for electric vehicle using heat pipes. *International Journal of Thermal Sciences,* 12, Volume 134, pp. 517-529.

Smith, K. & Wang, C. Y., 2006. Power and thermal characterization of a lithium-ion battery pack for hybrid-electric vehicles. *Journal of Power Sources,* 9, 160(1), pp. 662-673.

Sridhar, A., 2013. Single phase and boiling heat transfer under steady and pulsating confined jet impingement.

Steger, F., Krogh, J., Meegahapola, L. & Schweiger, H. G., 2022. Calculating Available Charge and Energy of Lithium-Ion Cells Based on OCV and Internal Resistance. *Energies 2022, Vol. 15, Page 7902,* 10, 15(21), p. 7902.

Suarez, C. & Martinez, W., 2019. Fast and Ultra-Fast Charging for Battery Electric Vehicles - A Review. *2019 IEEE Energy Conversion Congress and Exposition, ECCE 2019,* 9.pp. 569-575.

Sundin, D. W. & Sponholtz, S., 2020. Thermal management of Li-ion batteries with single-phase liquid immersion cooling. *IEEE Open Journal of Vehicular Technology,* Volume 1, pp. 82-92.

Tarawneh, C., 2006. *Chapter 11 Supplemental Material: LMTD Method for Multipass and Cross-Flow Heat Exchangers.* [Online]
Available at:
https://faculty.utrgv.edu/constantine.tarawneh/Heat%20Transfer/ch11_supp.pdf

Tete, P. R., Gupta, M. M. & Joshi, S. S., 2021. Developments in battery thermal management systems for electric vehicles: A technical review. *Journal of Energy Storage,* 3, Volume 35, p. 102255.

The Parker Bay Company, 2023. *Equipment Database: Mining Trucks.* [Online] Available at: https://parkerbaymining.com/mining-equipment/mining-trucks

The Royal Society, 2020. Ammonia: zero-carbon fertiliser, fuel and energy store.

Tung, S. C., Woydt, M. & Shah, R., 2020. Global Insights on Future Trends of Hybrid/EV Driveline Lubrication and Thermal Management. *Frontiers in Mechanical Engineering,* 10, Volume 6, p. 74.

Vargas, R. S., Gonda, V. & Ruiz, L. C., 2018. Thermal analysis and control for heating of an extrusion die.

Verbruggen, F. et al., 2018. *Evaluation of the state-of-the-art of full-electric medium and heavy-duty trucks.* Kobe City, s.n.

Vikram, S., Vashisht, S. & Rakshit, D., 2022. Performance analysis of liquid-based battery thermal management system for Electric Vehicles during discharge under drive cycles. *Journal of Energy Storage,* 11, Volume 55, p. 105737.

Wang, J. et al., 2011. Cycle-life model for graphite-LiFePO4 cells. *Journal of Power Sources,* 4, 196(8), pp. 3942-3948.

Wang, Q., Jiang, B., Li, B. & Yan, Y., 2016. A critical review of thermal management models and solutions of lithium-ion batteries for the development of pure electric vehicles. *Renewable and Sustainable Energy Reviews,* 10, Volume 64, pp. 106-128.

Wang, X. et al., 2022. A critical review on thermal management technologies for motors in electric cars. *Applied Thermal Engineering*, 1, Volume 201, p. 117758.

Wang, Y. et al., 2020. Experimental Performance of a Solar Air Collector with a Perforated Back Plate in New Zealand. *Energies 2020, Vol. 13, Page 1415,* 3, 13(6), p. 1415.

Watari, T. et al., 2019. Total material requirement for the global energy transition to 2050: A focus on transport and electricity. *Resources, Conservation and Recycling,* 9, Volume 148, pp. 91-103.

Weinert, J. X., Burke, A. F. & Wei, X., 2007. Lead-acid and lithium-ion batteries for the Chinese electric bike market and implications on future technology advancement. *Journal of Power Sources,* 10, 172(2), pp. 938-945.

Wu, K. et al., 2012. Investigation on Li4Ti5O12 batteries developed for hybrid electric vehicle. *Journal of Applied Electrochemistry,* 12, 42(12), pp. 989-995.

Wu, W. et al., 2019. A critical review of battery thermal performance and liquid based battery thermal management. *Energy Conversion and Management,* 2, Volume 182, pp. 262-281.

Xia, G., Cao, L. & Bi, G., 2017. A review on battery thermal management in electric vehicle application. *Journal of Power Sources,* 11, Volume 367, pp. 90-105.

Xu, J., Lan, C., Qiao, Y. & Ma, Y., 2017. Prevent thermal runaway of lithium-ion batteries with minichannel cooling. *Applied Thermal Engineering,* Volume 110, pp. 883-890.

Yang, S. et al., 2019. A review of lithium-ion battery thermal management system strategies and the evaluate criteria. *electrochemsci.org,* Volume 14, pp. 6077-6107.

Ye, Y. et al., 2012. Electro-thermal modeling and experimental validation for lithium ion battery. *Journal of Power Sources,* Volume 199, pp. 227-238.

Yokoyama, A., Osaka, T., Imanishi, Y. & Sekiya, S., 2011. Thermal Management System for Electric Vehicles. *SAE International Journal of Materials and Manufacturing,* 4(1), pp. 1277-1285.

Yue, H., Zhao, Y., Ma, X. & Gong, J., 2012. Ethylene glycol: properties, synthesis, and applications. *Chemical Society Reviews,* 5, 41(11), pp. 4218-4244.

Yuksel, T., Litster, S., Viswanathan, V. & Michalek, J. J., 2017. Plug-in hybrid electric vehicle LiFePO4 battery life implications of thermal management, driving conditions, and regional climate. *Journal of Power Sources,* 1, Volume 338, pp. 49-64.

Zadeh, P. G., Gholamalizadeh, E., Wang, Y. & Chung, J. D., 2022. Electrochemical modeling of a thermal management system for cylindrical lithium-ion battery pack considering battery capacity fade. *Case Studies in Thermal Engineering,* 4, Volume 32, p. 101878.

Zeng, Y. et al., 2021. A review of thermal physics and management inside lithium-ion batteries for high energy density and fast charging. *Energy Storage Materials,* 10, Volume 41, pp. 264-288.

Zhang, X. et al., 2022. A review on thermal management of lithium-ion batteries for electric vehicles. *Energy,* 1, Volume 238, p. 121652.

Zhang, X., Peng, H., Wang, H. & Ouyang, M., 2018. Hybrid Lithium Iron Phosphate Battery and Lithium Titanate Battery Systems for Electric Buses. *IEEE Transactions on Vehicular Technology,* 2, 67(2), pp. 956-965.

Zhao, G., Wang, X., Negnevitsky, M. & Zhang, H., 2021. A review of air-cooling battery thermal management systems for electric and hybrid electric vehicles. *Journal of Power Sources,* 7, Volume 501, p. 230001.

Appendices

Appendix I: MHDEV activity data

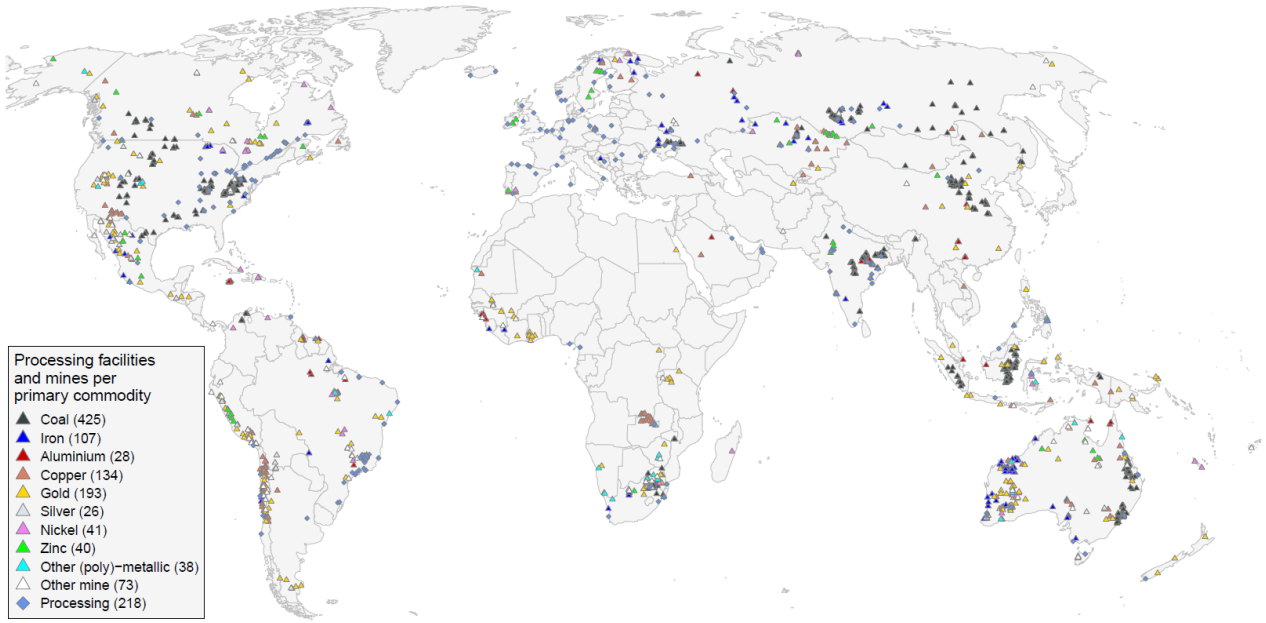

Figure 21: Global locations of metal and coal mining (Fineprint, 2023)

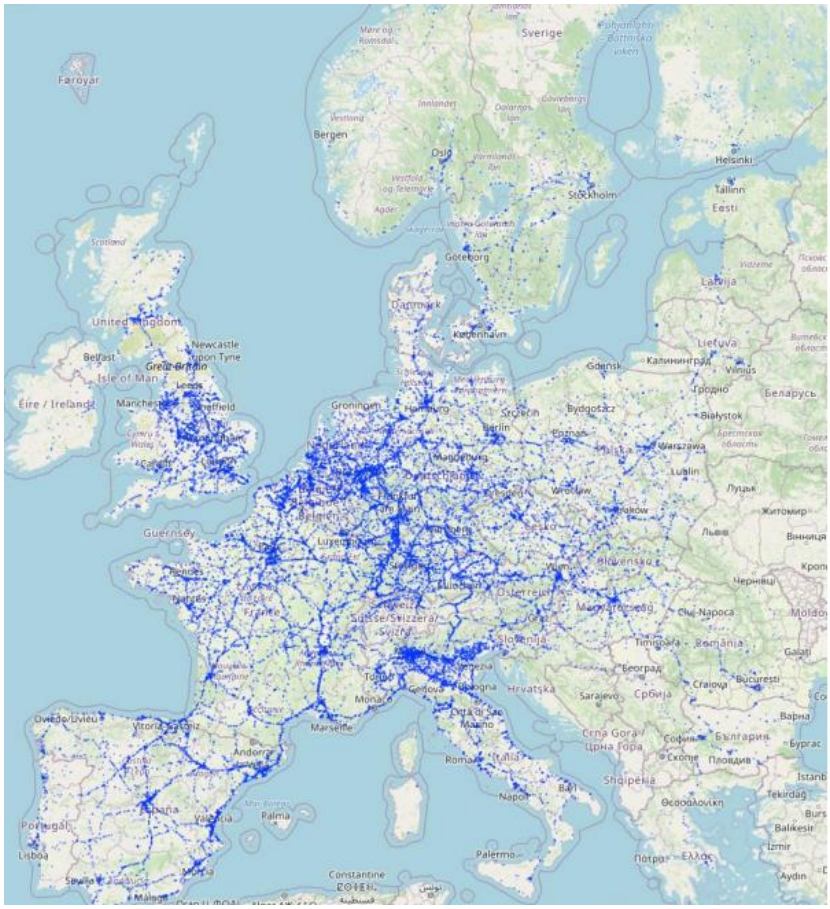

Figure 22: Truck stop locations of long-haul trucks (Fraunhofer, 2021)

Appendix II: Battery specification list overview

Part number	Manufacturer	Battery Type	Capacity [mA * hr]	Vnominal [V]	Weight [g]	Energy density [mAhr/g]
ALM12V7	A123	Lithium - ion	4600	13.2	840	5.48
AMP20M1HD	A123	Lithium - ion	19600	3.3	496	39.52
ANR26650M1	A123	Lithium - ion	2300	3.3	72	31.94
PD3032	Korea_Powercell	Lithium - ion	180	3.7	7.2	25.00
NCA103450	Panasonic	Lithium - ion	2200	3.6	38.3	57.44
NCA463436A	Panasonic	Lithium - ion	680	3.6	12.4	54.84
NCA593446	Panasonic	Lithium - ion	1260	3.6	20.6	61.17
NCA623535	Panasonic	Lithium - ion	1050	3.6	17.6	59.66
NCA673440	Panasonic	Lithium - ion	1220	3.6	20.3	60.10
NCA793540	Panasonic	Lithium - ion	1515	3.6	24.7	61.34
NCA843436	Panasonic	Lithium - ion	1275	3.6	23	55.43
NCR18500A	Panasonic	Lithium - ion	1900	3.6	33.5	56.72
NCR18650BD	Panasonic	Lithium - ion	3030	3.6	49.5	61.21
NCR18650BF	Panasonic	Lithium - ion	2835	3.6	46.5	60.97
NCR18650PF	Panasonic	Lithium - ion	2700	3.6	48	56.25
UF103450P	Panasonic	Lithium - ion	1880	3.6	38.5	48.83
UF463450F	Panasonic	Lithium - ion	960	3.7	18.5	51.89
UF553443ZU	Panasonic	Lithium - ion	1000	3.7	18.7	53.48
UF653450S	Panasonic	Lithium - ion	1250	3.7	25.1	49.80
UR18650A	Panasonic	Lithium - ion	2150	3.6	44	48.86
UR18650ZTA	Panasonic	Lithium - ion	2900	3.7	49	59.18
UR18650F	Sanyo	Lithium - ion	2300	3.7	44.5	51.69
T18650	Tenergy	Lithium - ion	2200	3.6	45	48.89
U1_12XP	Valence	Lithium - ion	40000	12.8	6520	6.13

Appendix III: Studied battery specification sheet

Panasonic

Lithium Ion

NCA793540

Features & Benefits

- High energy density
- Long, stable power and long run time
- Ideal for portable communications, portable computing, DSC and Camcorder.

* At temperatures below 10°C, charge at a 0.35C rate.

Specifications

Rated capacity(1)	Min. 1485mAh
Capacity(2)	Min. 1515mAh Typ. 1570mAh
Nominal voltage	3.6V
Charging	CC-CV, Std. 1061mA, 4.20V, 4.0 hrs
Weight (max.)	24.7g
Temperature	Charge*: 0 to +45°C Discharge: -20 to +60°C Storage: -20 to +50°C
Energy density	Volumetric: 473 Wh/l Gravimetric: 216 Wh/kg

(1) At 20°C (2) At 25°C

Dimensions

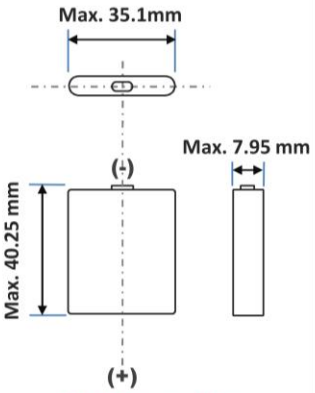

For Reference Only

Charge Characteristics

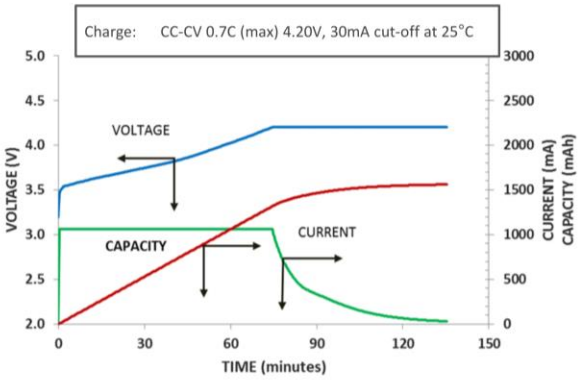

Cycle Life Characteristics

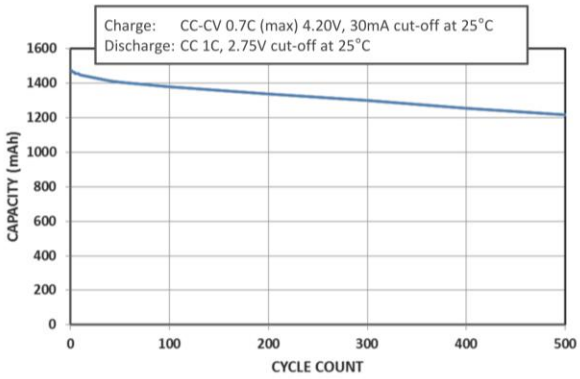

Discharge Characteristics (by temperature)

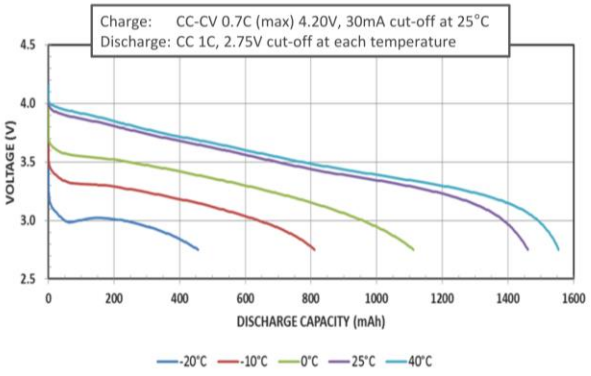

Discharge Characteristics (by rate of discharge)

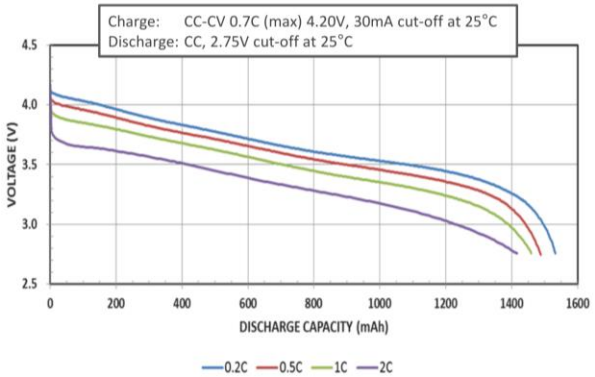

The data in this document is for descriptive purposes only and is not intended to make or imply any guarantee or warranty.

Jun. 2016 | Copyright© 2016 All Rights Reserved.

Appendix IV: MATLAB calculation model

General specifications

```
% Battery cell specifications
D_cell  = 0.00795;              % cell thickness
W_cell  = 0.0351;               % cell width
H_cell  = 0.04025;              % cell height
m       = 0.0247;               % weight of cell [kg]
Abat_tot = (2*H_cell*W_cell) + (2*H_cell*D_cell) + (2*W_cell*D_cell);      % total battery
cell surface area [m2]
R_cell  = 0.02;                 % cell internal resistance [Ohm]

% Battery pack specifications
E_pack = 500;                   % battery pack energy capacity [kWh]
nr_p = 220;                     % number of battery cells in parallel
nr_s = 417;                     % number of battery cells in series
n_cells = nr_p*nr_s;            % total number of battery cells in the pack
pack_weight = n_cells*m;        % total weight of the cells in the battery pack

% Charging specifications
P_charge = 4.5*10^6;            % charging power [MW]
U_charge = 1500;                % charging voltage [V]
I_charge = P_charge/U_charge;   % charging current [A]
```

Determining cell power characteristics

```
% Ah: when cells in parallel, add the cells Ah. In series system, Ah is not increased
% V: When cells in parallel, voltage stays same. When in series, system voltage is increases
% A: When cells in parallel, add the cells current. When in series, A is not increased
% P: just a multiplication of V and A

C_rate = P_charge/E_pack;

U_cell = U_charge/nr_s;
I_cell = I_charge/nr_p;
P_cell = U_cell*I_cell;
```

Determining cell heat generation

```
% assuming no heat loss of the battery cell to its surroundings
% (adiabatic), this section calculates what the temperature of the cell
% will be as a result of a heat load from one charging session

% using Ohmic heating equation to determine heat generation in cell
Q_gen_cell = R_cell*(I_cell^2);
```

C-rate and duration of charging session

```
% using energy stored in pack to calculate duration of the charging session and the C-rate
C_rate = P_charge/(E_pack*1000);                                    % C rate of charging
t_charge = (E_pack*1000*3600)/P_charge;                             % charging time to fully
charge the battery pack [s]
```

Cell heat generation plot

```
% making a plot to visualize how the charging efficiency decreases for higher charging powers
I_plot = linspace(0, 3000, 31);                                    % a range of power
values through battery pack
I_cell_plot = I_plot./nr_p;                                        % a range of power
values through battery cell

% making a vector to use as the x-axis in the plot
P_cell_plot = I_cell_plot*U_cell;                                  % converting the
I_cell_plot to power for battery cell as its more relatable
P_pack_plot = I_cell_plot*nr_p*U_cell*nr_s;                        % converting to power
for the whole pack

% using Ohmic heating equation to determine heat generation in cell
Q_gen_cell_plot = R_cell*(I_cell_plot.^2);                         % heat generated per
cell [W]

%plot
figure;
x1 = P_pack_plot;
y1 = Q_gen_cell_plot;
plot(x1,y1, '-', 'LineWidth', 2)
title ('Battery cell heat generation from Ohmic Heating')
xlabel ('Power [W]')
ylabel ('Heat generation [W]')

hold on;
```

Power loss percentage

```
P_loss = ((Q_gen_cell)/P_cell)*100;                                % determining
percentage of charging power that is lost to heat, at the current set power (ratio of actual
power in and loss from heat) [%]
P_loss_plot = (Q_gen_cell_plot./P_cell_plot)*100;                  % making a plot to
visualize this power loss at varying charging power

figure;
x2 = P_pack_plot;
y2 = P_loss_plot;
y22 = 100-P_loss_plot;
yyaxis left
plot(x2,y2, '-', 'LineWidth', 2)
ylim([0,100])
ylabel ('Power loss [%]')
hold on;

yyaxis right
plot (x2, y22, '-', 'LineWidth', 2)
title('Charge efficiency for various charging power')
ylim([0,100])
xlabel ('Power [MW]')
ylabel ('Charging efficiency [%]')

legend ('power loss', 'charge efficiency')

hold on;
```

Appendix V: BTMS Simulink Model

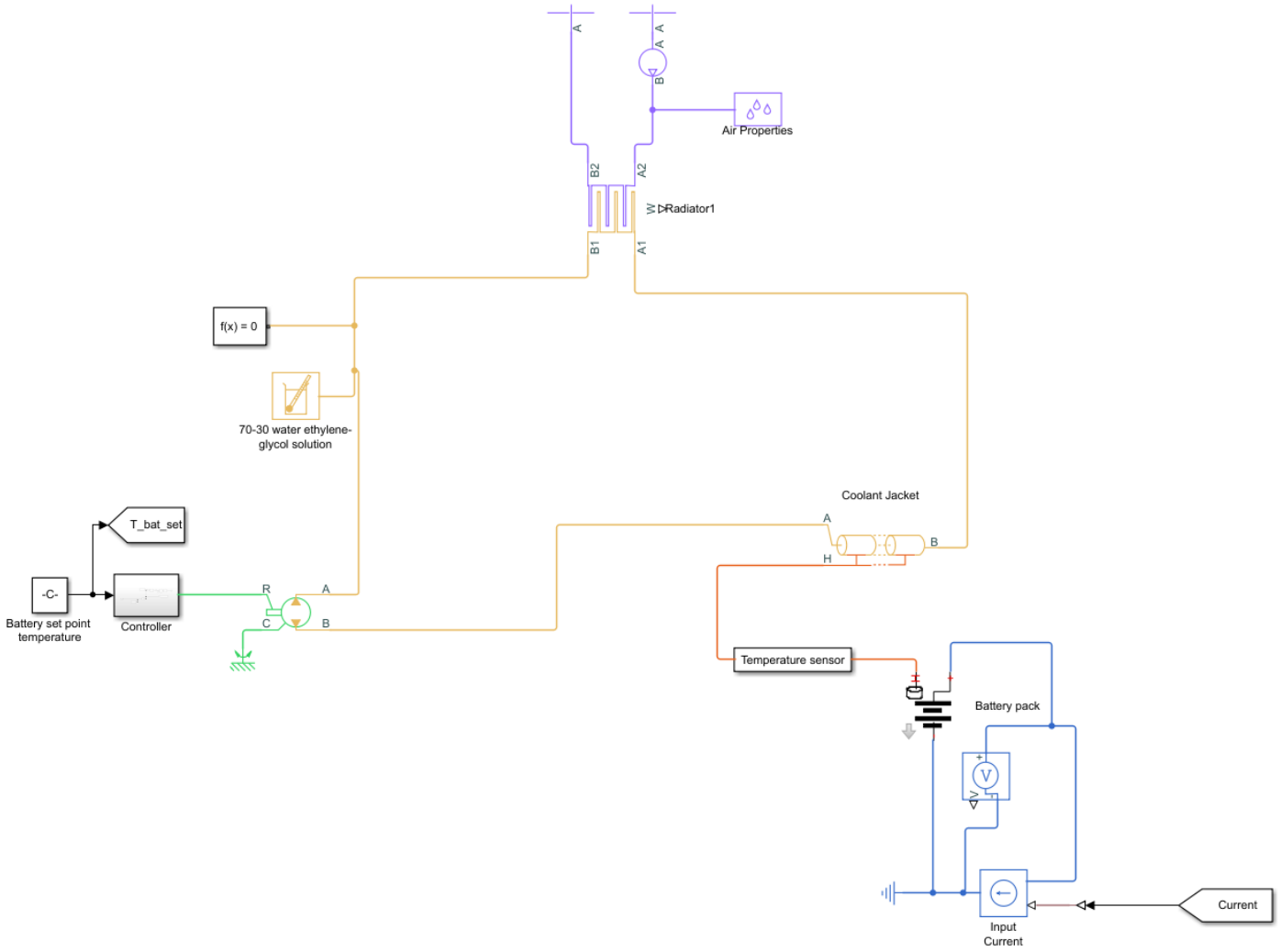

Figure 23: Overview of the BTMS Simulink model

Appendix VI: Refrigerants thermal specifications

Refrigerant	$\log(P/1) = A/T + B$	Molar mass $g \cdot mol^{-1}$	T_b (°C)	T_b K	C_p $kJ \cdot kg^{-1} \cdot K^{-1}$	C_p $J \cdot mol^{-1} \cdot K^{-1}$	ΔH $kJ \cdot kg^{-1}$	ΔH_{molar} $J \cdot mol^{-1}$	$C_p - \Delta H_{molar}/T_b$ $J \cdot mol^{-1} \cdot K^{-1}$
R717 (Ammonia)	$A = -1218.6$; $B = 7.0751$	17.03	−33.35	239.8	2.297	39.12	1369	23 314	−58.11
R134a	$A = -1231.1$; $B = 6.9447$	102	−26.11	247.0	0.7942	81.01	217.9	22 226	−8.96
R1234yf	$A = -1098.2$; $B = 6.5146$	114	−29.49	243.7	0.8127	92.65	180.3	20 554	8.29
R1234ze(E)	$A = -1249.4$; $B = 6.8754$	114	−19.28	253.9	0.7782	88.71	215.2	24 533	−7.92
R123	$A = -1509.6$; $B = 6.9594$	152.9	27.78	300.9	0.7128	108.99	170.6	26 085	22.31
R410a	$A = -1101.2$; $B = 6.9304$	72.6	−51.45	221.7	0.8097	58.78	272.9	19 813	−30.58
R290 (propane)	$A = -1123.5$; $B = 6.8116$	44.1	−42.1	231.1	1.461	64.43	425.8	18 778	−16.84
R32	$A = -1109.1$; $B = 6.9656$	52	−51.66	221.5	0.8767	45.59	381.9	19 859	−44.07
R407C	$A = -1108.2$; $B = 6.7988$	86.2	−43.63	229.5	0.7616	65.65	244.9	21 110	−26.33
R600a (i-butane)	$A = -1255.7$; $B = 6.7519$	56.06	−11.68	261.5	1.558	87.34	365.9	20 512	8.89
R22	$A = -1168.4$; $B = 6.9678$	86.5	−40.82	232.3	0.6227	53.86	233.9	20 232	−33.22
R50 (methane)	$A = -444.23$; $B = 5.9815$	16.04	−161.5	111.7	2.218	35.58	510.8	8 193	−37.81
R600 (n-butane)	$A = -1300.3$; $B = 6.7196$	56.06	−0.5273	272.6	1.65	92.50	384.8	21 572	13.37

Table 16: Specifications of common refrigerants (Ally, et al., 2019)

Appendix VII: Refrigerants environmental specifications

Refrigerant group	Refrigerant example	ODP	GWP_{100}	Atmospheric lifetime (years)	Flammability
CFCs	R-11, R-12, R-115	0.6–1	4750–14400	45–1700	Nonflammable
HCFCs	R-22, R-141b, R-124	0.02–0.11	400–1800	1–20	Nonflammable
HFCs	R-407C, R-32, R-134a	0	140–11700	1–300	Nonflammable or mildly flammable
HFOs	R-1234fy, R-1234ze, R-1234yz	0	0–12	-	Mildly flammable
Natural refrigerants	CO_2(R744), NH_3(R717), HC (Propane (R-290), n-Butane(R-600) , iso-Butane (R-600a))	0	0	Few days	HCs: Highly flammable R-717: Flammable R-744: Nonflammable

Table 17: Specifications related to the environmental effects of refrigerants (Ally, et al., 2019)

Appendix VIII: Specification sheet WEG coolant

Temp.	Volume Percent Ethylene Glycol									
°C	0%	10%	20%	30%	40%	50%	60%	70%	80%	90%
-35							2.845	2.613	2.371	
-30						3.089	2.867	2.637	2.398	2.149
-25					3.319	3.108	2.889	2.662	2.424	2.178
-20					3.335	3.128	2.911	2.686	2.451	2.207
-15				3.548	3.352	3.147	2.933	2.710	2.478	2.236
-10				3.562	3.369	3.166	2.954	2.734	2.504	2.265
-5			3.759	3.576	3.386	3.185	2.976	2.759	2.531	2.294
0		3.939	3.771	3.590	3.403	3.205	2.998	2.783	2.558	2.323
5	4.229	3.947	3.782	3.604	3.419	3.224	3.020	2.807	2.584	2.352
10	4.195	3.956	3.794	3.619	3.436	3.243	3.042	2.831	2.611	2.381
15	4.168	3.965	3.805	3.633	3.453	3.263	3.063	2.855	2.638	2.410
20	4.147	3.974	3.816	3.647	3.46:	3.282	3.085	2.880	2.664	2.439
25	4.132	3.982	3.828	3.661	3.486	3.301	3.107	2.904	2.691	2.468
30	4.121	3.991	3.839	3.675	3.503	3.321	3.129	2.928	2.717	2.497
35	4.115	4.000	3.851	3.690	3.520	3.340	3.151	2.952	2.744	2.526
40	4.114	4.009	3.862	3.704	3.537	3.359	3.172	2.977	2.771	2.555
45	4.115	4.017	3.874	3.718	3.554	3.379	3.194	3.001	2.797	2.584
50	4.120	4.026	3.885	3.732	3.56:	3.398	3.216	3.025	2.824	2.613
55	4.128	4.035	3.897	3.746	3.587	3.417	3.238	3.049	2.851	2.642
60	4.138	4.044	3.908	3.761	3.604	3.437	3.260	3.074	2.877	2.671
65	4.150	4.052	3.920	3.775	3.621	3.456	3.281	3.098	2.904	2.700
70	4.164	4.061	3.931	3.789	3.637	3.475	3.303	3.122	2.931	2.729
75	4.179	4.070	3.943	3.803	3.654	3.495	3.325	3.146	2.957	2.758
80	4.196	4.079	3.954	3.817	3.671	3.514	3.347	3.171	2.984	2.787
85	4.213	4.087	3.966	3.831	3.688	3.533	3.369	3.195	3.011	2.816
90	4.231	4.096	3.977	3.846	3.705	3.553	3.390	3.219	3.037	2.845
95	4.249	4.105	3.989	3.860	3.721	3.572	3.412	3.243	3.064	2.875
100	4.267	4.113	4.000	3.874	3.738	3.591	3.434	3.268	3.091	2.904
105	4.285	4.122	4.012	3.888	3.755	3.610	3.456	3.292	3.117	2.933
110	4.303	4.131	4.023	3.902	3.772	3.630	3.478	3.316	3.144	2.962
115	4.321	4.140	4.035	3.917	3.788	3.649	3.499	3.340	3.171	2.991
120	4.338	4.148	4.046	3.931	3.805	3.668	3.521	3.365	3.197	3.020

Table 18: Specific heat in kJ/kgK of various compositions of DOWTHERM SR-1 water ethylene glycol (Dow, 2020)

Appendix IX: Vapor-compression refrigeration diagrams

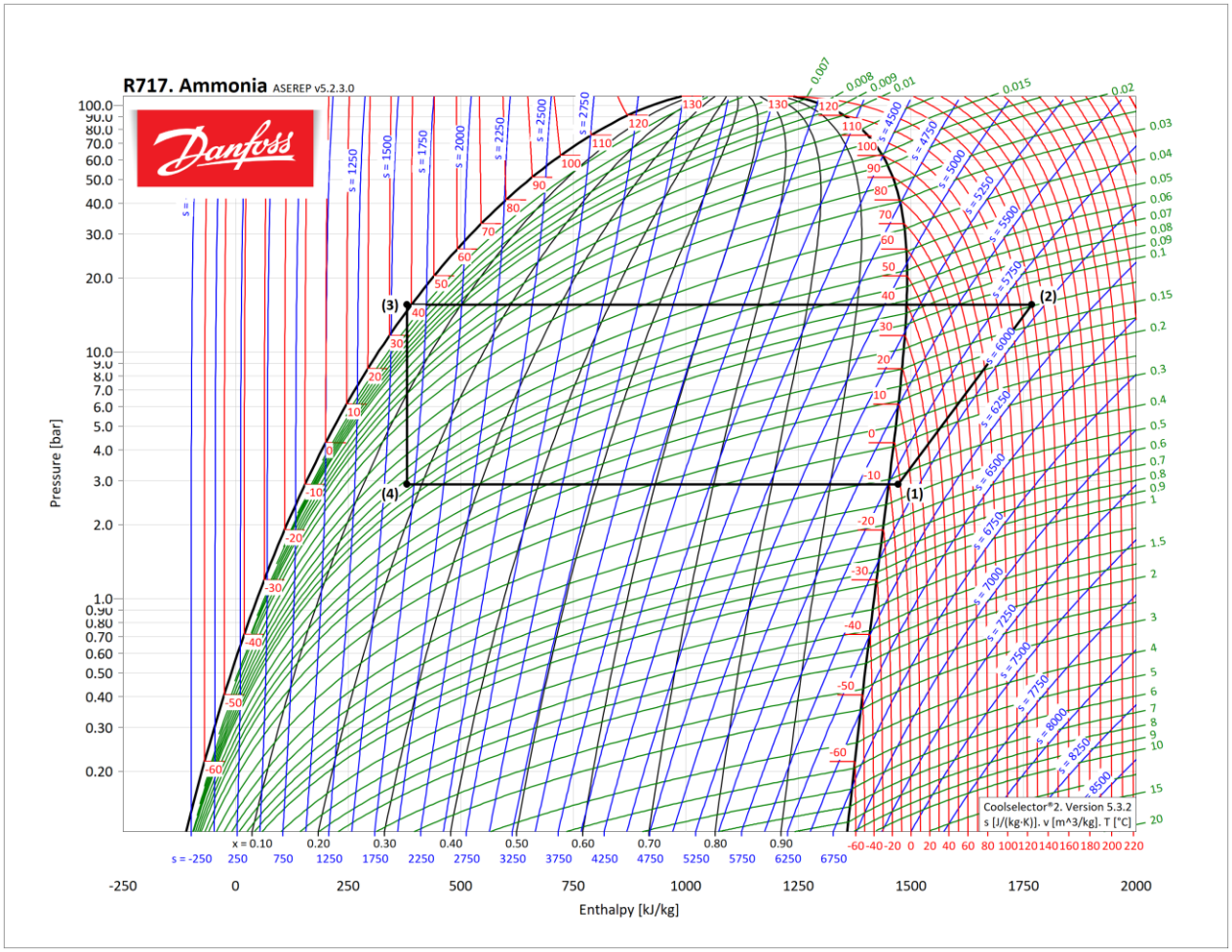

Figure 24: Log-ph diagram of R717

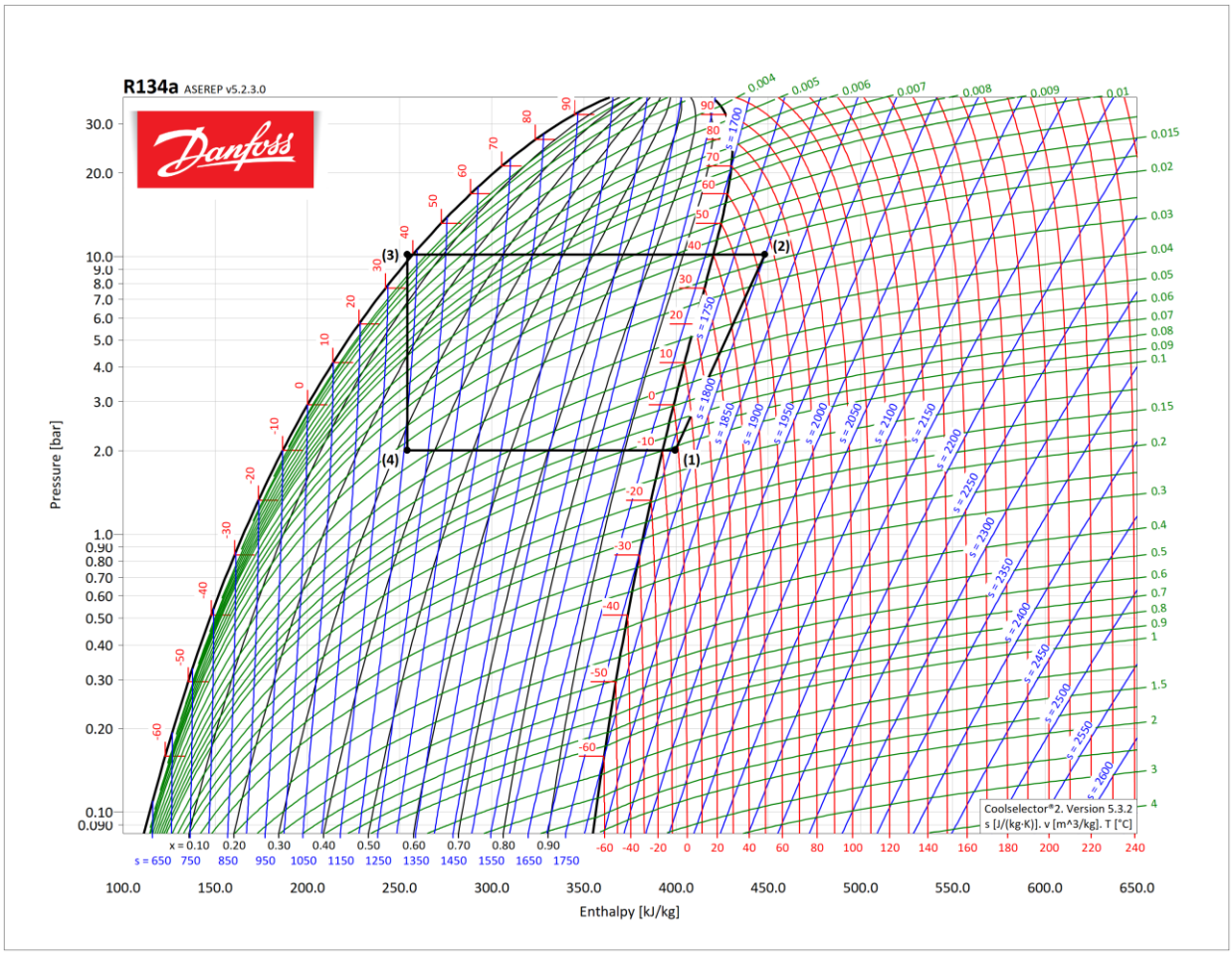

Figure 25: Log-ph diagram of R134a

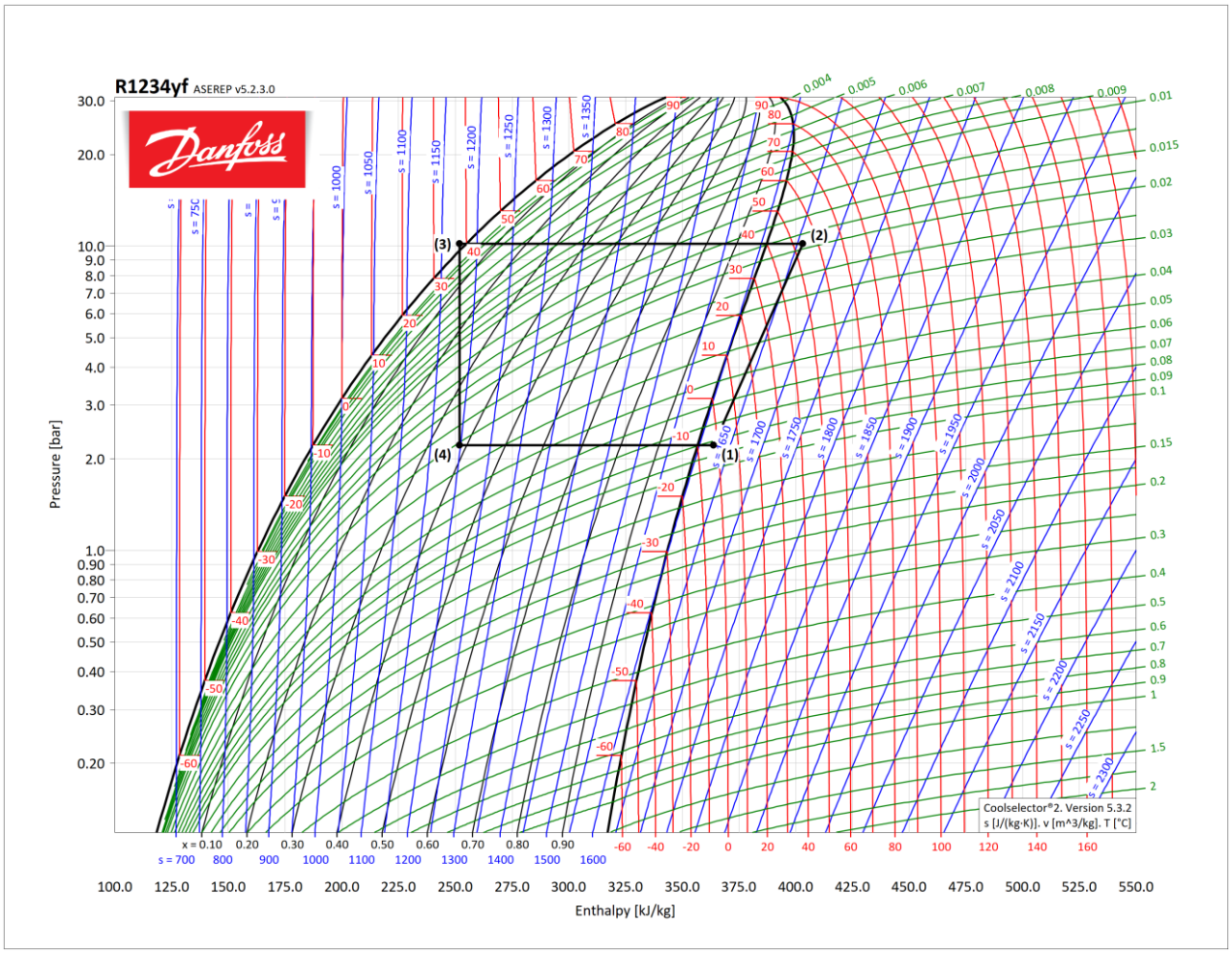

Figure 26: Log-ph diagram of R1234yf

Appendix X: Overall coefficients air-cooled exchangers

Btu/(°F · ft² · h)

Condensing	Coefficient	Liquid cooling	Coefficient
Ammonia	110	Engine-jacket water	125
Freon-12	70	Fuel oil	25
Gasoline	80	Light gas oil	65
Light hydrocarbons	90	Light hydrocarbons	85
Light naphtha	75	Light naphtha	70
Heavy naphtha	65	Reformer liquid streams	70
Reformer reactor effluent	70	Residuum	15
Low-pressure steam	135	Tar	7
Overhead vapors	65		

Gas cooling	Operating pressure, lb./sq. in. gage	Pressure drop, lb./sq. in.	Coefficient
Air or flue gas	50	0.1 to 0.5	10
	100	2	20
	100	5	30
Hydrocarbon gas	35	1	35
	125	3	55
	1000	5	80
Ammonia reactor stream			85

Bare-tube external surface is 0.262 ft²/ft.
Fin-tube surface/bare-tube surface ratio is 16.9.
To convert British thermal units per hour-square foot-degrees Fahrenheit to joules per square meter-second-kelvins, multiply by 5.6783; to convert pounds-force per square inch to kilopascals, multiply by 6.895.

Table 19: Overall heat transfer coefficients for air-cooled heat exchangers on bare-tube basis (Green & Southard, 2019)

Appendix XI: Calculation cooling plate temperature gradient

As heat transfer by conduction through the metal wall of a cooling plate is a thermal resistance that is encountered, it has to be determined how significant the effect of this thermal resistance is on the temperature gradient through the metal wall of a cooling plate.

This thermal resistance phenomena is described by Fourier's law:

$$\dot{Q} = \frac{\Delta T}{R}$$

- Where $\dot{Q}$ is the heat flux through the plane in W
- ΔT is the temperature difference between the two ends of the material in K
- R is the thermal resistance in K/W

The thermal resistance is defined as:

$$R = \frac{L}{\lambda * A}$$

- Where L is the thickness of the cooling plate in m
- λ is the thermal conductivity of the cooling plate in $\frac{W}{mK}$
- A is the area of the plane through which heat transfer takes place in m^2

The Fourier equation for 1D steady heat transfer by conduction can be simplified to:

$$q' = \frac{\lambda}{L}\,(T_{bat} - T_s)$$

- Where T_{bat} is the maximum battery temperature that occurs at the surface of the battery cell in K
- T_s is the temperature of the coolant channel wall inside the cooling plate in K
- λ is the thermal conductivity of the cooling plate material in W/mK
- q' is heat flux through the cooling plate material defined in W/m^2

Calculating this q' based on the battery contact surface area shown in Appendix III gives a heat generation of:

$$q' = \frac{\dot{Q}_{cell}}{A_{cell}} = \frac{3.729}{3.199 * 10^{-4}} = 11622.3\ W/m^2$$

Assuming a thermal conductivity of aluminum of 235 W/mK and solving for a cooling plate wall thickness of 1 mm gives:

$$11622.3 = \frac{235}{0.001}\,(T_{bat} - T_s)$$

$$(T_{bat} - T_s) = 0.0495\ ℃$$

This result indicates that for each additional millimeter of cooling plate wall thickness, the difference between the battery surface temperature and the cooling plate channel wall temperature increases with $0.0495\ ℃$. As this temperature difference is significantly small, it is assumed in this study that the battery surface temperature is equal to the temperature of the cooling channel wall inside a cooling plate where convection to a coolant takes place.

Appendix XII: R717 Compressor specifications

Figure 27: Ammonia compressor unit with on top the screw compressor and on the bottom a 3-stage oil separator (GEA, 2021)

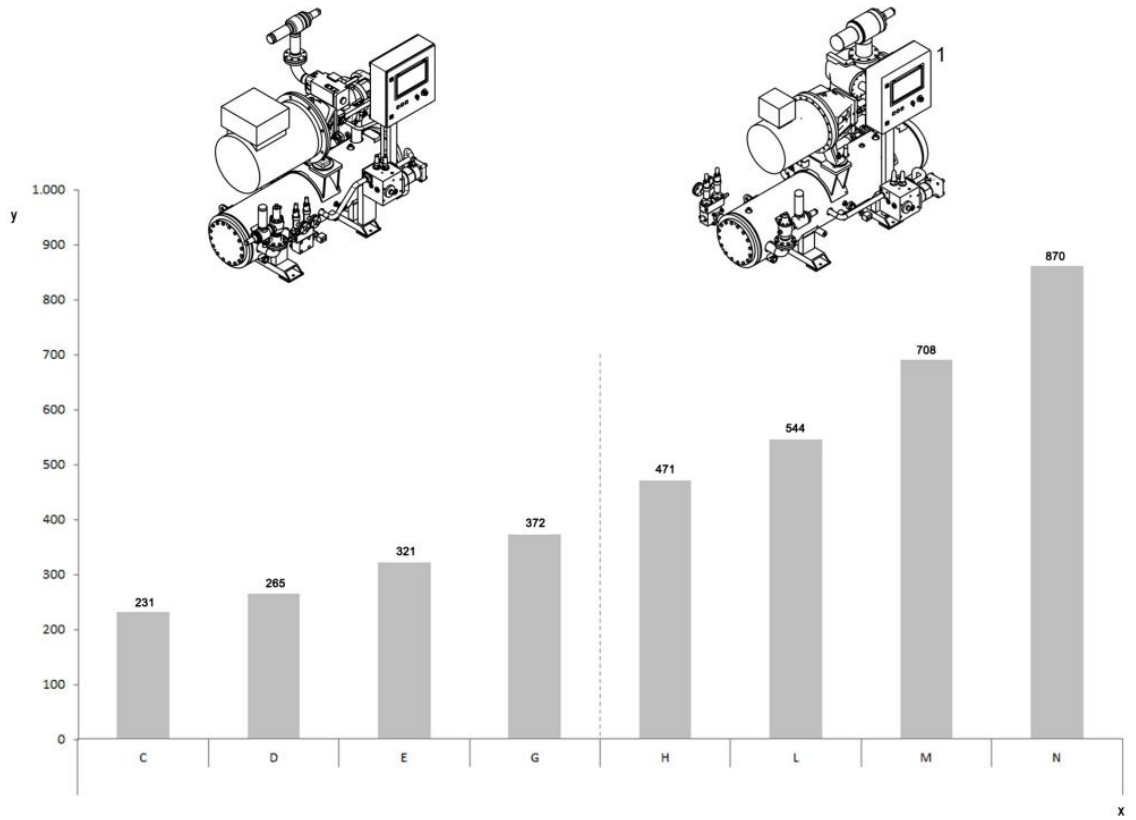

y	Swept volume in m³/h at 2940 rpm
x	Compressor frame size
1	Oil separator (installed horizontally)

Figure 28: Variations of GEA ammonia compressor and their volumetric flow rate (GEA, 2021)

GEA Grasso M	Motor speed (rpm)	Cooling capacity (kW)			Dimensions* (mm)			Weight* (kg)
		R717 −10/+35 °C	R717 −40/−10 °C	R290 −10/+35 °C	L	W	H	without motor
GEA Grasso M-C	3,600 4,500	172 219	54 68	143 181	2,200	1,225	1,950	1,350
GEA Grasso M-D	3,600 4,500	206 262	64 81	171 217	2,200	1,225	1,950	1,450
GEA Grasso M-E	3,600 4,500	247 313	76 96	205 259	2,200	1,225	1,975	1,550
GEA Grasso M-G	3,600 4,500	293 372	88 111	243 308	2,300	1,225	1,975	1,650
GEA Grasso M-H	3,600 4,500	374 471	116 147	308 389	2,550	1,225	1,950	1,725
GEA Grasso M-L	3,600 4,500	432 544	134 169	356 449	2,550	1,225	1,950	1,800
GEA Grasso M-M	3,600 4,500	568 715	176 222	468 590	2,600	1,225	2,025	1,875
GEA Grasso M-N	3,600 4,500	698 879	220 274	576 725	2,600 2,950	1,225 1,325	2,075 2,175	1,925 2,125

Table 20: Ammonia compressor specifications (GEA, 2023)

Appendix XIII: Air-cooled condenser specification sheet

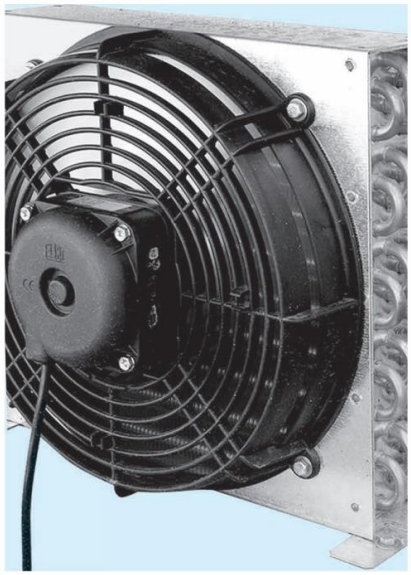

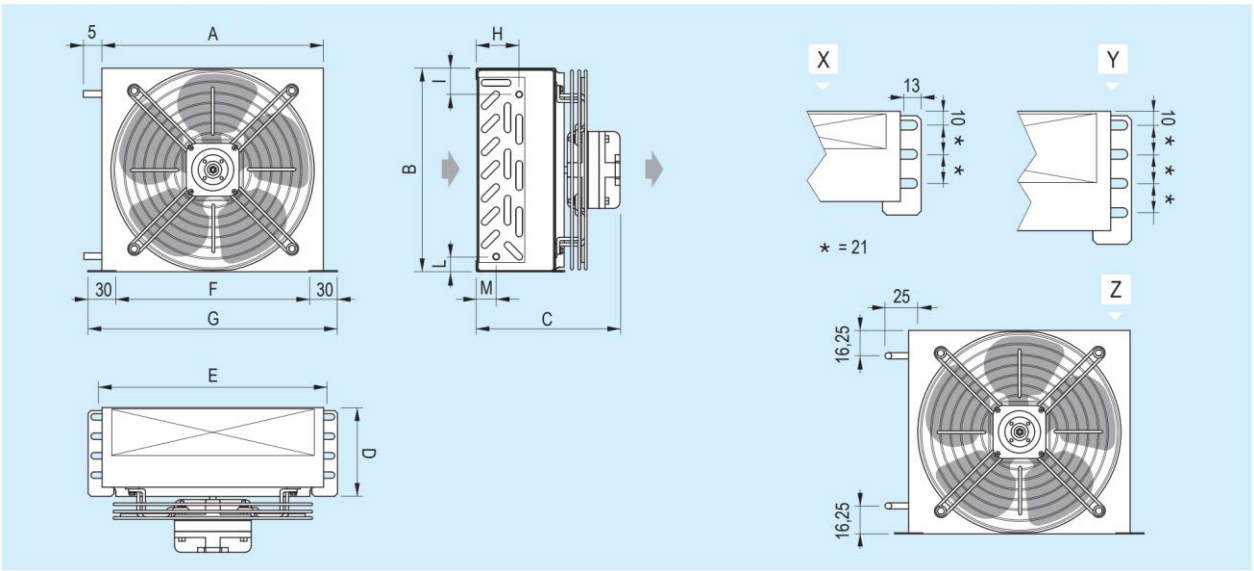

Model		036	045	057	048	063	077	066	087	107	089	117	140	168	179	213	234
Dimensions	A	210	210	210	240	240	240	270	270	270	300	300	300	360	380	380	380
Abmessungen	B	192	192	192	220	220	220	255	255	255	280	280	280	305	320	320	320
Размеры	C	138	164	164	139	165	165	140	164	164	140	166	166	166	199	199	213
mm	D	78	103	103	78	103	103	77	102	102	77	102	102	102	103	103	116
	E	214	214	214	244	244	244	274	274	274	304	304	304	364	384	384	384
	F	180	180	180	210	210	210	240	240	240	270	270	270	330	350	350	350
	G	240	240	240	270	270	270	300	300	300	330	330	330	390	410	410	410
	H	8,75	33,75	46,25	8,75	33,75	46,25	8,75	33,75	46,25	8,75	33,75	46,25	46,25	33,75	46,25	-
	I	14,75	14,75	27,75	16,25	16,25	28,75	9,25	9,25	21,75	9,25	9,25	21,75	21,75	16,25	28,75	16,25
	L	14,75	27,25	14,75	16,25	28,75	16,25	8,25	20,75	8,25	8,25	20,75	8,25	8,25	28,75	16,25	16,25
	M	21,25	8,75	21,25	21,25	8,75	21,25	21,25	8,75	21,25	21,25	8,75	21,25	21,25	8,75	21,75	-

Model	Capacity W		Air flow	Sound pressure lev.	Rows	Inner volume	Internal surface	External surface	Fan motors		Total power	Total absorption	Drawing reference	Connect.	Net weight
Modell	Leistung W		Luftmenge	Schalldruck-pegel	Rohrreihen	Innen-volumen	Innen-oberfläche	Außen-oberfläche	Motorventilatoren		Gesamt-leistung	Gesamt-stromauf.	Zeichnungs-hinweis	Anschlüsse	Netto-gewicht
Модель	Произво-дительность W		Расход воздуха	звук	Ряды	Вместимость	Внутренняя поверхность	Наружная поверхность	Двигатели вентиляторов		Общая мощность	Общий потребляемый ток	Ссылочный чертеж	Соединения	Масса нетто
	R404A	R448A	m³/h	LPA 3 m	n.	l	m²	m²	Ø	V/ph/Hz	W	A		Ø (mm)	kg
036	362	372	240	31	2	0,11	0,1	0,5	172	230/1/50	38	0,23	X	7	2,4
045	452	465	220	31	3	0,16	0,1	0,8	172	230/1/50	38	0,23	Y	7	2,7
057	566	582	210	31	4	0,23	0,1	1,0	172	230/1/50	38	0,23	Y	7	2,8
048	484	497	330	33	2	0,15	0,1	0,7	200	230/1/50	38	0,23	X	7	2,7
063	630	648	300	33	3	0,22	0,1	1,0	200	230/1/50	38	0,23	Y	7	3,1
077	765	786	290	33	4	0,3	0,1	1,3	200	230/1/50	38	0,23	Y	7	3,3
066	659	677	450	33	2	0,22	0,2	1,0	230	230/1/50	38	0,23	X	7	2,7
087	870	894	400	33	3	0,33	0,3	1,4	230	230/1/50	38	0,23	Y	7	3,2
107	1066	1096	380	33	4	0,43	0,3	1,9	230	230/1/50	38	0,23	Y	7	3,4
089	887	912	630	37	2	0,26	0,2	1,2	254	230/1/50	46	0,31	X	7	3,8
117	1169	1201	580	37	3	0,38	0,3	1,8	254	230/1/50	46	0,31	Y	7	4,3
140	1403	1442	520	37	4	0,53	0,4	2,9	254	230/1/50	46	0,31	Y	7	4,5
168	1680	1727	620	37	4	0,69	0,6	3,2	254	230/1/50	46	0,31	Y	7	5,2
179	1790	1840	870	44	3	0,55	0,4	2,5	300	230/1/50	75	0,47	Y	7	6,4
213	2126	2185	800	44	4	0,73	0,6	3,4	300	230/1/50	75	0,47	Y	7	6,7
234	2340	2405	740	44	5	0,91	0,7	4,2	300	230/1/50	75	0,47	Y - Z	8	7,3

Table 21: Air-cooled condenser specifications (Modine, 2023)

Appendix XIV: Battery pack configuration

This section describes a proposed configuration of the battery cells and describes the dimensions that result from this configuration.
The proposed battery cell configuration consists out of 5 packs. In each of the packs, 12 cells rows are placed in the battery's height direction, 139 rows of cells in the width direction, and contains 11 banks stacked on top of each other. The total size of each of the 5 packs is shown in Table 22, taking into account 2mm battery spacing in each direction between the cells as recommended by Lopez et al. (2015).

Dimension	battery cell dimensions [m]	number of cells	pack size without cell spacing [m]	pack size with cell spacing [m]
height	0.04025	12	0.483	0.504
length	0.0351	11	0.386	0.406
width	0.00795	139	1.105	1.381
		18348		

Table 22: Overview of battery pack size

Appendix XV: Automotive battery pack SAE standards

Standard	Title	Scope
SAE J240	Life test for Automotive Storage batteries	Life test simulates automotive service when the battery operates in a voltage regulated charging system
SAE J1766	Recommended Practice for EV & Hybrid Vehicle Battery Systems Crash Integrity Testing	Specifies test methods and performance criteria which evaluate battery spillage, retention and electrical isolation during specified crash tests
SAE J1797	Packaging of Electric Vehicle Battery Modules	Provides for common battery designs through the description of dimensions, termination, retention, venting system, and other features required in an EV application
SAE J1798	Recommended Practice for Performance Rating of Electric Vehicle Battery Modules	Common test and verification methods to determine EV battery module performance. Document describes performance standards and specifications.
SAE J2185	Life test for heavy-duty Storage batteries	Simulates heavy-duty applications by subjecting the battery to deeper discharge and charge cycles than those encountered in starting a vehicle
SAE J2289	Electric-Drive Battery Pack System: Functional Guidelines	Describes practices for design of battery systems for vehicles that utilize a rechargeable battery to provide or recover traction energy
SAE J2344	Technical Guidelines for Electric Vehicle Safety	Defines safety guideline information that should be considered when designing electric vehicles for use on public roadways
SAE J2380	Vibration Testing of Electric Vehicle Batteries	Describes the vibration durability testing of an EV battery module or battery pack.
SAE J2464	Electric Vehicle Battery Abuse Testing	Describes a body of tests for abuse testing of EV batteries.
SAE J2929	Electric and Hybrid Vehicle Propulsion Battery System Safety Standard	Safety performance criteria for a battery systems considered for use in a vehicle propulsion application as an energy storage system galvanically connected to a high voltage power train

Table 23: Society of Automotive Engineers (SAE) mechanical design standards for battery packs (Arora, 2017)

Appendix XVI: Pathway to green ammonia production

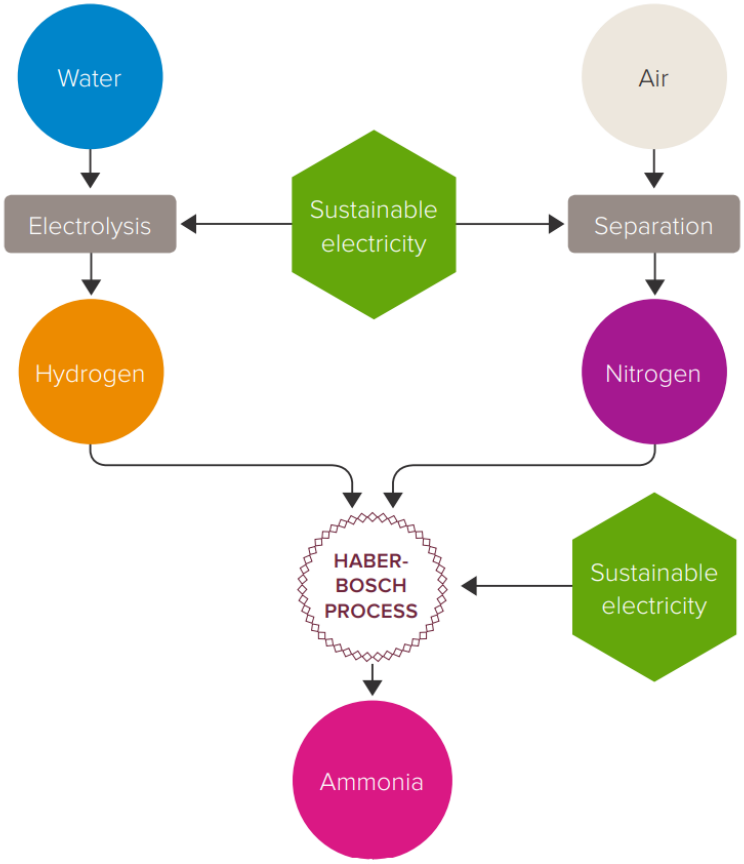

Figure 29: Green ammonia production process (adapted from The Royal Society, (2020))

Appendix XVII: Simulink battery variables

Property	Value used
Number of series connected cells	20
Initial cell charge deficit (A*hr)	0
Initial cell temperature (K)	303.15
Cell mass (kg)	2.5
Cell specific heat (J/kgK)	795

Table 24: Simulink battery general- and thermal variables

	Em open circuit voltage (V)			R0 terminal resistance (Ohm)			R1 cell resistance (Ohm)			C1 capacitance (Farad)		
SOC	5 °C	20 °C	40 °C	5 °C	20 °C	40 °C	5 °C	20 °C	40 °C	5 °C	20 °C	40 °C
0	3.4966	3.5057	3.5148	0.0117	0.0085	0.009	0.0109	0.0029	0.0013	1913.6	12447	30609
0.1	3.5519	3.566	3.5653	0.011	0.0085	0.009	0.0069	0.0024	0.0012	4625.7	18872	32995
0.25	3.6183	3.6337	3.6402	0.0114	0.0087	0.0092	0.0047	0.0026	0.0013	23306	40764	47535
0.5	3.7066	3.7127	3.7213	0.0107	0.0082	0.0088	0.0034	0.0016	0.001	10736	18721	26325
0.75	3.9131	3.9259	3.9376	0.0107	0.0083	0.0091	0.0033	0.0023	0.0014	18036	33630	48274
0.9	4.0748	4.0777	4.0821	0.0113	0.0085	0.0089	0.0033	0.0018	0.0011	12251	18360	26839
1	4.1923	4.1928	4.193	0.0116	0.0085	0.0089	0.0028	0.0017	0.0011	9022.9	23394	30606

Table 25: Simulink battery electrical variables